2004-48

Final Report

Rapid Assessment of Distortional Stresses in Multi-Girder Steel Bridges

Research

Technical Report Documentation Page

1. Report No.	2.	3. Recipients Accession No.
MN/RC – 2004-48		

4. Title and Subtitle	5. Report Date
Rapid Assessment of Distortional Stresses in Multi-Girder Steel Bridges	September 2004
	6.

7. Author(s)	8. Performing Organization Report No.
Benjamin Severtson Frederick Beukema Arturo E. Schultz	

9. Performing Organization Name and Address	10. Project/Task/Work Unit No.
University of Minnesota Department of Civil Engineering 500 Pillsbury Drive S.E. Minneapolis, MN 55455-0116	11. Contract (C) or Grant (G) No. (c) 81655 (wo) 14

12. Sponsoring Organization Name and Address	13. Type of Report and Period Covered
Minnesota Department of Transportation Research Services Section 395 John Ireland Boulevard Mail Stop 330 St. Paul, Minnesota 55155	Final Report
	14. Sponsoring Agency Code

15. Supplementary Notes

http://www.lrrb.org/PDF/200448.pdf

16. Abstract (Limit: 200 words)

Multi–girder steel bridges are found as part of the transportation infrastructure of countries throughout the world. These bridges are typically constructed with a steel reinforced concrete deck rigidly attached to the top flange of steel girders. The deck and the transverse steel members distribute loads laterally between bridge girders. The weld connecting transverse stiffeners to the girder web are commonly terminated several inches away from the girder flanges to avoid overlapping with the web–to–flange connection weld, leaving a short, unstiffened portion of the girder web—the web gap. The large flexibility of the web gap region relative to the other components forces it to accommodate the majority of the distortion.

Since 1998, several research efforts have investigated methods for predicting the amount of web gap stress a bridge will experience during its service life. Phase I of this research resulted in a simple equation for estimating web gap stress using data collected during field testing and subsequent finite modeling of a skew supported bridge with staggering bent–plate diaphragms. Phase II produced an approximate method for predicting diaphragm differential deflection of skew supported bridges with bent–plate diaphragms. The combined result of Phase I and Phase II was a useful method for predicting peak web gap stress in skewed multi–girder steel bridges with staggered bent–plate diaphragms.

The next step was to develop a reliable procedure for the rapid assessment of distortional stresses in steel bridges that includes a test of the applicability of this procedure to bridges with geometries differing from those that formed the basis of the previous research. As a consequence of this most current research, the authors propose changes and recommend modifications of previously developed methods of field measurement and assessment.

17. Document Analysis/Descriptors		18.Availability Statement
Steel bridges Stresses Assessment	Infrastructure Multi-girder	No restrictions. Document available from: National Technical Information Services, Springfield, Virginia 22161

19. Security Class (this report)	20. Security Class (this page)	21. No. of Pages	22. Price
Unclassified	Unclassified	134	

RAPID ASSESSMENT OF DISTORTIONAL STRESSES IN MULTI-GIRDER STEEL BRIDGES

Final Report

Prepared by:

Benjamin Severtson
Frederick Beukema
Arturo E. Schultz
Department of Civil Engineering
University of Minnesota

September 2004

Published by:

Minnesota Department of Transportation
Research Services Section, MS 330
395 John Ireland Boulevard
St. Paul, Minnesota 55155-1899

Acknowledgements

This research would not have been possible without the generous support of the Minnesota Department of Transportation (Mn/DOT). The authors would also like to extend their thanks to Erik Wolhowe, Poachen Mma and Gary Peterson of the Office of Bridges and Structures for their help and guidance throughout the course of this project. Special thanks are due to Mark Pribula and others at the Mn/DOT Metro Division Office of Maintenance for their assistance with field data collection.Thanks must also be given to Paul Bergson, who provided practical knowledge for the field instrumentation and testing portion of this project. The authors are also indebted to the previous researcher in this line of research, Evan Berglund, for his help throughout various portions of this project. Thanks are also extended to fellow graduate students Clifford Youngberg, Robert Fitzpatrick, Hussam Mahmoud, Christopher Drake, Jonathon Wacker, Nathan Erpested, Bulent Erkman, Christine Freisinger, and Xiping Lie for their assistance during many aspects of this project including the instrumentation and truck testing phases of the research.

Table of Contents

List of Figures

List of Tables

List of Equations

Executive Summary

Fatigue cracking from out-of-plane web stresses due to distortional deformation has been a well-documented problem in steel bridges. One situation leading to out-of-plane distortion arises when transverse stiffeners serving as diaphragm connection plates are not attached to the girder tension flange in the negative moment region. Often, in such connections, the stiffener-to-web weld is terminated away from the flange, thus leaving a portion of the web unstiffened, and this region is frequently referred to as the web gap. When girders connected by a diaphragm undergo a differential deflection, the web gap accommodates most of the out-of-plane deformation inducing large out-of-plane stresses in the web.

Research has been performed by various researchers over the past two decades to investigate the sources and causes of distortional fatigue as well as methods to reduce or eliminate the problem. The Minnesota Department of Transportation (Mn/DOT) has sponsored research at the University of Minnesota since 1998 to develop tools for rapid assessment of distortional stress in steel girder bridges. In Phase I of this program, a formula for the prediction of the peak web gap stress in steel girder bridges was proposed by Jajich [1]. This equation was developed based upon field observation and finite element modeling of a skew supported bridge with staggered, bent-plate diaphragms. This equation requires geometrical parameters of the bridge and the differential deflection of the diaphragm as its inputs. In a subsequent research project (Phase II of the Mn/DOT distortional fatigue rapid assessment program), Berglund developed an approximate formula for the prediction of the maximum amount of differential deflection a bridge could experience [2]. The derivation was based upon the results of an extensive parameter study using finite element models of entire bridges. These models were developed and refined using field data collected during the previous project and attributes commonly found in the Mn/DOT bridge inventory.

The first part of the Phase III research project (i.e., Phase IIIA) was aimed at investigating the distortional stress phenomenon, and to test the applicability of the

formulas proposed in Phases I and II. Two bridges were selected for instrumentation and monitoring, the first of which was a skewed bridge with staggered cross-braced diaphragms (i.e., Plymouth Ave. Bridge in Minneapolis), as well as a square bridge with back-to-back diaphragms (i.e., 7th St. Bridge in St. Paul). Analysis for the field data recorded for these bridges indicated that the Jajich and Berglund formulas do not predict the measured web gap stresses and diaphragm differential deflections as accurately as was expected.

Phase IIIA research activities included a finite element parameter study of a model of the skewed bridge with cross-braced diaphragms (i.e., Plymouth Ave. Bridge) to further investigate the distortional stress behavior. The finite element model represented part of the bridge which included one diaphragm and the portions of the attached girders between successive lateral supports, and it was constructed and refined to match field measurements. The parametric study indicated that web gap stress is primarily generated by rotations of the top flange and the transverse stiffener, and that these rotations could be approximated by linear functions of the assumed diaphragm rotation (i.e., the ratio of differential deflection and girder spacing). It was also determined that lateral deflection of the web gap does not appear to play a significant role in the generation of web gap stress. Making use of the previously described findings allowed for the modification of the peak web gap stress formula for bridges with staggered cross-braced diaphragms. Also, given the small amounts of measured differential deflection and stress in the 7th St. Bridge, it is believed that distortional stress will not be a significant problem in bridges with back-to-back diaphragms.

In the second part of this research (i.e., Phase IIIB), a finite element model of the entire Plymouth Ave. Bridge was developed and calibrated using the recorded field data. The methods used to model the diaphragms and the sidewalk, and the decision to model the horizontal braces, significantly influenced the results by increasing prediction accuracy. A series of simulated truck tests showed that the cross-braces had a significant reducing effect on differential deflections, an effect that was not included in the Berglund prediction formula.

On the basis of the previous observations, it was concluded that the Berglund formula, which was developed for bent-plate diaphragm bridges, needed modification if it is to be extended to cross-brace diaphragm bridges. Thus, a modification factor was developed to account for the reduction in differential deflection effected by the cross-braced diaphragms. A parametric study was performed on a series of bridge models with cross-brace diaphragms to identify the discrepancy between differential deflections for bent-plate and cross-brace diaphragm bridges. The numerical data from the finite element parametric study was used to define the modification factor for use with the Berglund formula in order to predict differential deflections in bridges with cross-braced diaphragms.

Chapter 1 *Introduction*

1.1 *Background*

Multi-girder steel bridges are found commonly in the transportation infrastructure of the United States and countries around the world. These bridges are typically constructed with a steel reinforced concrete deck rigidly attached to the top flange of steel girders by means of headed shear studs. This practice allows the steel and concrete to act compositely and makes the system very efficient for spanning the distances commonly required in today's highway system. The concrete deck and transverse steel members act to distribute vertical loads laterally between bridge girders. These transverse members are commonly referred to as diaphragms.

Diaphragms also function to resist lateral loads and to provide lateral bracing. The lateral bracing function is important during the construction process, prior to the pouring and hardening of the concrete deck, when the deck cannot provide the needed lateral restraint. The lateral bracing function is also important during the service life of the bridge in the negative moment regions where the bottom flanges of the girders are in compression. In this case the concrete deck is too distant to provide the needed restraint to the bottom flanges of the girders.

Diaphragms are connected to the girders by means of diaphragm connection plates. The diaphragm connection plates are transverse stiffeners that are welded to the girders and to which the diaphragms are typically bolted. The weld connecting the transverse stiffeners that serve as diaphragm connection plates to the girder web are commonly terminated several inches away from the girder flanges to avoid overlapping with the web-to-flange connection weld. This practice leaves a short, unstiffened portion of the girder web that is commonly referred to as the web gap.

Prior to 1985, it was standard practice not to weld transverse stiffeners to the girder tension flange. Such construction techniques can lead to fatigue problems when transverse stiffeners are used as connection plates for diaphragms. Lateral distortion of the web gap occurs when adjacent girders connected by a diaphragm experience different amounts of vertical deflection. Due to its stiffness, the diaphragm experiences a rotation in response to the differential vertical deflection, and the diaphragm rotation forces the web to undergo out-of-plane distortion. The large flexibility of the web gap region, relative to that of the deck, diaphragm and other components, forces it to accommodate the majority of the distortion.

Differential deflections are magnified by the angle of skew between a bridge and its supports, so skewed bridges are more susceptible to this phenomenon than square bridges. Moreover, back-to-back diaphragms reduce the magnitude of the out-of-plane deformation of the girders, because a diaphragm behind a web gap that is undergoing distortion poses a large lateral stiffness that reduces the magnitude of the imposed deformation. Thus, the mechanism of web gap distortion is of greatest concern in bridges with staggered diaphragms. Since staggered diaphragms are used only in skewed bridges, the mechanism of web gap distortion is of greatest concern in skewed bridges.

Web gaps in negative moment regions are especially susceptible to this problem. In such regions, the top flanges of the girder are the tension flanges to which welded connection to the transverse stiffeners is avoided. The stiff concrete decks and the headed shear stud connections restrain the top flanges of the girders, so the web gaps must accommodate all of the out-of-plane distortion. The corresponding concentration of distortion in the web gap leads to out-of-plane web stresses at the toe of the transverse stiffener. Given the small thickness of the web relative to the depth of the girders, the out-of-plane web stresses are several times larger than the corresponding flange stresses.

Over many loading cycles, the higher stresses in the web gap region can lead to fatigue cracking. Previous research has included some efforts to investigate the source of distortional stresses in web gaps. However, most previous research efforts have focused

on methods for lessening or eliminating web gap stresses once they are identified. Although current design codes have requirements that mitigate the sources of these stresses in new bridges, guidance on how to deal with this problem in existing structures is limited. Thus, further research is needed to provide bridge owners with methods to effectively assess bridges susceptible to this problem. The research documented in this report is aimed at providing rapid procedures for assessing distortional stresses in steel girder bridges on skew.

1.2 *Objectives*

Prior to 1998, little research effort had been expended on methods for predicting the amount of web gap stress a bridge will experience during its service life. Since then, the Minnesota Department of Transportation (Mn/DOT) has funded research to provide insight into this problem and develop expedient procedures for the estimation of peak values of web gap stress and the associated diaphragm differential deflection [1, 2]. In Phase I of this program, Jajich derived a simple equation for estimating web gap stress using data collected during field testing and subsequent finite element modeling of a skew supported bridge with staggered bent-plate diaphragms [1]. This prediction method requires several parameters defining the geometry of the bridge, as well as the differential deflection of bridge girders at the diaphragm location where the peak web gap stress is sought.

In a subsequent Mn/DOT research project (Phase II), Berglund proposed an approximate method for predicting diaphragm differential deflection of skew supported bridges with bent-plate diaphragms [2]. An extensive parameter study using finite element models of skewed bridges meeting the characteristics of those in the Mn/DOT inventory was used as the basis for this prediction method. Several bridge geometry parameters are also necessary for the use of this method. Jajich's web gap stress formula coupled with Berglund's differential deflection formula comprise a useful and expedient method for predicting peak web gap stress in skewed multi-girder steel bridges with staggered bent-plate diaphragms.

The next step in developing a procedure for rapid assessment of distortional stresses in steel girder bridges comprises a test of the applicability of this procedure to bridges with geometries differing from those that formed the basis of the previous research. In 2001, Mn/DOT approved such a project, the details of which are documented in the present report (Phase III). This project included the selection and monitoring of two bridges to determine their susceptibility to distortional fatigue. One of these bridges was square (i.e., the supports were not skewed) and had back-to-back diaphragms, while the other bridge was skewed but had cross-brace diaphragms. The data collected during this process was compared with the methods developed by Jajich [1] and Berglund [2] to verify their applicability to bridges with different details and geometry. As a consequence of this verification, modification of these previously developed methods is recommended, and changes are proposed as part of the present study.

1.3 *Outline*

This report begins with a brief introduction on the topic of distortional stresses in steel girder bridges. The objectives of the present research and a brief outline of the contents of this report are also included.

Chapter 2 provides a review of literature on the problem of out-of-plane distortion of the web gap region, including efforts made to determine its sources as well as techniques to mitigate the problem. Previous Mn/DOT research, which provides the basis and motivation for the present study, is also reviewed.

Chapter 3 discusses the selection and instrumentation of the two bridges studied in the project documented in this report. The equipment used in the monitoring of these bridges is also described.

Chapter 4 presents the means and methods of data collection during the truck load testing of the selected bridges.

Chapter 5 reviews the methodology and data collection schemes used for the long term monitoring portion of this research.

Chapter 6 examines the data collected during truck testing and long-term monitoring. Comparison of the data collected with each testing approach, as well as with previously developed prediction methods, is also presented.

Chapter 7 describes the formulation and use of a finite element (FE) micro-model of a portion of the Plymouth Ave. Bridge. The micro-model includes one diaphragm and portions of the two connected girders and deck, and a refined finite element mesh is used for the purpose of determining localized stresses in the web gap region. Results of a parameter study conducted using this model are also given.

Chapter 8 combines the most important observations reached from the FE parameter study and the implications of these findings on the estimation of web gap stresses. As a consequence of these findings, Jajich's equation for the prediction of the peak web gap stress [1] is modified, and a variant of this formula is proposed.

Chapter 9 concerns the construction and calibration of a finite element macro-model of the Plymouth Ave. Bridge. The macro-model includes all girders, diaphragms, deck and supports in the Plymouth Ave. Bridge for the purpose of calculating differential vertical deflections at the diaphragm locations. Because of its size, the macro-model utilizes a coarser FE mesh than the micro-model. Results of a sensitivity study of parameters affecting calibration are also discussed.

Chapter 10 describes the simulated truck tests on the calibrated macro-model, the results of which explain the discrepancies between analytic predictions and field data for differential deflections on the Plymouth Ave. Bridge.

Chapter 11 presents the development of a modification factor that reduces the differential deflection magnitude from the Berglund deflection formula [2] so that it may be used in assessing bridges with cross-brace diaphragms.

Chapter 12 summarizes the results of this research as well as the applications and importance of these findings.

Chapter 2-*Literature Review*

2.1 Overview

There exists a considerable amount of literature documenting distortional fatigue problems in steel bridges. Research investigating these problems can be broken down into two main categories. The first category includes field observation of the causes of distortional stresses, extent of fatigue damage and characteristics common to affected bridges. The second category documents laboratory experiments exploring the sources of distortional stresses and the effectiveness of retrofit procedures. Several methods of retrofitting affected bridge details have been proposed to eliminate or reduce distortional stresses. Research in this area has brought about changes in design codes and led to design guidelines that will limit the effects of distortional fatigue on future structures. Information regarding the causes and severity of distortional fatigue as well as guidelines for the design and maintenance of steel bridges have greatly benefited from the field and laboratory research performed in this area.

2.2 Stress Mechanism

The welds connecting transverse stiffeners to girder webs are often terminated away from the flanges to avoid welding near the flange-to-web welded connection. This practice leaves an unstiffened portion of the web that is several inches long and which is commonly referred to as the web gap. Prior to 1985, connection of transverse stiffeners to girder tension flanges was discouraged due to fatigue concerns. After 1985, such connections have been allowed using either bolts or welds, with designers often preferring to use a bolted connection so as to avoid the fatigue problems associated with welds. The absence of such a connection in pre-1985 steel girder bridges makes this region prone to out-of-plane distortion that generates large stresses in the web gap.

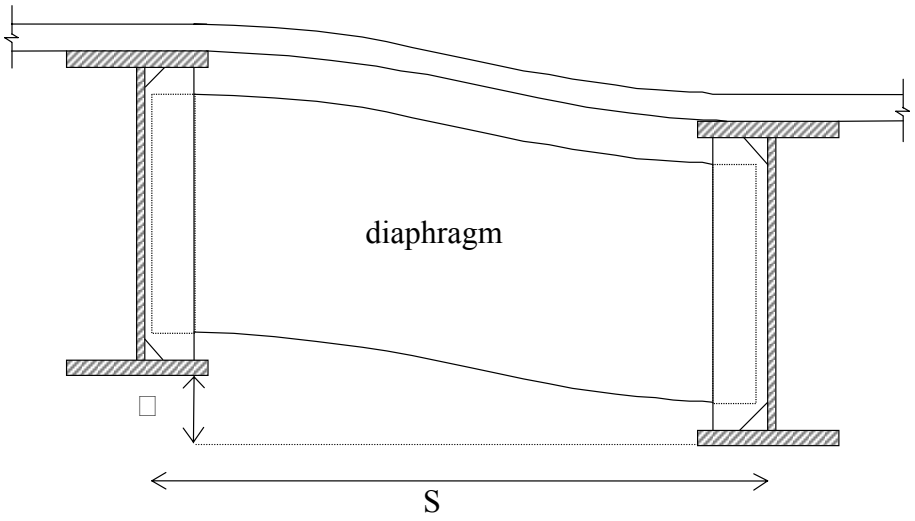

Figure 2.1 Differential Deflection of Girders

When transverse stiffeners are used as connection plates for diaphragms, large out-of-plane stresses can be induced in the girder webs. This situation occurs when adjacent girders undergo different amounts of vertical deflection from vehicular traffic (Figure 2.1). Due to the high stiffness of the diaphragm, this differential deflection, Δ, causes the diaphragm to undergo a rigid body rotation. Due to its large flexibility relative to that of the diaphragm, the deck and other components, the web gap attracts the majority of the out-of-plane distortion (Figure 2.2). Large stresses are generated in this area by virtue of concentrating the distortion over the small web gap length, often only one or two inches long. Due to the severity of the stresses and the prevalence of this detail, distortional stresses are considered the largest source of fatigue cracking in steel bridges [3].

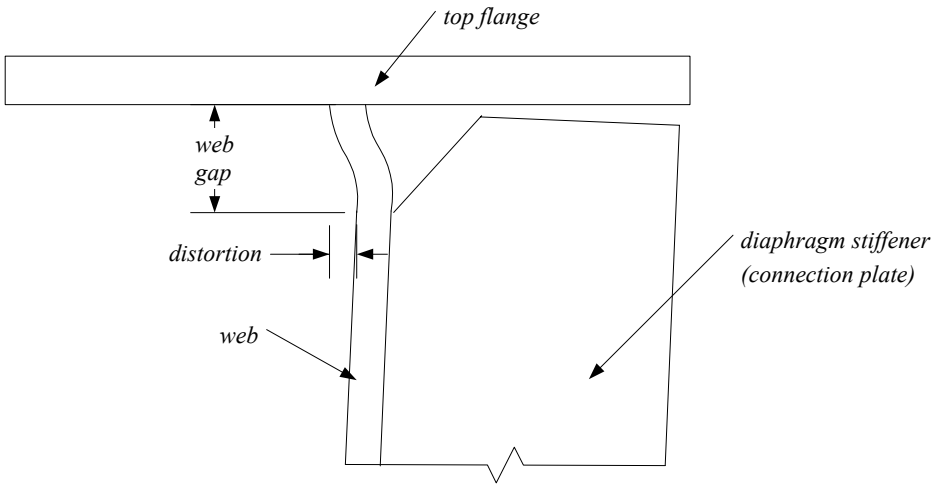

Figure 2.2 Girder Web Gap Distortion

Many field studies have investigated the fatigue cracking of unstiffened web gaps and their findings support the previously discussed behavior, in addition to demonstrating the need for further research to provide a better understanding of this problem [4, 5, 6]. Distortional fatigue cracks are often observed to form parallel to the primary bending stresses in the bridge. Thus, these cracks are not problematic until they have propagated away from the area of distortion and their growth is influenced by the primary bending stresses, which causes them to grow perpendicular to these stresses.

Laboratory testing has found that this detail has the equivalent fatigue resistance of an American Association of State Highway and Transportation Officials (AASHTO) category C detail for hot spot stresses [7]. Research has also shown that the stresses at the web-flange weld are often larger than those at termination of the stiffener. Thus one could expect cracks to form at either location, and such occurrences have been observed. However, the smooth profile of the web-flange connection provides a greater fatigue resistance than that of the stiffener weld termination, thus making cracks less likely to form in the web-flange connection region.

Field and laboratory work has shown that the magnitude of the distortional stress is often hard to predict. It has been proposed that the web gap be modeled as a short beam with fixed supports undergoing a lateral deflection, δ, without end rotation [8]. Using the slope deflection equation one can derive a relationship between the lateral deflection of the web gap and the web gap stress. If one assumes that all of this lateral deflection is created by the rigid body rotation of the diaphragm about its base, one can arrive at the relationship shown in Figure 2.3.

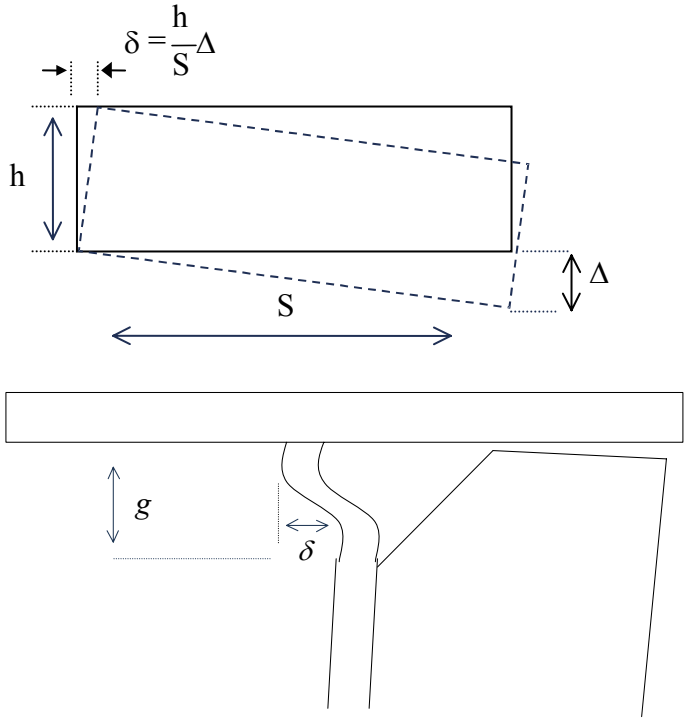

Figure 2.3 Diaphragm Rotation and Web Gap Deflection

Substituting this relationship into the equation for the web gap stress described above, one arrives at the formula given in Equation 2.1. Where E is Young's Modulus, t_w is the thickness of the web, h is the depth of the diaphragm, S is the girder spacing, g is the length of the web gap, and Δ is the amount of differential vertical deflection between adjacent girders, as shown in Figure 2.3. In this report, Equation 2.1 is referred to as Fisher's formula for web gap stress.

$$\sigma_{wg} \approx \frac{3Et_w}{g^2}\delta = \left(\frac{3Et_w}{g^2}\right)\left(\frac{h\Delta}{S}\right)$$

Equation 2.1

Accurate quantification of distortional stresses is not as simple as the preceding derivation might imply. Prediction of the amount of girder differential deflection is a very difficult task due to interaction of the concrete slab, steel reinforcement, girders and diaphragms. Even if the differential deflection in known, it has been shown that the web gap stress is sensitive to small changes in the geometry of the surrounding structure, and thus a large variability in response can be expected. This conclusion is further supported by the erratic crack growth that has been observed when the web gap length is less than five times the web thickness [9]. Given the factors complicating the prediction of web gap stresses, field measurement is still considered to be the only reliable method to determine the intensity of distortional stresses in steel bridges.

2.3 Retrofitting

Due to the prevalence of distortional fatigue problems, a number of researchers have performed work to develop methods for correcting these problems. Retrofitting solutions for distortional fatigue problems are typically based on one of two different philosophies. The first method relies on increasing the stiffness of the system so that it can better handle the stresses placed upon it. This goal is often achieved by positive attachment of the transverse stiffener plate to the girder flange. Such connections often incorporate bolted and/or welded plates, angles or tees [7, 10, 11]. See Figure 2.4 for a "positive attachment" retrofitting example.

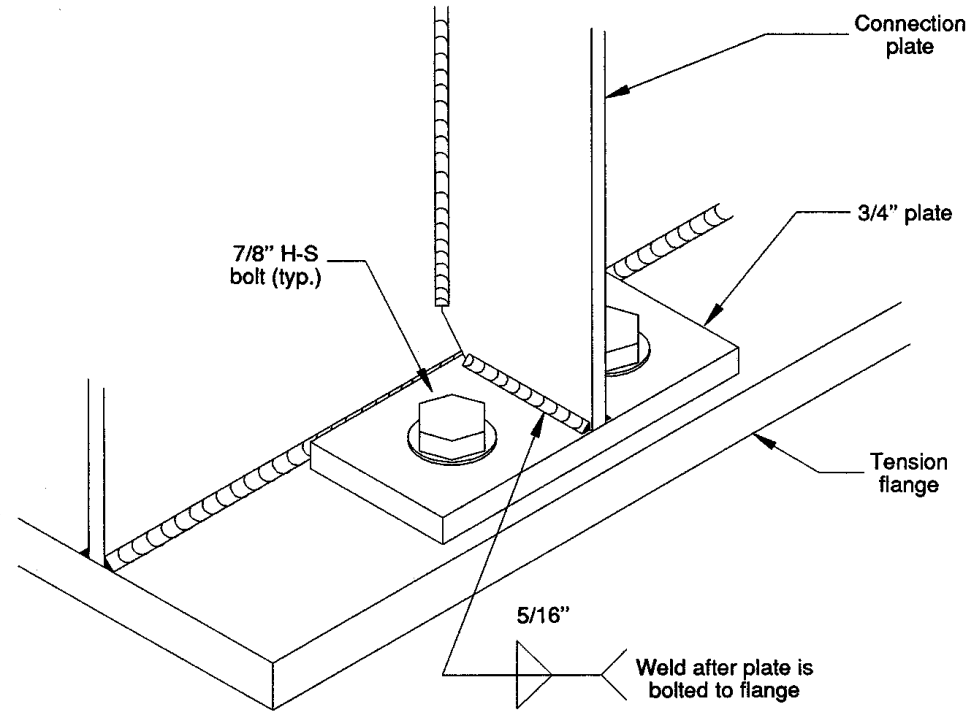

Figure 2.4 Bolted Base Plate Retrofit Example [3]

Various retrofit connection details have been shown to reduce web gap stresses and arrest crack growth, but these options are often expensive and time consuming due to field conditions and the locations of problem areas. Field weld quality is hard to assure due to corrosion and dirt buildup during service life, preheat requirements and the overhead location of the web gap. Welding also requires that the bridge be closed during the retrofit operations so as to reduce structure movement. Bolted solutions are also difficult because they require access to the top flange in the negative moment, and thus the removal of the reinforced concrete deck is necessary. Bolted connections have also been shown to be less rigid then their welded counterparts, and therefore it is desirable to employ rigid splice components in these connections. Sufficient stiffness can be achieved by using components, such as tees, with a thickness of 0.75 inches or greater.

To prevent the further propagation of any cracking, drilling holes at crack tips is recommended when positive attachment retrofitting is undertaken. It has also been

shown that hole drilling is effective at stopping crack propagation, but only when the distortional stresses are below 15 ksi [7].

Current design codes by the American Association of State and Highway Transportation Officials (AASHTO) require the positive attachment of transverse stiffeners to the girder flanges [12]. It has been shown that welded attachments to the tension flange are no worse than similar attachments made to the web [7]. It should also be noted that positive attachments to the flanges will only reduce out-of-plane distortion by a sufficient amount if the web gap length is greater than 2 inches or 4 times the web thickness, whichever is greater. For further guidance in the fatigue evaluation of steel bridges, including the assessment of fatigue loading, stress ranges and remaining life, see National Cooperative Highway Research Program (NCHRP) Report 229, Fatigue Evaluation Procedures for Steel Bridges[13].

The second retrofitting philosophy involves increasing the flexibility of system so as to reduce the concentration of stresses. Increasing the web gap length by removing a portion of the transverse stiffener has been shown to significantly reduce the growth rate of fatigue cracks [7]. However, for this method to be effective, the new web gap length must be at least 20 times the web thickness [7]. Another method to reduce the stiffness of the connection involves the loosening or removal of bolts from the diaphragm connection. Loosening of bolts lowers the stiffness of the diaphragm connection and has been shown to reduce the out-of-plane distortion and its corresponding stresses [14]. However, care must be taken to ensure that bolts do not become completely loosened by vibrations of bridge, which would create the hazard of falling nuts and bolts.

Complete removal of the diaphragm is also a solution and would eliminate the source of the distortional stresses. Research has shown the removal of diaphragms has a negligible effect on the capacity of a bridge [15]. Diaphragms often provide essential lateral bracing in the negative moment region as well as strength for resisting lateral forces from wind and seismic excitation, therefore, complete diaphragm removal should not be performed without careful prior analysis.

2.4 Mn/DOT Project Background

Given the prevalence of the distortional fatigue problem, the Minnesota Department of Transportation (Mn/DOT) funded research in 1998 (Phase I) to provide further investigation of this problem [1]. The purpose of this research was to 1) instrument and monitor a skew supported multi-girder steel bridge in the field, 2) assess the frequency and magnitude of distortional fatigue stresses at web gap locations and 3) evaluate the impact of these stresses on the fatigue life of the bridge [1]. To accomplish this goal Bridge #27734 at the intersection of Interstate Highway 94 (I-94) and 694 (I-694) in Brooklyn Center, Minnesota was instrumented and monitored. Long-term monitoring of the bridge under ambient traffic loading was performed to determine the actual stresses to which the bridge is subjected. The response of the bridge under known loading was investigated by testing of the bridge with fully loaded Mn/DOT sand trucks driving at highway speeds.

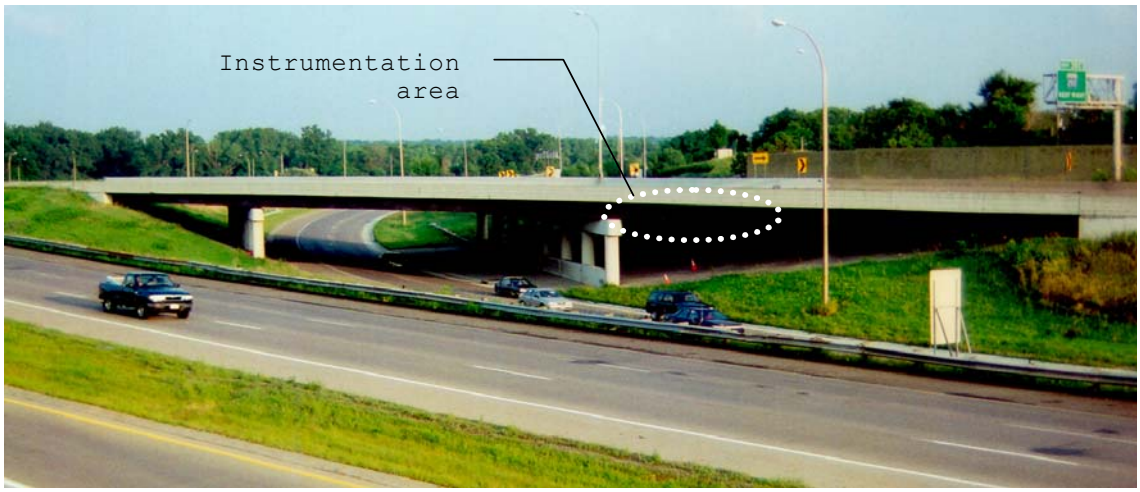

Figure 2.5 Bridge #27734, Looking South

This monitoring revealed that web gap stresses were 2-2.5 times that of the flange stresses. A detailed finite element (FE) analysis of the web gap region showed that the maximum stresses were much higher than those recorded in the field. The large stress gradient in the web gap region and the location of the strain gages accounted for these discrepancies. The FE analysis also determined that the out-of-plane distortion of the

web gap was primarily created by a rotation of the diaphragm about the termination of the transverse stiffener.

With the mode of web gap deformation known, it was then possible to model the web gap as a small fixed-fixed beam. Assuming that all of the differential deflection between girders is translated into this rotation yields the expression $\theta = \Delta/S$. Combining this relationship with the slope deflection equation modified for this mode of deformation produces a simple equation for the prediction of the peak web gap stress, Equation 2.2.

$$\sigma_{wg} = 2E \cdot \left(\frac{t_w}{g}\right)\left(\frac{\Delta}{S}\right) \qquad \textbf{\textit{Equation 2.2}}$$

Equation 2.2 is referred to as the Jajich web gap stress formula, and Jajich found that stresses calculated using Equation 2.2 correlate well with results from FE analysis. The Jajicj stress formula is dependent only on geometric parameters of the bridge, as defined previously, and the differential deflection of bridge girders at the diaphragm location, Δ. Having derived a formula to estimate web gap stresses [1], further research (Phase II) was focused on developing a procedure for estimating diaphragm differential deflection [2]. To accomplish this task, an FE model of the entire instrumented bridge was created and refined to match the field data. Using this refined model, parametric studies were performed to determine the influence of various parameters on the differential deflection of adjacent bridge girders [2].

The primary parameter study of this research focused on the influence of girder spacing, angle of skew, and main span length on differential deflection. A secondary study considered the effects of concrete deck thickness, adjacent span length and diaphragm depth on differential deflection, as well as considering additional values for girder spacing to augment the primary study. From these studies it was shown that main span length, angle of skew, girder spacing and concrete deck thickness all have a significant impact on the amount differential deflection. It was observed that for varying values of skew and span lengths that the value of Δ/S remained fairly constant. Using this

relationship, an approximate formula for the value of Δ/S was obtained, and it is given in Equation 2.3.

$$\frac{\Delta}{S} = \frac{A \cdot L^2 + B \cdot L + C}{L} \qquad \textit{Equation 2.3}$$

This equation, which is referred to as the Berglund deflection formula, relates the maximum ratio of differential deflection and girder spacing seen in a bridge to the main span length and several constants. The constants A, B and C are dependent on the angle of skew of the bridge and can be determined through interpolation from Table 2.1.

Table 2.1 Polynomial Equation Constants Based on Angle of Skew

	Constants (*L* in meters)		
(deg.)	*A*	*B*	*C*
20	-0.00001327	0.001486	-0.008639
40	-0.00001227	0.001522	-0.01034
60	-0.00001714	0.002185	-0.02328
	Constants (*L* in inches)		
(deg.)	*A*	*B*	*C*
20	-3.370E-07	0.001486	-0.3399
40	-3.115E-07	0.001522	-0.4065
60	-4.352E-07	0.002185	-0.9156

Berglund also recognized that use of the Jajich stress formula (Equation 2.2) requires knowledge of the web gap length, g. However, this quantity may not be known with accuracy because it is a detailing dimension that is usually not specified in bridge plans. Through inspection of the Mn/DOT bridge inventory, Berglund determined that the ratio of the web thickness, t_w, to the web gap length, g, could be approximated using Equation 2.4, in absence of actual bridge geometry. In this equation K is equal to –0.002858 when L is in meters and -0.00007260 when L in is inches.

$$\frac{t_w}{g} = K \cdot L + 0.4091 \qquad \textit{Equation 2.4}$$

Equation 2.2, when used in conjunction with Equation 2.3, allows for the prediction of the web gap stress based solely upon the geometry of the bridge in question. If the actual

web gap length is not known then Equation 2.4 can be used as an approximation. It is also noted that Berglund developed modification factors for Equation 2.3 based upon the axle configuration of the truck being considered as well as the concrete deck thickness.

Chapter 3-*Instrumentation*

3.1 Bridge Selection

The stress prediction formula developed by Jajich and the diaphragm differential deflection formula proposed by Berglund are both based on field data taken from Bridge #27734 at the intersection of I-94 and I-694 in Brooklyn Center, Minnesota. This three-span bridge has a sixty degree angle of skew and staggered bent plate diaphragms. In order to determine the applicability of the Jajich and Berglund formulas to dissimilar bridges in the Mn/DOT inventory, it was determined that two other bridges should be selected and instrumented in order to monitor their distortional fatigue response in Phase IIIA of the Mn/DOT program on rapid assessment of distortional stress in steel bridges.

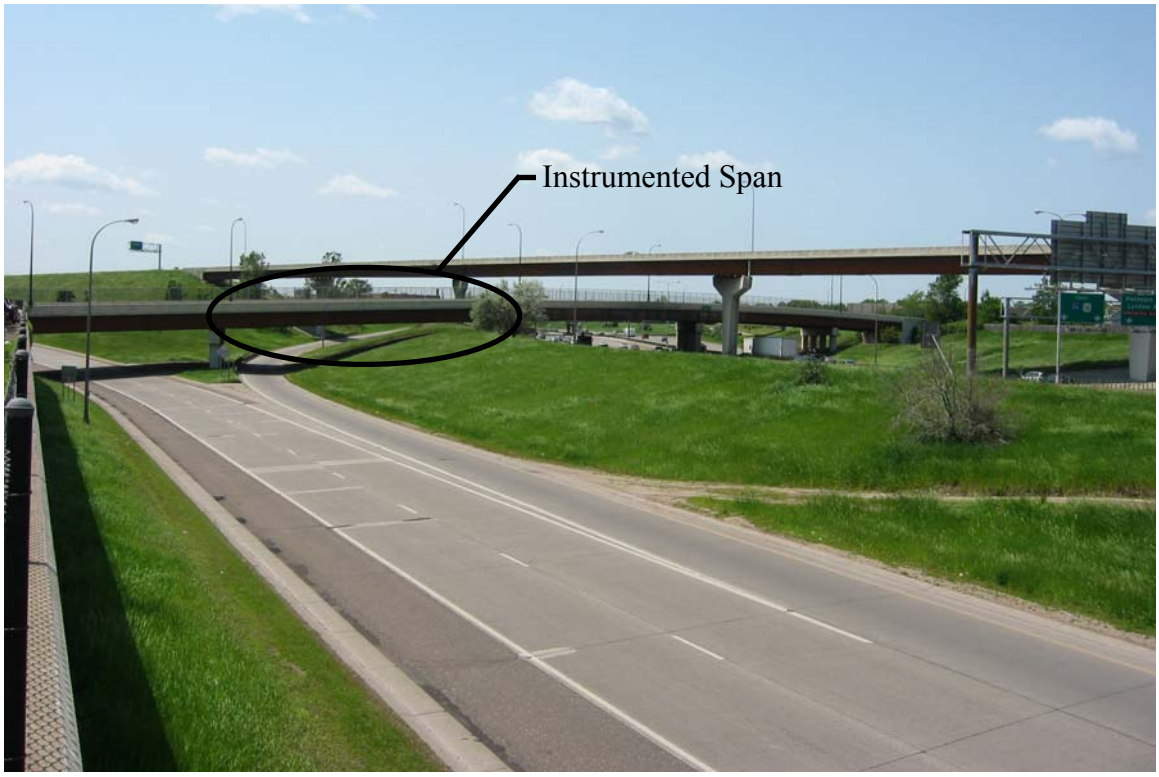

Figure 3.1 Plymouth Avenue Bridge, Looking South

To this end, Bridge #27796, Plymouth Avenue over Interstate Highway 94 and ramps in Minneapolis, Minnesota, was selected for study. This five-span bridge has a 45.5° angle

of skew and staggered X-braced diaphragms. In addition, Bridge #62028, conveying 7th Street over railroad tracks in St. Paul, Minnesota, was selected for observation. This square bridge has five spans with back-to-back bent plate diaphragms. By studying these bridges it is expected that a greater understanding of the girder web distortional phenomenon can be gained and the applicability of the previous research can be tested.

Figure 3.2 7th Street Bridge, Looking North

3.2 Objectives

In order to determine the distortional fatigue behavior of the selected bridges, a variety of field measurements must be taken. These measurements include strains in bridge components, and these strains can be correlated to stresses. Displacement of the bridge components must also be measured so that an accurate picture of the bridge deformation can be established. The bridges were monitored under known loading during truck testing as well as under unknown loading by ambient traffic during long-term monitoring. These measurements allow insight into the mechanism of the out-of-plane distortion in a controlled case as well as the behavior of the bridges under service conditions.

3.3 Equipment

In order to gather data from the bridges, a wide array of equipment was required. This equipment was used during the field instrumentation, truck testing and long term monitoring of the two bridges. An overview of important equipment required to complete this work follows.

3.3.1 Somat eDAQ Field Computer

The Somat eDAQ field computer was used to collect data during the long-term monitoring portion of this research. The system used contains eight low-level analog channels used for collecting data from strain gages. The eDAQ was powered using two 100 amp-hour deep-cycle marine batteries. Data was collected at 100 Hz for the entire duration of the long term monitoring study.

3.3.2 Campbell PC9000

The Campbell PC9000 data acquisition unit was used to collect data from instruments during truck testing. The Campbell configuration used was able to monitor twelve analog DC channels, which were used for the position transducers and LVDT's, as well as twenty-four 350-ohm three-quarter bridge strain gage channels. Data was recorded at 66.7 Hz during truck testing.

3.3.3 Strain Gages

Texas Measurements AW-6-11-01LT weldable strain gages were used in both bridges to monitor strains at various locations. Twenty-four strain gages were placed on the Plymouth Ave. Bridge and twenty-one gages were placed on the 7th St. Bridge in the locations presented in section 3.4. The 350-ohm strain gages were designed to function over a wide temperature range and in harsh environments, and, therefore, were found suitable to endure winter climate conditions in Minnesota during the long-term monitoring study. The gages were attached to the bridges by spot welding after the surface had been prepared by removal of any paint or corrosion.

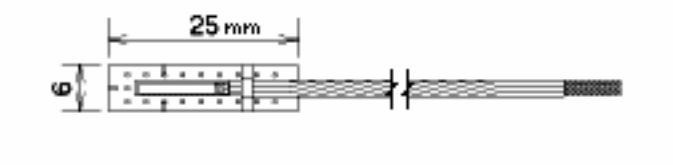

Figure 3.3 Texas Measurements AW-6-11-0LT Strain Gage

Figure 3.4 Field Placement of Strain Gages

3.3.4 Linear Voltage Differential Transducers

Four Lucas Schaevitz GCA-121-250, ±0.25 inch and four Lucas Schaevitz GCD-121-500, ±0.5 inch linear voltage differential transducers (LVDT's) were used during truck testing to measure the horizontal and vertical displacements of the web stiffener plate with respect to the bridge girders. The LVDT's were clamped to the stiffener plate to insure stability throughout testing. Electrical power to the LVDT's was provided by a generator and AC-to-DC converters, with the output signals recorded by the PC9000 data acquisition unit.

Figure 3.5 LVDT Placement for Measuring Relative Horizontal Deflection

3.3.5 Position Transducers

Four UniMeasure P510 series linear position transducers were used during truck testing to measure the absolute vertical deflection of bridge girders. The transducers provide an output signal of 0 to 10 volt DC, which corresponds to a total displacement range of 3 inches. Given that the transducers are not suited to extended periods of outdoor use, they were installed on the day of truck testing. The transducers were attached to boards, which were placed on the ground and weighted to ensure stability during testing. Boards with steel wire cables attached were clamped into place on the bottom of the bridge girders and then attached to the position transducers such that the wire in the transducer was in the middle of its displacement range. The position transducers were placed at girder mid-span locations for one-half of the testing and at the diaphragm locations for the other one-half.

Figure 3.6 UniMeasure Position Transducer

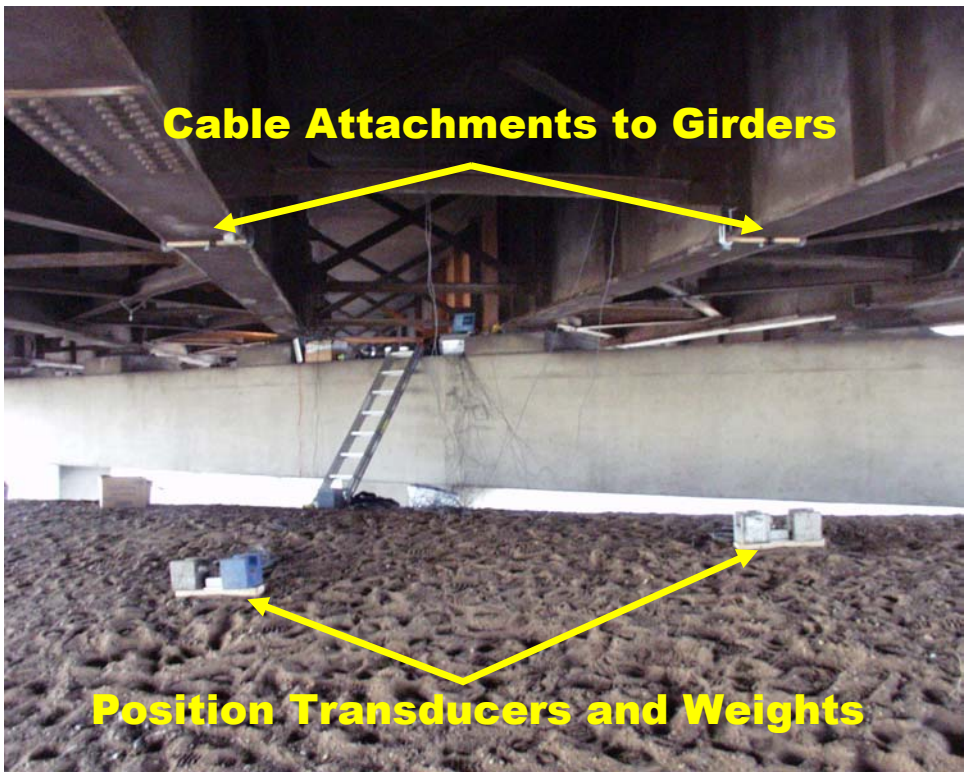

Figure 3.7 Position Transducer Placed in Field at Diaphragm Locations

3.4 Instrumentation

Strain gages were placed at several locations on the selected bridges so that the strains associated with (1) distortional stresses in the girder web, and (2) bending stresses in the girder flanges could be monitored. The locations at which strain gages were placed on each bridge are shown in Figure 3.8 and Figure 3.9.

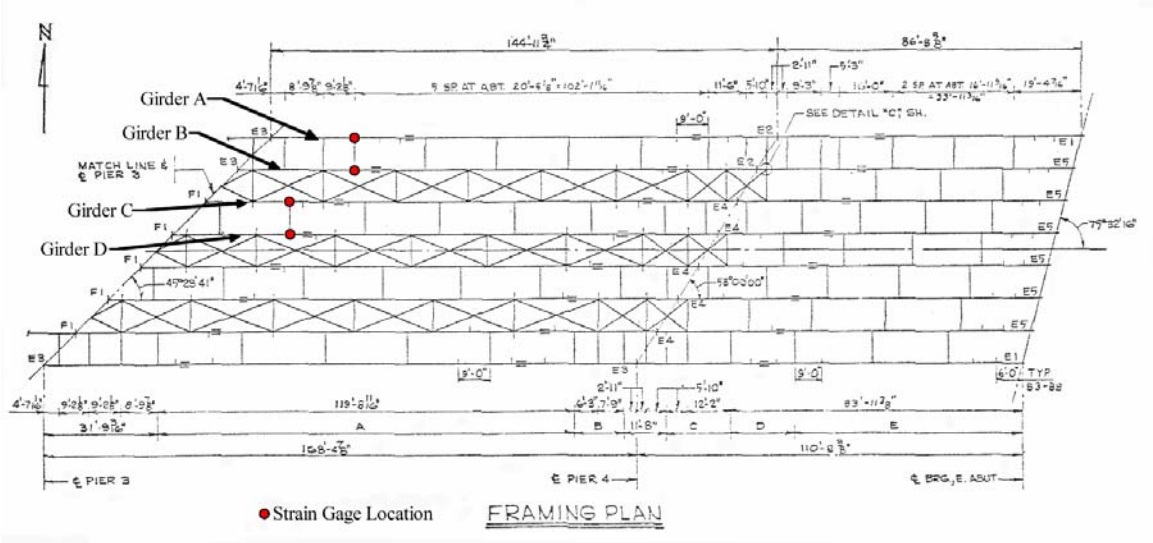

Figure 3.8 Plymouth Avenue Bridge Strain Gage Locations

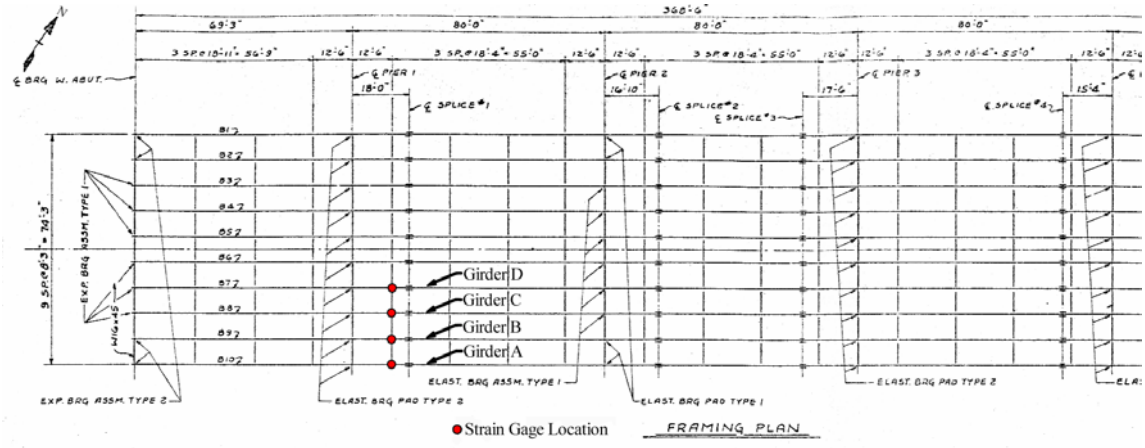

Figure 3.9 7th Street Bridge Strain Gage Locations

At each strain gage location shown in Figure 3.8 and Figure 3.9, several individual strain gages were placed. One strain gage was placed on the bottom of the girder flange and four or five strain gages were placed on the web of the girder. See Figure 3.10 for a detailed description of the strain gage placement on the bridge girder. Five strain gages were placed on the girder web at those locations where a diaphragm was located only on one side of the web, whereas those girders with back-to-back diaphragms had only four strain gages placed on the web.

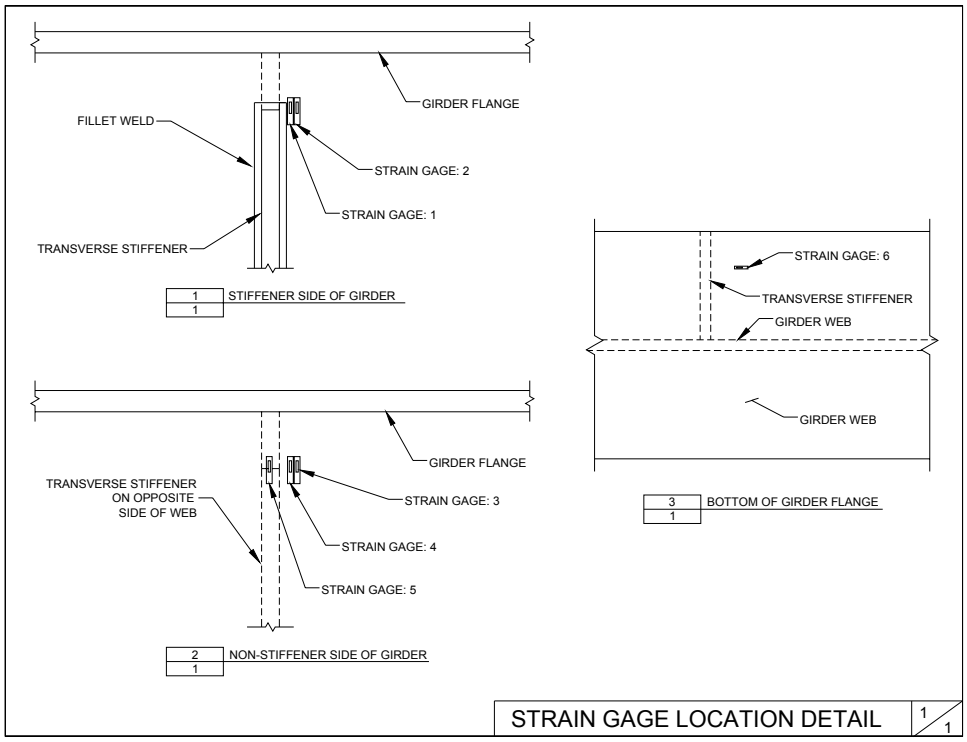

Figure 3.10 Individual Strain Gage Placement at an Instrumentation Location

Chapter 4-*Truck Testing*

4.1 Overview

The testing of the bridges with loaded trucks allows the researchers to monitor the response of the selected bridges to known loads. These known loads can then be correlated with the recorded stress ranges and can then be compared with the predictions made using the methods developed in previous research.

4.2 Procedure

Truck testing took place for several hours during morning and afternoon sessions over several days. Two Mn/DOT sand trucks, loaded to a total weight of 50 kips were used during each day of testing. The trucks made several passes over the bridges in a side-by-side configuration, as well as singly, in both the right and left lanes, over the instrumented portions of each bridge. The trucks traveled at a speed of approximately 30 miles per hour in conjunction with normal bridge traffic during testing.

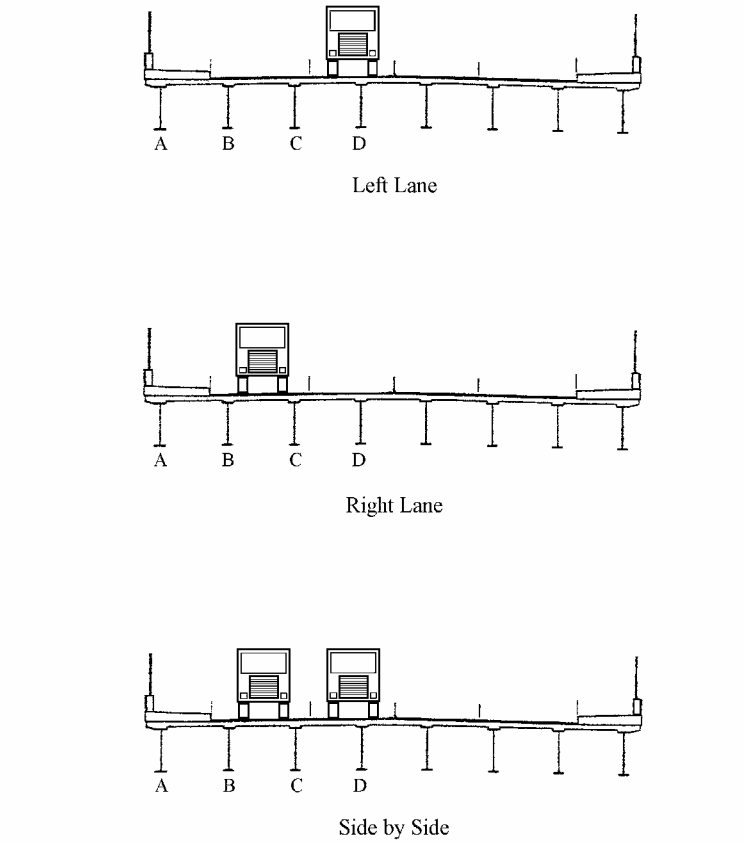

Figure 4.1 Truck Lane Configurations

The Campbell PC9000 was used to collect data continuously during testing. The time at which the Mn/DOT sand trucks passed over the instrumented section of the bridge was also recorded. An example of the strain gage data recorded during a truck pass is shown in Figure 4.2. The relative maximum and minimum values for each gage occur as the truck passes over the instrumented span. Although the data recorded is dynamic in nature it, the fatigue resistance of a bridge is determined using only the relative maximum and minimum values of stress experienced. The methodology used in the analysis of the data collected during truck testing is described in section 6.2.

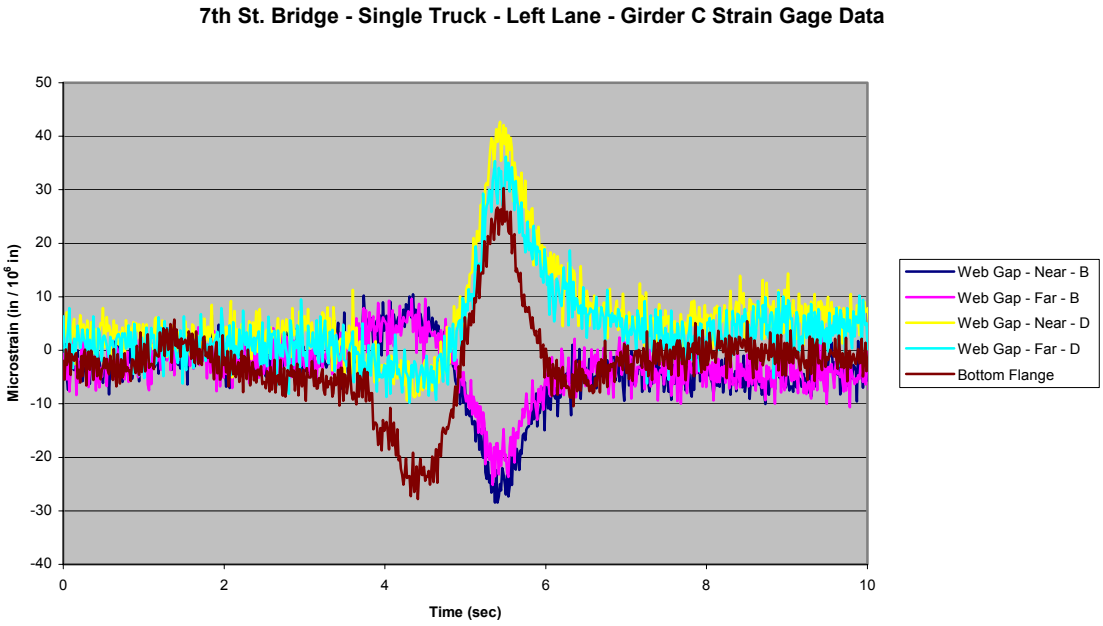

Figure 4.2 Truck Testing Strain Gage Data Example

Chapter 5-*Long-Term Monitoring*

5.1 Overview

In order to determine the strains caused by normal traffic loading, a long-term monitoring study was conducted for both bridges. This study also allowed for verification of the truck testing results.

5.2 Data Recorded

Given the large amount of data generated by continuous monitoring of strain gages, it was necessary to reduce the amount of data that was actually recorded by the field computer to a manageable amount. Due to the dynamic nature of the events of interest, it was found sufficient to record only the number and magnitudes of strain cycles experienced by the strain gages. This task is accomplished by using so-called data modes available in the Somat software which operates the eDAQ field computer. The "rainflow data" mode allows the user to record only the number and magnitude of strain cycles seen in continuous data. The burst history data mode allows the user to record continuous data for a specified period of time. A variety of triggering conditions for the recording of a burst history are available, such as when a strain value exceeds a specified amount, or if some mathematical combination of several channels meets a certain value. Given the limitations of the eDAQ field computer, it was only possible to record rainflow data from eight strain gages at one time.

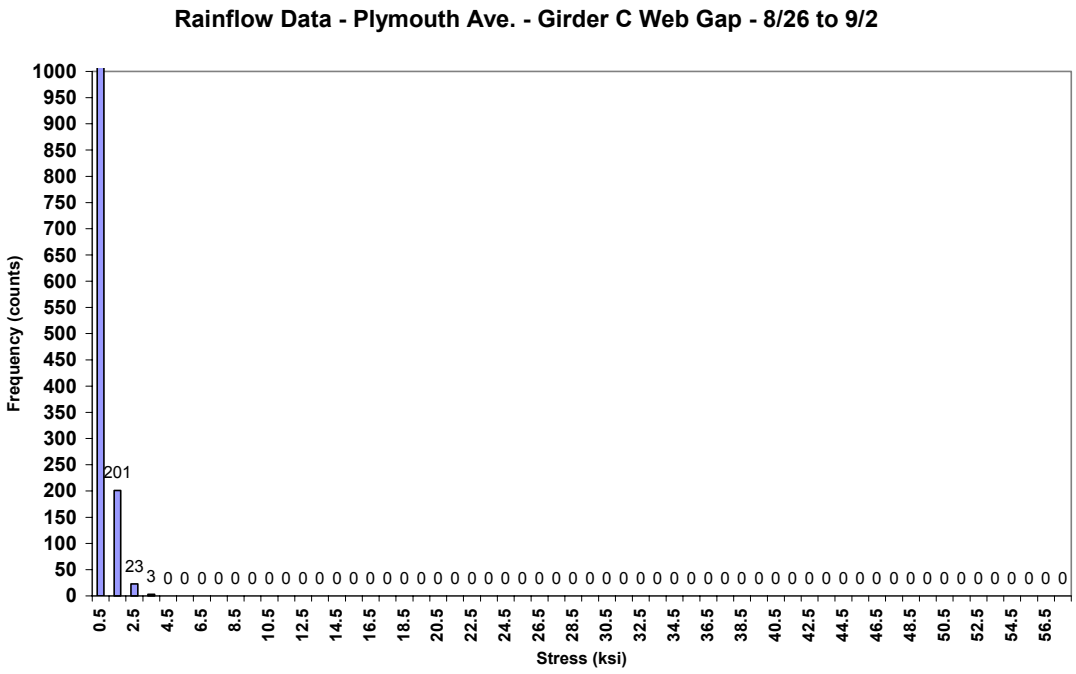

Figure 5.1 Rainflow Data Example

The burst history data mode was used to record time histories of sufficient length to capture the complete response of large trucks passing over the bridge. It would be ideal to record a burst history when the change in strain exceeded a certain value. Due to the drift experienced in the zero value of gages over time, it was determined that using a specific strain value as a triggering condition would not yield consistent results. During distortional fatigue events, one side of the girder web is placed in tension, with the opposite in compression, thus the triggering condition was set such that burst histories were recorded when the difference in strain measured by gages on opposite sides of the web exceeded an absolute maximum value. This value was set at approximately 100 microstrain, but it was adjusted throughout the monitoring process to reduce or increase the number of burst histories recorded, as memory space allowed. Due to the memory limitations of the eDAQ, and the data intensive nature of time history data, burst histories were recorded only to verify that the instrumentation was working properly. Long-term monitoring data sets were recorded for one week time periods due to the memory and

power requirements of the eDAQ field computer, as well as to allow a consistent time period for later comparison.

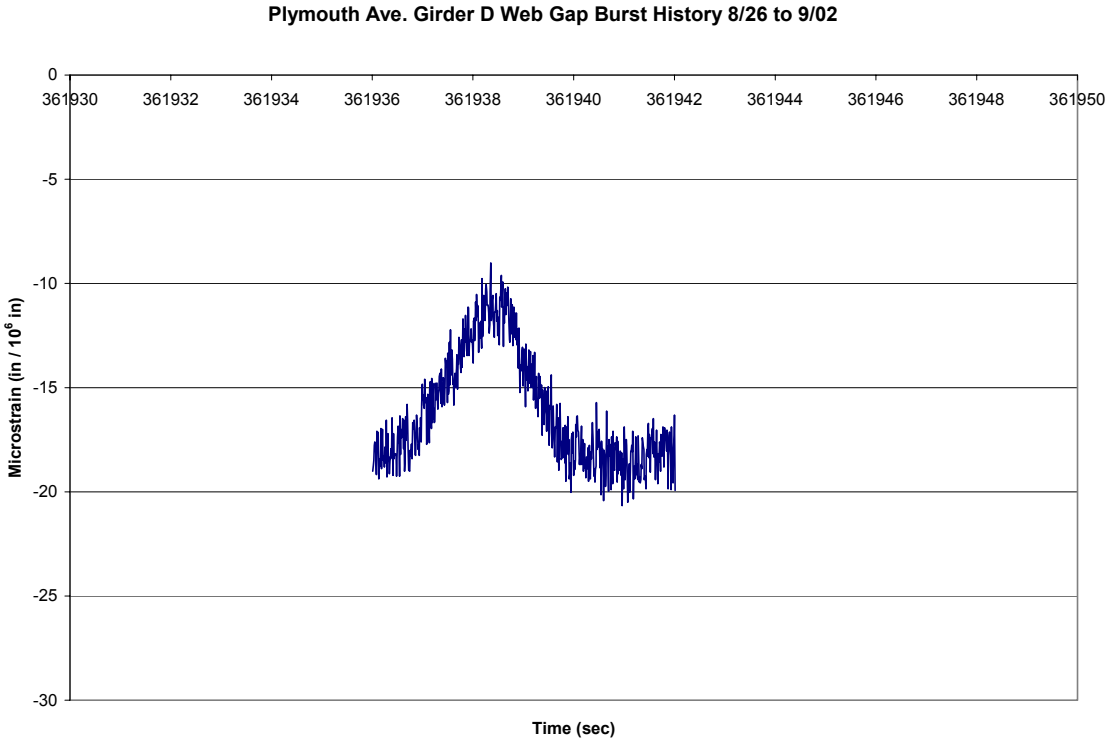

Figure 5.2 Burst History Data Example

Figure 5.1 provides an example of rainflow data collected from a strain gage on the Plymouth Ave. Bridge over a one-week time period. A data set such as this was recorded once a week for each monitored gage. Figure 5.2 shows an example of a burst history collected for a strain gage placed on the Plymouth Ave. Bridge. As mentioned earlier, the burst history data was only used to provide verification that the instruments and eDAQ field computer were functioning properly. Analysis of the long term monitoring data collected is provided in section 6.3.

Chapter 6-*Data Analysis*

6.1 Overview

Large quantities of data were collected during truck testing and long-term monitoring. This data was manipulated and filtered to provide meaningful information about the distortional fatigue behavior of the two bridges. The important findings of the data analysis process are presented here.

6.2 Truck Testing

The Campbell PC9000 was used to record data continuously throughout the truck load testing of both bridges. This procedure generated a large amount of time history data. To provide useable information, this data was manipulated in the manner described below. Given that the trucks were traveling at speeds of approximately 30 mph, it took them roughly three seconds to pass over the instrumented span. Using the time at which the truck passed over the instrumented location, time segments of approximately thirty seconds in length surrounding the truck pass were extracted from the continuous data. Given that it was unlikely for a given instrument to be at its zero value, the data for each instrument was adjusted to a new average zero value based upon several seconds of undisturbed data prior to the truck passing.

An average maximum or minimum value was calculated for each instrument by averaging the data over a period of 0.075 seconds centered about the absolute maximum or minimum value for each truck pass. This averaging was performed to limit the influence of ambient signal noise on the data. It was found that the average maximum or minimum value calculated for each instrument was fairly consistent for all of the truck passes. Nevertheless, the average maximum and minimum values for each instrument were averaged over all of the truck passes of the same type (i.e. left lane, right lane and side-by-side) to mitigate any influence from other traffic on the bridge, and it is these values that are presented in this report.

For comparison, the values predicted by the Berglund (Equation 2.3), Fisher (Equation 2.1) and Jajich (Equation 2.2) formulas are given. From the finite element modeling performed by Jajich, it is known that the peak web gap stress occurs near the center of the stiffener [1]. Since it is impossible to place strain gages in this location, a linear extrapolation was performed using the data from adjacent web gap gages. It was also found by this finite element modeling that the web gap stress decays rapidly as one moves away from the centerline of the stiffener. Thus, one could expect that the peak web gap stress generated by a finite element model of the web gap or any prediction equation to give significantly higher results than those found through a linear extrapolation of adjacent strain gages (Figure 6.1). The values found for the right and left lane truck passes are presented here with the data from the side-by-side truck passes omitted for clarity. For a more thorough presentation of data collected from all of the instruments used during the truck testing see Appendix A.

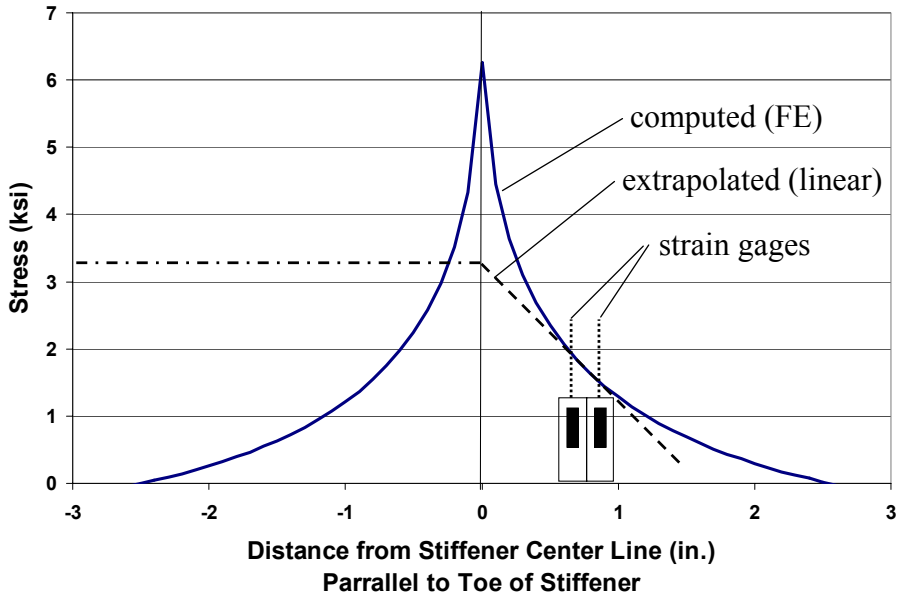

Figure 6.1 Comparison of Computed and Extrapolated Stresses.

6.2.1 Plymouth Ave. Bridge

The following tables present the important information found from the truck testing of the Plymouth Ave. Bridge.

Table 6.1 Comparison of Differential Deflection Data – Plymouth Ave.

Lane Loading	Diaphragm	Measured Differential Deflection (in)	Predicted Differential Deflection - Berglund (in)
Left	A-B	0.0372	0.0642
Left	C-D	0.0244	0.0642
Right	A-B	0.0365	0.0642
Right	C-D	0.0014	0.0642

Table 6.2 Comparison of Web Gap Stress Data and Predictions – Plymouth Ave.

Lane Loading	Diaphragm	Measured Web Gap Stress (ksi)	Extrapolated Web-Gap Stress (ksi)	Predicted Web Gap Stress - Fisher (ksi)	Predicted Web Gap Stress - Jajich (ksi)
Left	A-B	0.21	0.28	165.17	4.13
Left	C-D	1.47	1.60	97.56	2.71
Right	A-B	0.30	0.41	161.84	4.05
Right	C-D	0.47	1.20	5.65	0.16

From Table 6. it can be seen that the diaphragm differential deflection equation proposed by Berglund overestimates the measured differential deflection in this case. One should recall that the method for predicting differential deflection developed by Berglund gives the maximum differential deflection for an entire bridge. Berglund also found that the maximum stress tends to occur in the longest span of a bridge. Due to practical limitations, it was not possible to instrument in this location, and, thus, the maximum diaphragm differential deflection of this bridge probably might not have been recorded.

Comparing the measured stresses with those predicted by Fisher and Jajich it can be observed that the Jajich equation does provide more accurate results. However, it predicts a hot spot stress that is larger than the measured and extrapolated web gap stresses. It is expected that the Jajich equation will produce larger values due to the nature of the stress field around the peak web gap stress as described earlier. Also, given the extremely large

stresses predicted by the Fisher equation, it is unlikely that these values are an accurate representation of the peak web gap stresses occurring in the bridge.

6.2.2 7th St. Bridge

The significant findings from the analysis of the data collected during the truck testing of the 7th St. Bridge are displayed in the following tables.

Table 6.3 Comparison of Differential Deflection Data – 7th St.

Lane Loading	Diaphragm	Measured Differential Deflection (in)	Predicted Differential Deflection - Berglund (in)
Left	A-B	0.0264	0.0600
Left	B-C	0.0146	0.0600
Left	C-D	0.0039	0.0600
Right	A-B	0.0284	0.0600
Right	B-C	0.0016	0.0600
Right	C-D	0.0220	0.0600

Table 6.4 Comparison of Web Gap Stress Data and Predictions – 7th St.

Lane Loading	Diaphragm	Measured Web Gap Stress (ksi)	Extrapolated Web-Gap Stress (ksi)	Predicted Web Gap Stress - Fisher (ksi)	Predicted Web Gap Stress - Jajich (ksi)
Left	A-B	0.40	0.53	9.86	4.69
Left	B-C	0.54	0.64	5.47	2.60
Left	C-D	0.94	1.05	1.48	0.70
Right	A-B	0.73	0.99	10.61	5.05
Right	B-C	0.99	1.14	0.61	0.29
Right	C-D	1.13	1.52	8.21	3.91

Comparing the measured differential deflections in Table 6., with those predicted by Berglund one can see that the amount of differential deflection is also overestimated in this bridge. The overestimation occurs for several reasons, one reason being that square bridges tend to experience smaller amounts of differential deflection than skewed bridges. This difference comes about because of the differing lengths to the support from the applied loads for adjacent girders in skewed bridges. Another reason for the overestimation is that the Berglund method was developed for skew supported bridges, and was never intended for square bridges, like the 7th St. Bridge.

Examining the stresses measured in the 7th St. Bridge with those predicted by the Fisher and Jajich equations, one observes that neither method predicts the measured or extrapolated web gap stresses well. This may in part be caused by the inability of the measured or extrapolated stresses to capture the peak web gap stress based upon the locations at which stress measurements can be taken and the rapidly changing nature of the stress field away from the peak stress. The applicability of the Jajich equation to the 7th St. bridge can also be brought into question because it was developed using data collected from a bridge with staggered diaphragms. Recall that Jajich's research found the web gap stresses to be generated by a rotation of the diaphragm about the toe of the transverse stiffener. The rotation would be restrained by the back-to-back diaphragms, and thus the primary cause of web gap stresses would be minimized in the 7th St. Bridge, and, it would thus be expected that lower web gap stresses would occur.

6.3 Long-Term Monitoring

Long-term monitoring was conducted to provide further insight into the distortional fatigue response of the Plymouth Ave. and 7th St. bridges. Data sets were recorded for one-week intervals due to the memory and power requirement of the eDAQ field computer as well as to allow for a consistent time frame for future comparison. Given that the length of long-term monitoring was not the same for all gage configurations monitored, rainflow data will be reported as the average number of counts recorded for a one-week period.

It is noted that for certain weeks individual strain gages may have been deemed non-functional. This determination was based upon comparison of data between subsequent weeks as well as expected rainflow patterns. Gages determined to be non-functional recorded counts of an extremely large number at low strains or counts at unbelievably high strain values, and commonly the two cases would occur simultaneously. It is believed that these abnormal counts are the result of spikes in electrical signal that were not produced by strains in the base metal. These spikes could be of any value of strain and occur over a very short time frame, often only a single data point. Time history data was recorded during the truck testing of the 7th St. Bridge that

contained similar spikes. Although the origin of these disturbances is unknown, they exist and care should be taken when working with raw rainflow data.

6.3.1 Plymouth Ave. Bridge

Long-term monitoring data was collected for the Plymouth Avenue Bridge under two different configurations. The first configuration consisted of monitoring the back-to-back web gap strain gages on all of the girders, and this setup shall be referred to as the web gap configuration. The second configuration consisted of monitoring the back-to-back web gap strain gages on girders A and B, the bottom flange gages on girders A, B, and C as well as one web gap strain gage on girder C. This monitoring arrangement will be referred to as the A-B configuration. See Figure 3.8 for strain gage locations and girder labeling, as well as, Figure 3.10 for the placement of individual strain gages.

For clarity, the counts recorded for the lowest stress range, 0 to 1 ksi, have been omitted from the figures. Although one cannot make a direct correlation between number of stress cycles recorded during long-term monitoring and maximum stresses seen during truck testing, one can compare the relative difference in stresses experienced during truck testing. These differences in stress would be reflected in the long-term monitoring data by a comparatively greater number of stress cycles. Such a conclusion can be reached by assuming that the system remains elastic during loading, and thus any relative difference in stresses seen during the truck loading would be the same for other unknown loading cases occurring during long term monitoring.

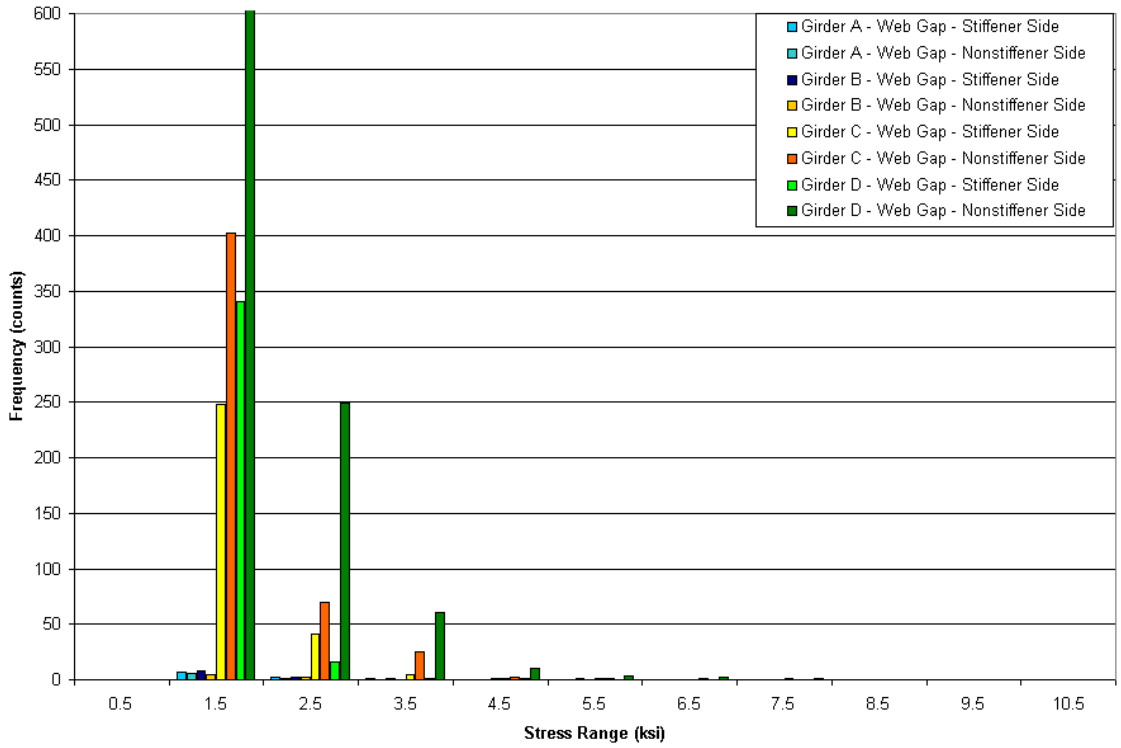

Figure 6.2 Plymouth Ave. Average Weekly Rainflow Data - Web Gap Configuration

Comparing the rainflow data taken using the web gap configuration (Figure 6.2) and truck test data (Table 6.2) one can see much agreement. Where higher web gap stresses were measured during truck testing, such as the web gap strain gages of girders C and D, higher counts, with respect to other gages, were also recorded during long-term monitoring. The larger number of counts recorded for gages placed on the non-stiffener side of the girder with respect to those placed on the side of the stiffener, such as for girders C and D, also correlate with higher stresses measured during truck testing.

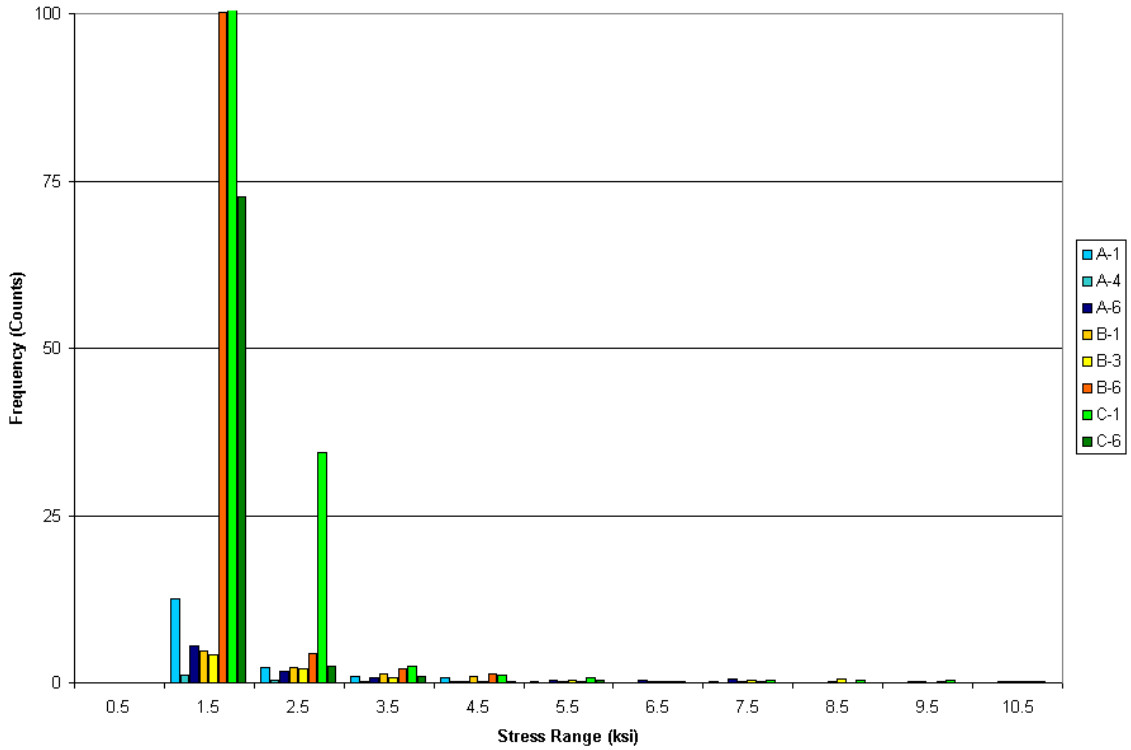

Figure 6.3 Plymouth Ave. Average Weekly Rainflow Data - A-B Configuration

Comparing the data recorded using the A-B configuration (Figure 6.3) with that recorded during truck testing (Table 6.4) one can also see agreement. Strains recorded for flange B during truck testing were much larger than web gap stresses on girders A and B as well as the flange stresses of girder A. This difference is reflected in the rainflow data by the greater number of stress cycles measured for the flange of girder B than the girder A and B web gap and girder A flange gages. Comparing the number of cycles recorded for the web gap and flange gages of girder C one sees a large discrepancy. This difference can be explained by the geometry on the bridge. When a truck drives in the left lane it is directly above girder D, and, therefore, its flange is most heavily stressed. But the diaphragm connecting girders C and D causes the web gap of girder C to see a high stress due to the differential deflection of the girders. This situation was confirmed by the truck test data.

6.3.2 7th St. Bridge

The long-term monitoring of the 7th St. Bridge was also conducted using two different strain gage configurations. The first configuration consisted of monitoring the back-to-

back web gap gages for girders C and D, the flange gages of girders B, C, and D, as well a web gap gage for girder B. This monitoring configuration is referred to as the C-D configuration. Similarly, the second configuration consisted of monitoring the back-to-back web gap gages for girders A and B, the flange gages for girders A, B and C, as well as a single web gap gage on girder C. This configuration is referred to as the A-B configuration. Refer to Figure 3.9 for information regarding strain gages locations and girder labeling, and Figure 3.10 for individual strain gage placement.

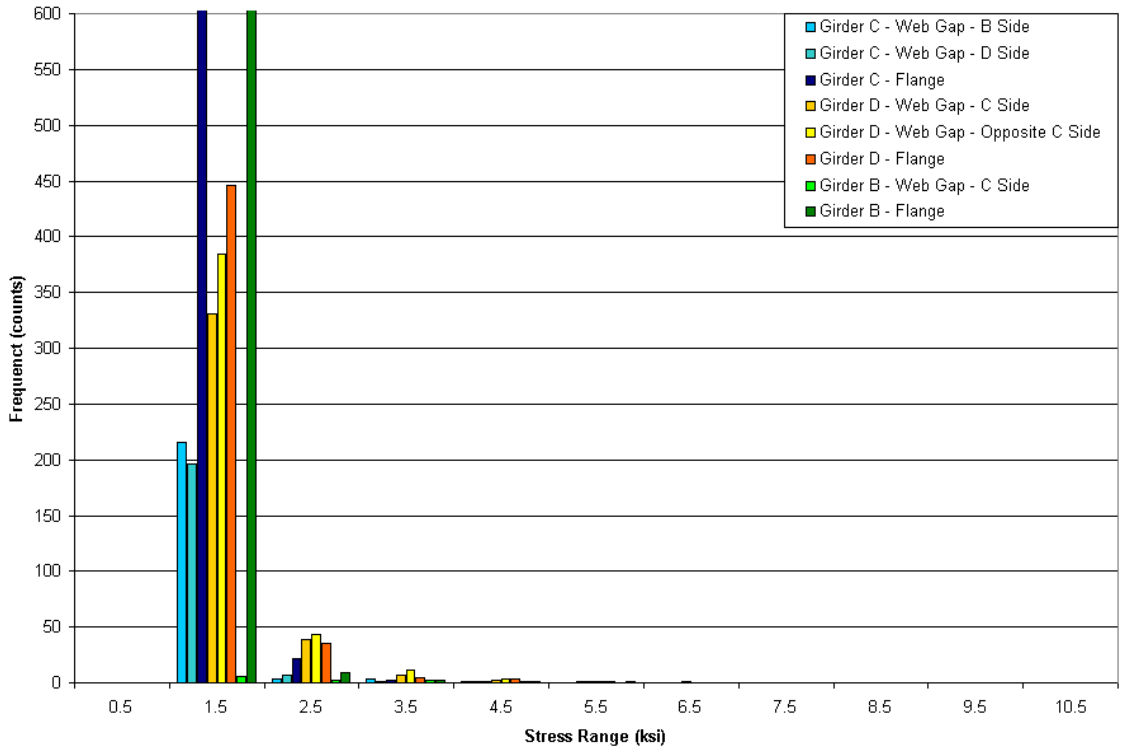

Figure 6.4 7th St. Average Weekly Rainflow Data - Girder C-D Configuration

Comparing the rainflow data collected under the C-D configuration with that taken during truck testing one can see many similarities. The counts for the web gap girder B gage are much lower than all the others, which is consistent with the truck testing data because that gage experienced significantly lower stresses than other gages. Also, one can observe that the gages on girder D had higher counts than other gages, this is consistent with the truck testing data when the truck passes in the right lane. The truck

testing data for the girder C gages shows that the flange will, on average, see higher stresses than the web gap, and this situation is reflected in the rainflow data by significantly higher counts for flange gage of girder C.

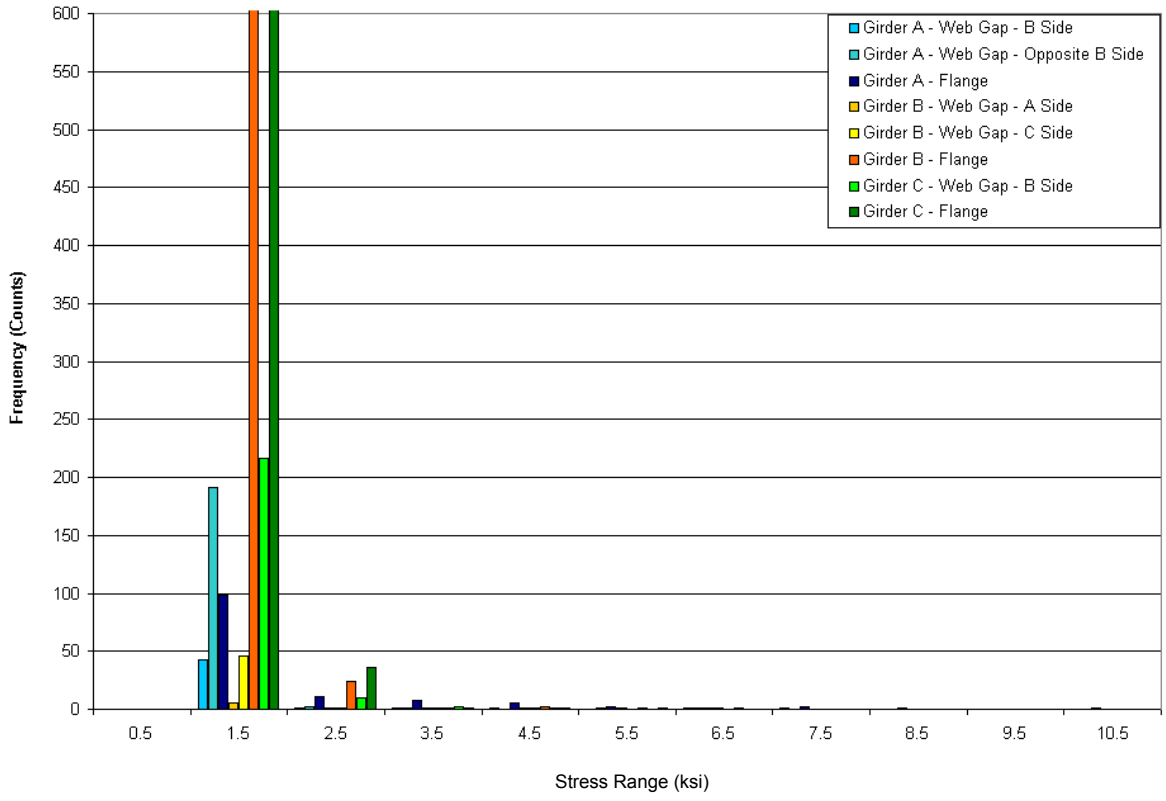

Figure 6.5 7th St. Average Weekly Rainflow Data - Girder A-B Configuration

Comparing the truck testing data with that taken under the A-B configuration one can see that the flange gages for girders B and C experienced similar number of stress cycles, this situation is consistent with the truck testing data where they both experienced similar levels of stress. Both of these gages also had many more counts than the other gages monitored, this also is reflected in the truck testing data by the much higher levels of stress experienced by these gages in comparison to the other strain gages.

The results of the long-term monitoring study reinforce the behavior of the bridges as determined during truck testing. The long-term monitoring data also shows that ambient traffic loading will produce higher stresses than those seen during truck testing. At the same time it should be noted that these higher stresses were not recorded with great frequency. Given that the traffic data for these bridges is not highly detailed it was not possible to correlate it with the number of counts recorded during the long term monitoring study.

Chapter 7-*Finite Element Diaphragm Modeling*

7.1 Overview

From the truck testing of the Plymouth Ave. Bridge it was observed that the Jajich equations, and more importantly the Fisher formula, do not accurately predict the measured or extrapolated peak web gap stresses. This result was expected, to a certain extent, due to the inability of these measuring schemes to capture the peak web gap stress. Thus, in order to determine the peak web gap stress experienced by the Plymouth Ave. Bridge, a finite element model was developed.

Another interesting aspect of the data taken during truck testing shows that the distance measured using an LVDT spanning from the transverse stiffener to the girder top flange decreased during truck loading. This observation suggests a mode of deformation different than that assumed by either the Fisher or Jajich model. Thus, to further investigate the distortional stress phenomenon, a finite element model of the X-braced diaphragm connecting girders C and D of the Plymouth Ave. Bridge (see Figure 3.8) was created. Diaphragm C-D of the Plymouth Ave. Bridge was selected for finite element modeling because it experienced the largest web gap stresses during truck testing.

7.2 Model Geometry

The computer program SAP2000 NonLinear [16] was chosen for the finite element diaphragm analysis of the Plymouth Ave. Bridge. The location of the modeled bridge segment, in reference to the entire structure, is shown in Figure 7.1. In order to limit the size of the model, only a small portion of the bridge could be represented, and locations at which to terminate the model, as well as the corresponding support conditions, needed to be determined.

The girder segments in the model were terminated at points where lateral bracing framed in from adjacent girders and, therefore, negligible lateral deflections could be assumed. At these locations a pin support was placed at the center of the bottom flange to restrain the lateral deflection. The portion of the concrete deck connecting the two girder segments was also modeled. The lateral deflection of the concrete deck was fixed along the edges parallel to the girders to represent the high stiffness of the portion of the deck not represented in the model. Furthermore, rotation of the concrete deck along the edge of the modeled region was constrained to that of the connected girder flange, but no additional restraint was assumed. This feature differs from the Jajich finite element model of the same region [1], in which the edge of the concrete deck at the boundary of the model, as well as the top flange of the connected girder, was restrained from rotation.

In addition to the full bridge cross-section, all components of the X-braced diaphragm were represented in the model. The dimensions and sizes of the bridge components were taken from bridge plans and field measurements. The concrete deck, steel girders, transverse stiffeners and gusset plates were modeled using shell elements. Frame elements were used to represent the angles in the X-braced diaphragm as well as various connecting elements that are discussed later. The entire finite element model of the diaphragm region is shown in Figure 7.2.

In order to accurately capture the stress field around the termination of the transverse stiffener, a 0.1 inch mesh was used to represent the vicinity of the web gap region. The scale of the mesh, as well as the configuration of the web gap in the model can be seen in Figure 7.3. To induce the out-of-plane distortion, the amount of differential deflection measured during truck testing, 0.0244 inches, was applied to the pin supports of girder D as a vertical deflection. The differential deflection of the bottom flanges at the diaphragm connection, where the field measurements were taken, was verified throughout the analyses and found to be very close to applied differential deflection.

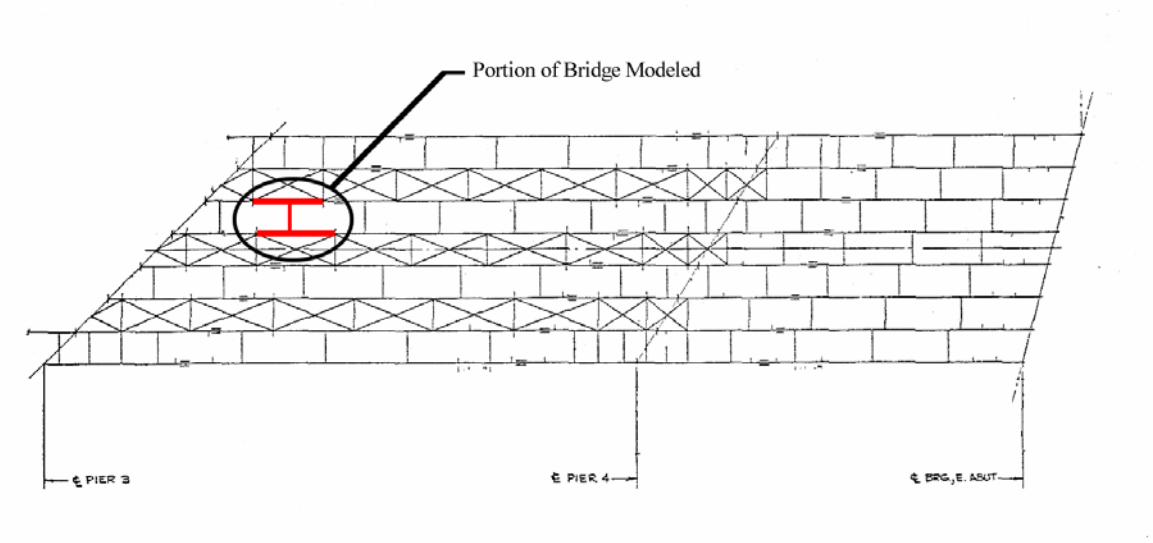

Figure 7.1 Location of Finite Element Model in Bridge

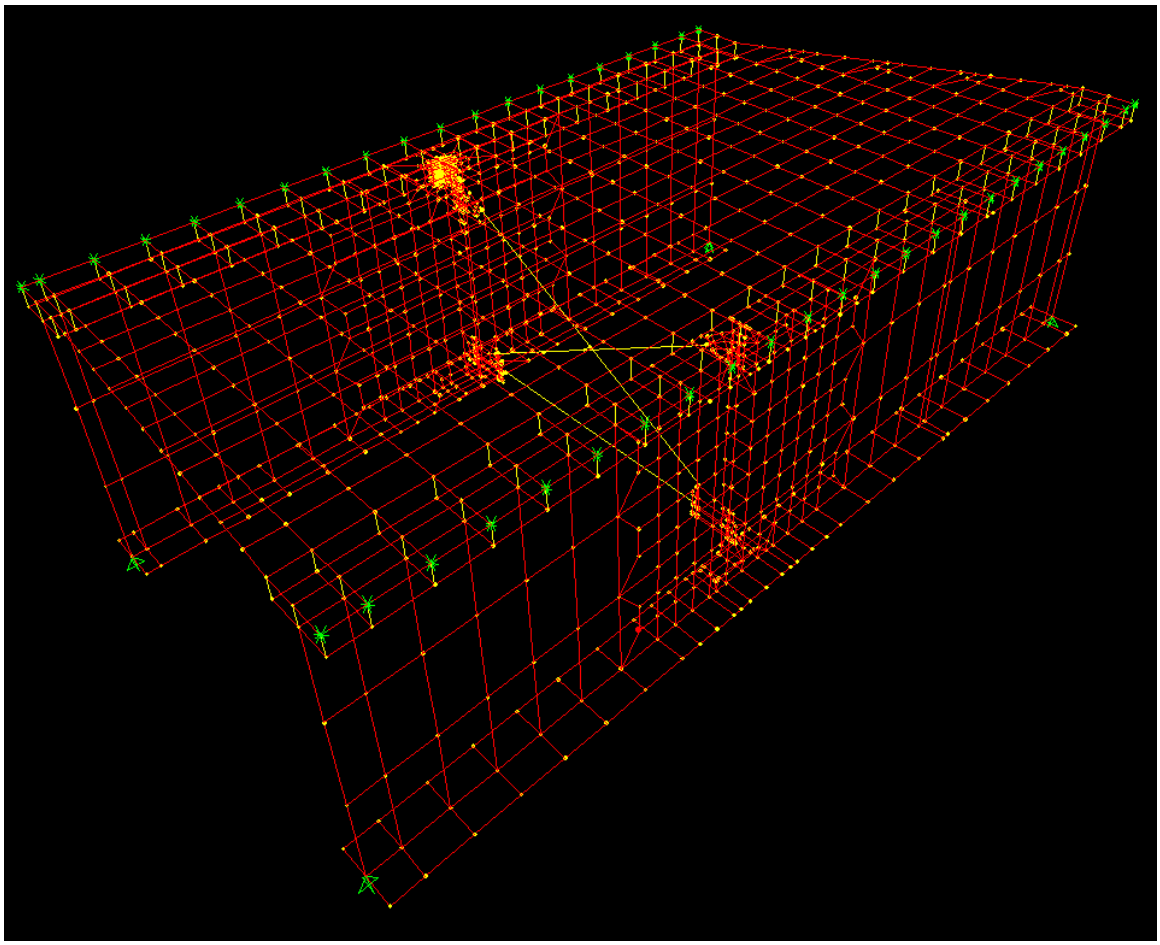

Figure 7.2 Finite Element Model of Diaphragm Connecting Girder C and D

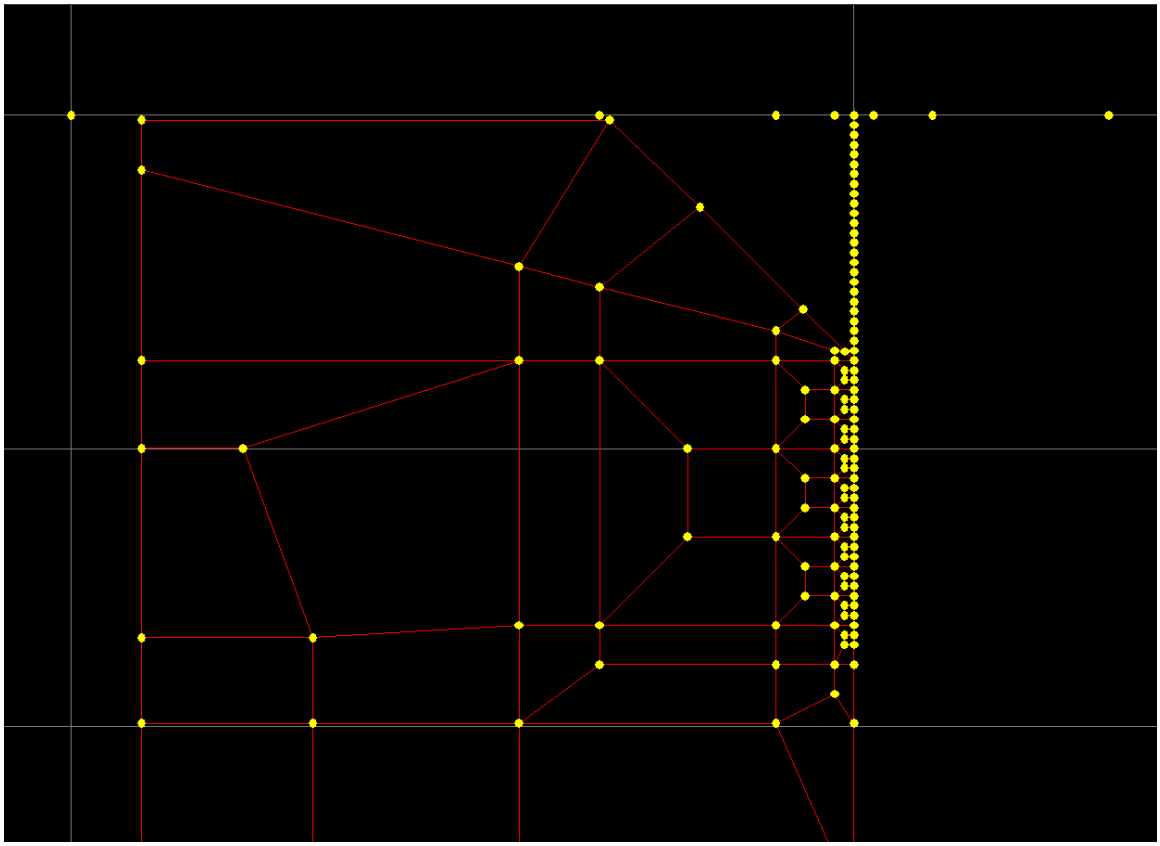

Figure 7.3 Cross Section of FE Model at Web Gap

7.3 Model Refinement

In order to ensure that the finite element model accurately represented the behavior of the actual structure, it was refined so as to match data taken during truck testing. After the properties of most model components had been determined from the bridge plans, the properties of two types of elements were left undetermined. The attributes of the frame elements connecting the concrete deck to top flange of the girders and the frame elements representing the bolts in the connection of the diaphragm gusset plates to the transverse web stiffener were selected as described below.

The frame elements connecting the concrete deck to the top flange of the girders were modeled such that their lateral stiffness matched the stiffness computed from the secant slope of the load-deflection equation for headed shear stud connections proposed by

Ollgaard, Slutter and Fisher [17]. In adjusting the model it was discovered that there exists an inverse relationship between this stiffness and the peak web gap stress given by the model. But, it was also noted the large changes in this stiffness did not cause significant changes to the calculated values of the peak web gap stress.

Having selected the properties of all other elements, only the properties of the frame elements representing the bolted connections used in the X-braced diaphragm remained undetermined. Given that the bolts are most likely placed in oversized holes and that their tightening would induce a frictional force between the diaphragm gusset plate and the transverse stiffener, the actual lateral stiffness of this connection is very difficult to determine. Fortunately, knowing all of the other attributes of the model, this value could be selected so as to match the stresses measured during truck testing. An increase in this stiffness was assumed to cause an increase in the peak web gap stress computed by the finite element model.

During the selection process, it was found that considerable changes in the stiffness of the X-brace bolted connection did not lead to significant changes in peak web gap stress. So as to accurately match the results of the finite element model with the strain gage data, the stresses in the areas covered by the strain gages were averaged to give a more accurate representation of what strain gages of finite dimensions would read were they placed in the model. By averaging over the area covered by a strain gage, the longitudinal and vertical variations in the stress field could be accurately accounted for. Thus, the finite element model was calibrated such that the stress measured by each web gap strain gage on girder C was predicted to within 10%.

7.4 Web Gap Deformation

Using the refined finite element model, the peak web gap stress and the mode of deformation of the web gap could be observed. The peak web gap stress in the finite element model was found to be 6.25 ksi. This value is much larger than the 1.47 and 1.36 ksi measured by strain gages in the field. This discrepancy occurs because the peak stress occurs at the centerline of the stiffener, where strain gages cannot be placed, and also

because the stress field decays rapidly in both the longitudinal and vertical directions away from this point, as can be seen in Figure 7.4. In fact, the Jajich formula (see Table 6.2) actually underestimates the 6.25-ksi calculated peak web gap stress at the centerline of the transverse stiffener.

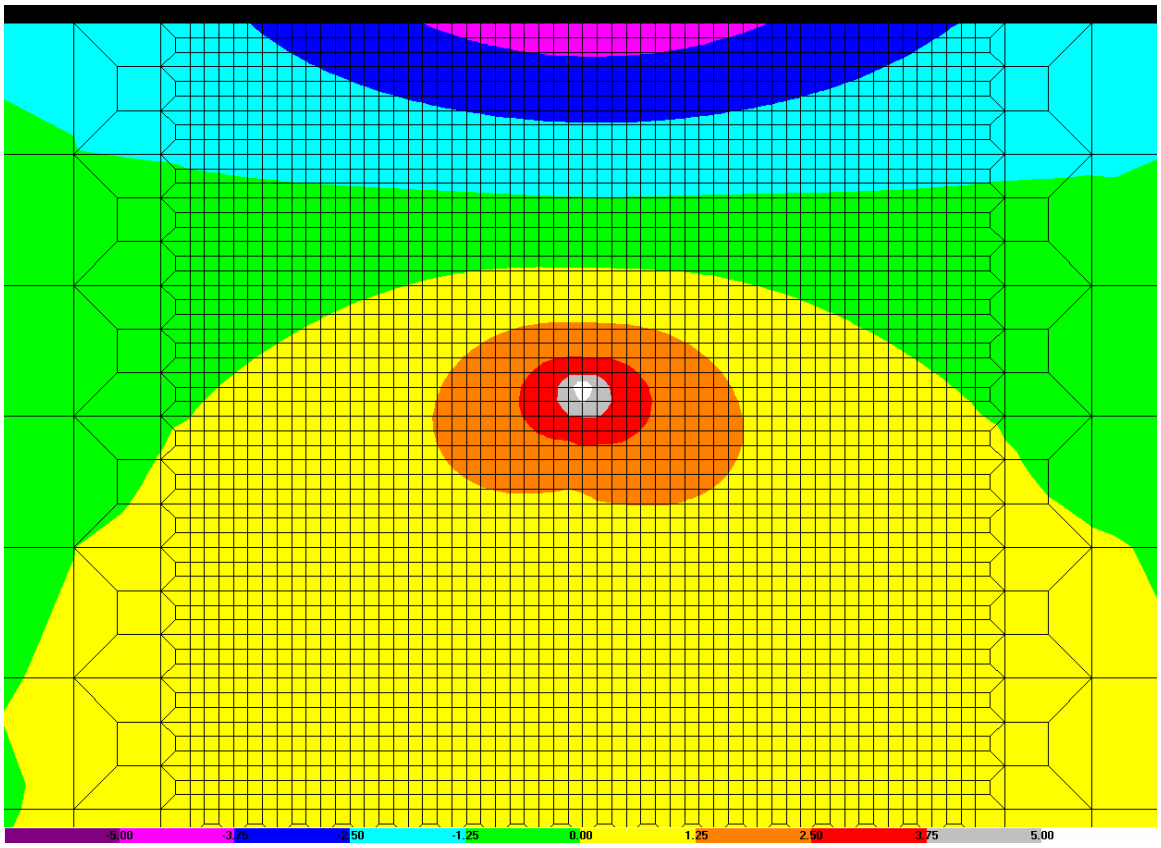

Figure 7.4 Web Stress in the Vertical Direction (ksi)

From the finite element model it was also found that, as noted by Jajich [1], the web undergoes very little lateral deflection. Thus, the web gap stress is primarily generated by the rotations of the top flange and the transverse stiffener. This situation can be observed in deformed shape of the web gap shown at a magnification of 500 times in Figure 7.5.

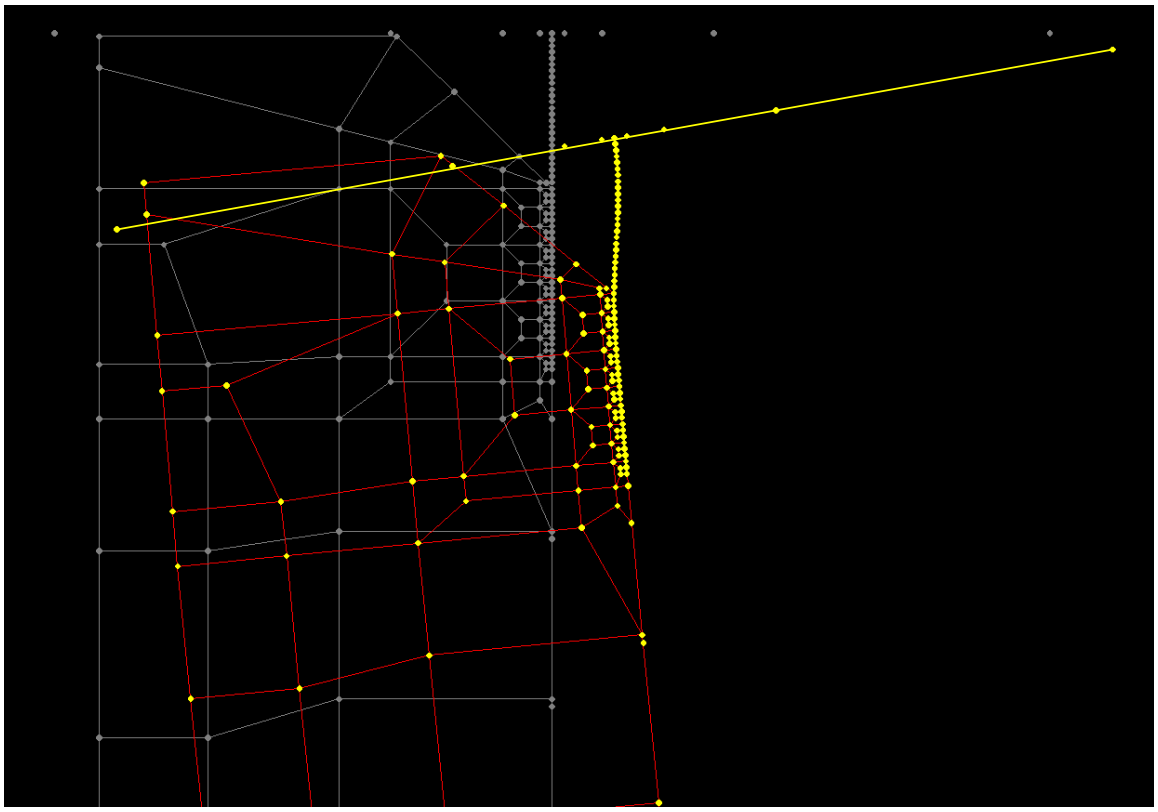

Figure 7.5 Deformed Shape of Web Gap Region Looking Parallel to the Web

In Figure 7.5, the top flange of a connected girder is seen to undergo a rigid body rotation such that the relative distance between the top of the stiffener plate and the top flange decreases. This mode of deformation is confirmed by the LVDT measurements recorded during truck testing, as shown in

Table 7.1. It is important to note that this movement is associated with rotation of the top and bottom of the web gap, and not with transverse (lateral) deflection. The observation of this phenomenon dictates a mode of deformation different from the one proposed by Fisher [8] and slightly different from the one proposed by Jajich [1]. The deformation illustrated in Figure 7.5 also explains the reason why their stress prediction equations did not hold for this bridge.

Table 7.1 Comparison of Model and Field Stiffener-Girder Relative Displacements

LVDT Measurement	Displacement, Field (in.)	Displacement, Model (in.)
Vertical	-0.00251	-0.00120
Horizontal	0.00147	0.00055

Although the finite element model constructed was able to reproduce the measured behavior of the actual bridge, several attributes of the model were approximate representations of the real structure that could be improved upon. The applied deflection of the girder segments did accurately represent the vertical differential deflection measured during truck testing. But, in addition to undergoing a vertical deflection the girders would have also experienced a certain amount of curvature. The amount of curvature experienced by the girders was unknown from field measurements and thus was not incorporated into the model. The pin supports used in the model did allow the lower flanges to undergo rotation. Whether or not the rotations that occurred in the model were representative of those that took place in the real structure is unknown, and thus the impact of this limitation of the model is unknown.

The lateral restraint of the concrete deck was chosen to represent the high axial stiffness of the portion of the deck not represented in the model. What was not represented in the model was the rotational stiffness that this unrepresented portion of the deck would have also provided. Given that a major component of the web gap stress is generated by the rotation of the top flange, any reduction in this rotation would cause a reduction in the web gap stress. The effect of these limitations could be determined through further study if the necessary values were found from a model of the entire bridge and then applied to the local model used in this research.

The model constructed also has its limitations with regards to the representation of the connection between the transverse stiffener and the girder web. The transverse stiffener was modeled using planar shell elements placed at the center line of the stiffener in the

real structure. These elements were rigidly connected to the girder web to simulate the welded connection used in the actual system. The main limitation of this modeling technique is that in the physical system the stiffener plate has real thickness, and is joined to the web by fillet welds along its edges.

There is little doubt that changing the model to more accurately represent the physical system would lead to changes in the web gap stress field. However, it is unknown what effect such an effort would have on the peak web gap stress. Given that the web gap stress is generated by a deformation of the web, it is unlikely that changing the location, but not the magnitude, of this deformation would significantly impact the peak value of web gap stress.

7.5 Parameter Study

A parameter study was performed to further investigate the distortional stress phenomenon for X-brace diaphragms because the current web gap stress prediction models did not hold for the case of the Plymouth Ave. Bridge. The web gap size, girder spacing, web thickness and the applied differential deflection of the finite element model were independently varied and the response of the model was monitored. The values of the parameters that were varied and the corresponding responses of the finite element model are listed in Table 7.2. The highlighted line in each group of parameters corresponds to the finite element model of the diaphragm that was calibrated with the field data, and the other lines correspond to variations of that model.

The range of values for web thickness and girder spacing were selected based upon the ranges of these parameters found in the Mn/DOT bridge inventory analyzed by Berglund [2]. The web gap lengths were selected to represent the range of values found in the Mn/DOT bridge inventory as well as the reports by other researchers [2, 6, 7]. The amount of applied differential deflection was varied between one-half and twice the amount measured during truck testing in order to simulate a variety of loading conditions. The following notation is used throughout the rest of this report, web gap length (g), diaphragm differential deflection (Δ), lateral deflection of stiffener toe with respect to the

top flange (δ), girder spacing (S), web thickness (t_w), rotation of the top of the web gap (θ_t), rotation of the bottom of the web gap (θ_b), and the peak web gap stress (σ_{wg}).

Table 7.2 Parameters Studied and FE Model Results

Parameter Changed	Value (in.)	σ_{wg} (ksi)	θ_t (rad.)	θ_b (rad.)	δ (in.)
g	1.7	4.08	0.000365	0.000176	-0.000133
g	2.0	5.13	0.000363	0.000178	-0.000091
g	2.3	5.93	0.000362	0.000180	-0.000034
g	2.5	6.25	0.000361	0.000182	0.000015
g	2.7	6.53	0.000360	0.000184	0.000064
g	3.0	7.24	0.000359	0.000187	0.000147
g	3.3	7.63	0.000358	0.000191	0.000239
S	100	6.60	0.000335	0.000216	0.000024
S	112	6.25	0.000361	0.000182	0.000015
S	124	5.98	0.000403	0.000151	-0.000003
t_w	0.4375	12.62	0.000366	0.000181	0.000669
t_w	0.5625	6.25	0.000361	0.000182	0.000015
t_w	0.6875	3.15	0.000355	0.000187	-0.000290
Δ	0.012	4.21	0.000262	0.000084	0.000053
Δ	0.020	5.53	0.000326	0.000147	0.000029
Δ	0.022	5.85	0.000342	0.000163	0.000023
Δ	0.0244	6.25	0.000361	0.000182	0.000015
Δ	0.027	6.68	0.000381	0.000203	0.000007
Δ	0.029	7.01	0.000397	0.000218	0.000001
Δ	0.049	10.31	0.000556	0.000376	-0.000060

From the results of the parameter study shown in Table 7.2 it can be seen that all of the parameters have an impact on the magnitude of web gap stress. However, web thickness, t_w, has the largest influence on web gap stress, while girder spacing, S, has the least effect. It also can be noted that the values of both rotations and the lateral deflection of the web gap are affected by the variation of these parameters as well. This leads to the conclusion that the distortion of the web gap region is a complex problem and care must be taken in its analysis.

Chapter 8-*Stress Prediction Model*

8.1 Overview

The results of the parameter study demonstrated that the mode of out-of-plane distortion of the web gaps in the Plymouth Ave. Bridge is more complex than was assumed in previous research [1, 8], and that it is influenced by several of the geometrical properties of the system. In order to aid in the evaluation of bridges containing similar geometries, an effort was made to modify the simple equation developed by Jajich [1] for the prediction of peak web gap stress produced by the out-of-plane distortion of the web caused by the differential deflection of bridge girders.

8.2 Equation Derivation and Justification

Jajich idealized the web gap to be a fixed-fixed isotropic beam, thus allowing the use of the slope deflection equation as a representation of this system [1]. However, in the present case, no assumptions are made a priori regarding the magnitudes of the two end rotations and lateral displacement of the web gap. Thus, assuming a prismatic section, the web gap stress at the toe of the stiffener can be expressed in terms of the rotations and relative deflection of both ends of the web gap, as shown in Equation 8.1.

$$\sigma_{wg} = \frac{E \cdot t_w}{g}(2\theta_b + \theta_t + 3\frac{\delta}{g}) \qquad \textbf{Equation 8.1}$$

Jajich assumed that the rotation of the web gap at the flange connection and the relative lateral deflection (i.e., $\theta_t \approx \delta \approx 0$) vanish, and that the rotation of the web gap at the toe of the stiffener is equal to the assumed rigid body rotation of the diaphragm (i.e., $\theta_b \approx \Delta/S$) in order to obtain Equation 2.2 from Equation 8.1.

In general, it would be very difficult to determine θ_b, θ_t and δ for a diaphragm in a specific bridge without extensive field monitoring, so these values must be determined in another manner. Table 8.1 lists the results from the finite element study that was reported

previously in Table 7.2. However, in Table 8.1, the end rotations of the web gap, θ_b and θ_t, and the relative deflection, δ, are normalized by Δ/S to see the influence of diaphragm rotation on web gap stress.

Table 8.1 Parameter Study Results Normalized by Δ/S

Parameter Changed	Value (in)	σ_{wg} (ksi)	$\theta_t / (\Delta/S)$	$\theta_b / (\Delta/S)$	$(\delta/g) / (\Delta/S)$	Δ/S
g	1.7	4.08	1.63	0.79	-0.35	0.000224
g	2	5.13	1.62	0.79	-0.20	0.000224
g	2.3	5.93	1.62	0.81	-0.07	0.000224
g	2.5	6.25	1.61	0.81	0.03	0.000224
g	2.7	6.53	1.61	0.82	0.11	0.000224
g	3	7.24	1.60	0.84	0.22	0.000224
g	3.3	7.63	1.60	0.85	0.32	0.000224
S	100	6.6	1.34	0.87	0.04	0.000249
S	112	6.25	1.61	0.81	0.03	0.000224
S	124	5.98	1.98	0.74	-0.01	0.000203
t_w	0.4375	12.62	1.65	0.82	1.21	0.000221
t_w	0.5625	6.25	1.61	0.81	0.03	0.000224
t_w	0.6875	3.15	1.58	0.83	-0.51	0.000226
Δ	0.012	4.21	2.29	0.73	0.19	0.000115
Δ	0.02	5.53	1.76	0.80	0.06	0.000185
Δ	0.022	5.85	1.69	0.81	0.04	0.000203
Δ	0.024435	6.25	1.61	0.81	0.03	0.000224
Δ	0.027	6.68	1.55	0.82	0.01	0.000247
Δ	0.029	7.01	1.50	0.83	0.00	0.000264
Δ	0.049	10.31	1.26	0.86	-0.05	0.000440

The values for Δ/S in Table 8.1 were also taken from the finite element parameter study results that were previously reported in Table 7.2. Fairly consistent results are observed relating θ_b and θ_t to diaphragm rotation (Δ/S), but a similar case cannot be made for lateral displacement (δ). Thus it is proposed that θ_b and θ_t be approximated using linear functions of Δ/S. The average values for these ratios obtained from the finite element parameter study are listed in Table 8.2, and constant values proposed as approximations for these ratios are also given in Table 8.2.

Table 8.2 Average and Proposed Ratios for θ_t and θ_b

Average Values		Proposed Ratios	
$\theta_t / (\Delta/S)$	$\theta_b / (\Delta/S)$	$\theta_t / (\Delta/S)$	$\theta_b / (\Delta/S)$
1.64	0.81	1.7	0.9

From Tables 7.2 and 8.1, it can also be observed that a nearly constant value of δ occurs when Δ and S are varied, and that the magnitude of δ is negligible in many cases. Using the proposed ratios (Table 8.2) in the general web gap stress formula (Equation 8.1), and making use of the lateral deflection computed using the finite element model, the web gap stress can then be predicted. The values of the stress prediction equation with and without taking δ into consideration (i.e., assuming δ = 0) are shown in Table 8.3. The values for web gap stress listed as 'Model' are the values calculated using finite element analysis, and the values listed as 'Prediction' were obtained using Equation 8.1. Two different values were computed using Equation 8.1, in which the finite element values for δ were either included (i.e., 'w/ δ') or neglected (i.e., 'w/o δ').

Table 8.3 Comparison of Prediction Equation With and Without δ

Parameter Changed	Value (in)	Model σ_{wg} (ksi)	Prediction w/δ σ_{wg} (ksi)	Prediction w/o δ σ_{wg} (ksi)
g	1.7	4.08	5.27	7.52
g	2	5.13	5.28	6.39
g	2.3	5.93	5.24	5.56
g	2.5	6.25	5.23	5.11
g	2.7	6.53	5.16	4.74
g	3	7.24	5.06	4.26
g	3.3	7.63	4.95	3.87
S	100	6.6	5.88	5.70
S	112	6.25	5.23	5.11
S	124	5.98	4.62	4.64
t_w	0.4375	12.62	8.01	3.93
t_w	0.5625	6.25	5.23	5.11
t_w	0.6875	3.15	3.52	6.30
Δ	0.012	4.21	3.04	2.62
Δ	0.02	5.53	4.45	4.23
Δ	0.022	5.85	4.80	4.63
Δ	0.024435	6.25	5.23	5.11
Δ	0.027	6.68	5.69	5.63
Δ	0.029	7.01	6.04	6.03
Δ	0.049	10.31	9.58	10.05

The results listed in Table 8.3 show that neglecting δ for varying values of Δ and S does not significantly reduce the accuracy of the stress prediction formula (i.e., Equation 8.1). For the cases of varying t_w and g neglecting δ causes the web gap stress prediction to have an inverse relationship with the model stresses. It is noted that in the Plymouth

Ave. Bridge, as well as the I-94/I-694 Bridge studied by Jajich [1], significant lateral deflection of the web gap region was not observed during finite element modeling. On the basis of this observation, the presence of large lateral deflections in the web gap region of steel girder bridges in the Mn/DOT inventory is questioned. Moreover, lacking a simple means by which to predict δ with reasonable accuracy, it is recommended that δ be neglected in the stress prediction formula (Equation 8.1).

8.3 Simple Web Gap Stress Prediction Equation

A simplified version of the web gap stress formula is obtained from Equation 8.1 by substituting for θ_b and θ_t the ratios proposed in Table 8.2, i.e., $\theta_t \approx 1.7(\Delta/S)$ and $\theta_b \approx 0.9(\Delta/S)$, as well as neglecting δ (i.e., $\delta = 0$). The resulting web gap stress prediction formula is given in Equation 8.2.

$$\sigma_{wg} = 3.5 \cdot E \cdot \left(\frac{t_w}{g}\right)\left(\frac{\Delta}{S}\right) \qquad \textbf{\textit{Equation 8.2}}$$

Using this equation produces the results shown in the rightmost column in Table 8.4 for the various configurations considered in the parameter study. For comparison, the peak web gap stresses computed using the finite element model (i.e., 'Model') are also given.

Table 8.4 Predicted and Model Stress Comparison Assuming Ratios

Parameter Changed	Value (in)	Model σ_{wg} (ksi)	Prediction σ_{wg} (ksi)
g	1.7	4.08	7.52
g	2	5.13	6.39
g	2.3	5.93	5.56
g	2.5	6.25	5.11
g	2.7	6.53	4.74
g	3	7.24	4.26
g	3.3	7.63	3.87
S	100	6.6	5.70
S	112	6.25	5.11
S	124	5.98	4.64
t_w	0.4375	12.62	3.93
t_w	0.5625	6.25	5.11
t_w	0.6875	3.15	6.30
Δ	0.012	4.21	2.62
Δ	0.02	5.53	4.23
Δ	0.022	5.85	4.63
Δ	0.024435	6.25	5.11
Δ	0.027	6.68	5.63
Δ	0.029	7.01	6.03
Δ	0.049	10.31	10.05

As can be seen in Table 8.4, Equation 8.2 is a fairly good predictor of the peak web gap stress for various values of Δ and S. As has been previously noted, for values of g larger than that of the diaphragms in the Plymouth Ave. Bridge (g = 2.5 in.) and values of t_w smaller than that of the Plymouth Ave. Bridge (t_w = 9/16 in.), Equation 8.2 may underestimate peak web gap stress.

The use of the proposed equation can be further justified by comparing its results with those of the other peak web gap stress prediction formulas discussed in this report. From Table 8.5 it can be seen that the proposed formula (Equation 8.2) best predicts the peak web gap stress in the simulated truck test of the Plymouth Ave. Bridge given by the finite element (FE) model. The Fisher and Jajich formulas are given by Equations 2.1 and 2.2, respectively.

Table 8.5 Comparison of Peak Web Gap Stress Prediction Methods

Extrapolated Web Gap Stress (ksi)	Predicted Web Gap Stress - Fisher (ksi)	Predicted Web Gap Stress - Jajich (ksi)	FE Peak Web Gap Stress (ksi)	Proposed Web Gap Stress Prediction (ksi)
1.60	97.56	2.71	6.25	5.11

Chapter 9-*Finite Element Bridge Modeling*

9.1 Overview

The second part of the third Mn/DOT project on rapid assessment of distortional stress in steel bridges (Phase IIIB) focused on the differential deflection formula proposed by Berglund (Equation 2.3, and Table 2.1), because it does not appear to predict accurately the differential deflections measured during truck testing of the Plymouth Ave. Bridge (see 6.2.1). Remembering that the Berglund equation provides an approximate prediction of the maximum differential deflection in an entire bridge, it was suggested that this lack of accuracy could have occurred because the location instrumented on the Plymouth Ave. Bridge was not the most probable location of maximum differential deflection. Many positions of the bridge were not accessible for instrumentation because they spanned interstate highway 94.

Another aspect of the Berglund formula for differential deflection requiring further study concerns diaphragm type, because this formula was developed for bridges with bent-plate diaphragms. To determine if the Berglund equation was truly applicable to this bridge, further research was required. Given the degree of accuracy and confidence exhibited by the finite element analysis of the I94/I694 Bridge in Berglund's study [2], it was assumed that such a model would be similarly useful in this case. If a model of the Plymouth Ave. Bridge could be calibrated to the truck testing results, then areas of the bridge that could not be instrumented could be tested numerically to determine the maximum differential deflection. In addition, the influence of diaphragm type could be investigated as well.

9.2 General Model Features

The Plymouth Ave. Bridge was represented as a three-dimensional finite element model using the SAP2000 Nonlinear computer analysis program [16] (Figure 9.1). The deck and girder webs were modeled as shell elements while the diaphragms, sidewalks, and girder flanges were modeled as frame elements. Rigid elements connecting the top chord of the girders to the deck, spaced regularly along the length of the bridge, provided

composite action between the girders and deck (Figure 9.2). Berglund modeled the integral J-rail barriers of the I94/I694 Bridge, but in the case of Plymouth Ave., it was decided to neglect the F-rails, as they are discontinuous at intervals of 20'. The control joints in the I94/I694 Bridge were not full depth, leaving a portion of the rail continuous.

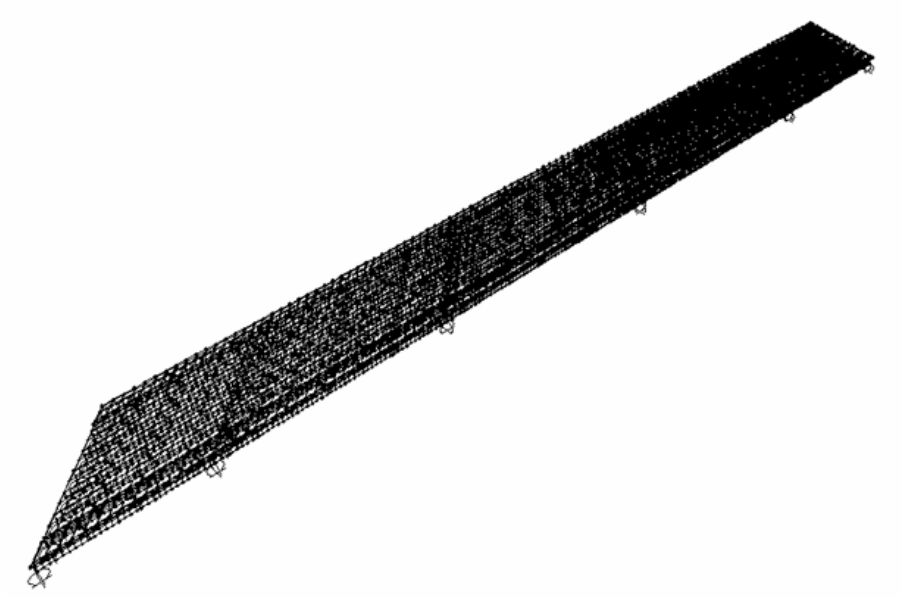

Figure 9.1 Finite Element Model of Plymouth Ave. Bridge

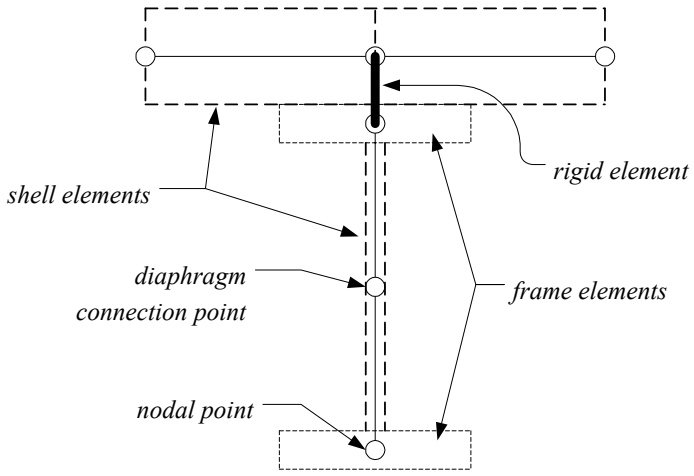

Figure 9.2 Berglund's Finite Element Model: Typical Partial Cross-Section

The I94/I694 Bridge features bent-plate diaphragms, which Berglund modeled as single line frame elements connected at mid-depth of the girder (Figure 9.3a). The Plymouth Ave. Bridge has cross-braces made up of steel angles. The first model of Plymouth Ave. utilized Berglund's single line element technique for modeling diaphragms, based on the assumption (supported by Berglund's study) that the method of modeling bent plate diaphragms mattered less to calculated differential deflection than the inclusion of the diaphragms. However, if the cross-braces in the Plymouth Bridge were to be modeled as single line elements, it was not clear what the cross-sectional properties of these elements should be, and any chosen cross-sectional area would always be arbitrary. The diaphragms were subsequently represented by four frame elements that connect at the top and bottom of each girder and, at their mid-length intersection, to each other (Figure 9.3b). This change in diaphragm representation introduced new issues of numerical instability, which were solved by modifying the restraint conditions of the cross-brace elements at their intersections and endpoints.

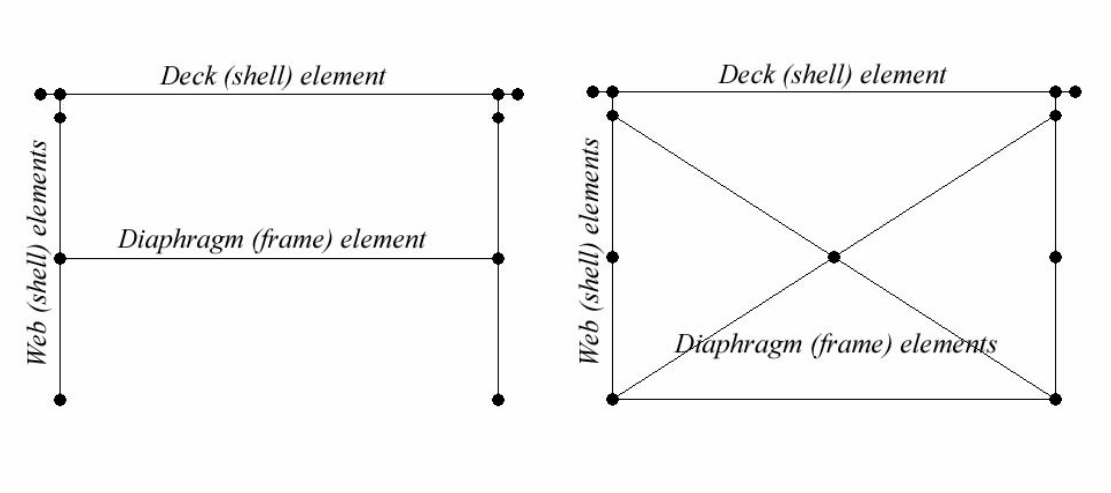

Figure 9.3 (a) Left: Single Line-Element Model for Bent-Plate Diaphragm (b) Right: Reconfigured Model for Cross-Brace Diaphragm

Further discussion of the diaphragm model is provided in section 9.4.6.

9.3 Model Modification and Verification

As shown in Figure 4.1, three different lane-loading configurations were used in truck tests on the Plymouth Ave. Bridge. All three load cases were replicated in calibrating the finite element bridge model. Truck loads of 222-kN (50-kips) were applied to the left and right lanes, individually and in combination. Field measurements of mid-span and diaphragm deflection of girders A, B, C, and D (Tables A.1-A.5) were used for comparison to the finite element analysis results.

Early analytical results did not show a high level of agreement to the field data. Several changes to the model were implemented, resulting in the final calibrated model properties given in Table 9.1. The calibrated model predicted with good accuracy vertical deflections at mid-span locations (Figures 9.4-9.6) and diaphragm differential deflections (Figure 9.7).

Table 9.1 Finite Element Model Properties

Calibrated Finite Element Model of Plymouth Ave. Bridge	
Span 1 Length	27.17 m (89.17 ft)
Span 2 Length	45.67 m (149.83 ft)
Span 3 Length	51.21 m (168 ft)
Span 4 Average Length	47.76 m (156.69 ft)
Span 5 Average Length	29.69 m (97.42 ft)
Girder Depth	1.829 m (72 in)
Girder Spacing	2.84 m (9 ft - 4 in)
Angle of Skew:	
West Abutment through Pier 3	45 deg - 28' - 41"
Pier 4	58 deg - 0' - 0"
East Abutment	75 deg - 32' - 16"
Deck Modulus of Elasticity	28.3 GPa (4100 ksi)
Sidewalk Modulus of Elasticity	24.8 GPa (3600 ksi)
Sidewalk Width	279.4 cm (110 in)
Sidewalk Height	25.4 cm (10 in)
Steel Modulus of Elasticity	200 GPa (29000 ksi)
Deck Thickness	22.86 cm (9 in)
Cross Brace Members	Angles LS4x4x5/16
Girder Flange Widths	35.56 - 40.64 cm (14 - 16 in)
Flange Thickness (w/ cover plates)	1.91 - 3.38 cm (0.75 - 8.57 in)
Lateral Brace Members	T-sections WT7x15
Support Conditions:	
Pier 3	elastomeric bearing pad (pin)
All other piers and abutments	elastomeric bearing pad (free)

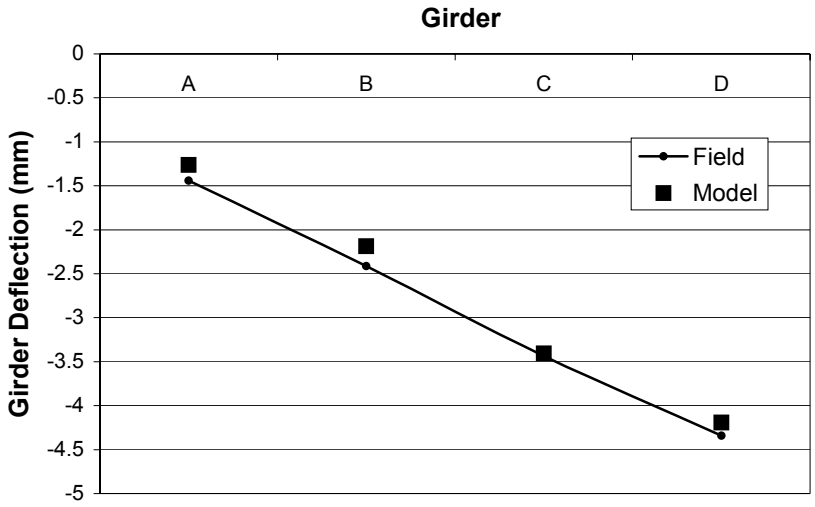

Figure 9.4 Mid-Span Deflection, Left Lane Loading

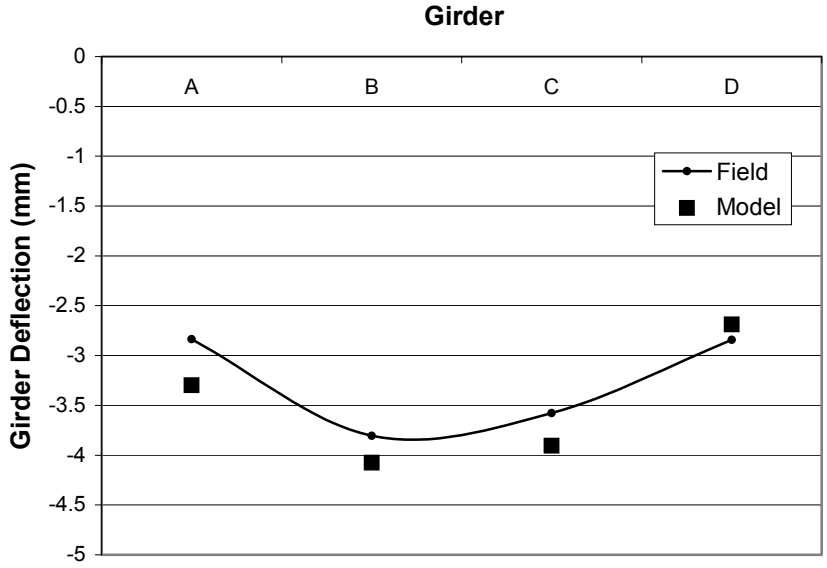

Figure 9.5 Mid-Span Deflection, Right Lane Loading

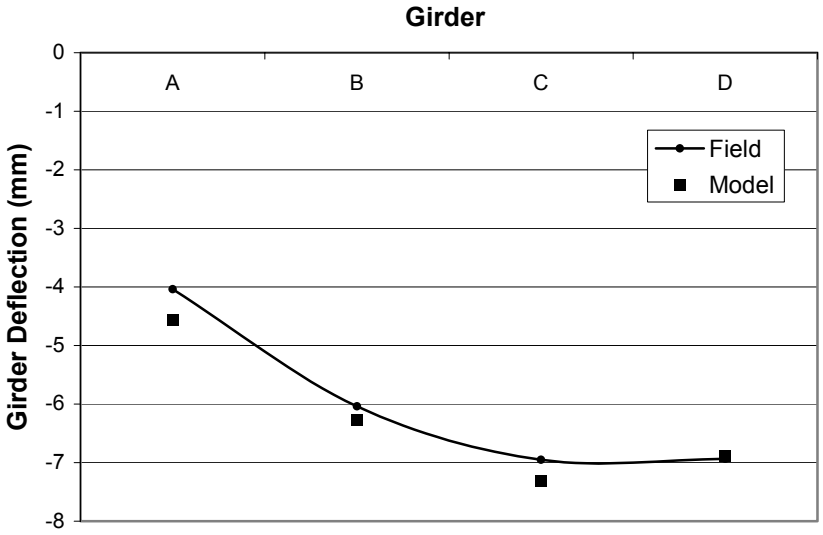

Figure 9.6 Mid-Span Deflection, Side-by-Side Loading

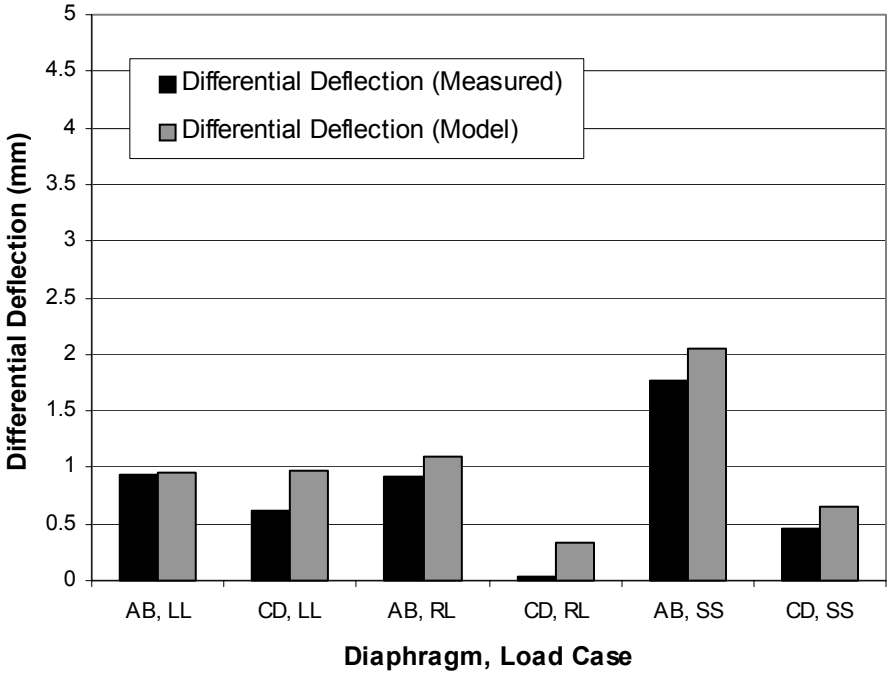

Figure 9.7 Differential Deflection of Instrumented Diaphragms

9.4 Model Sensitivity to Parameters

In the course of calibrating the finite element model of the Plymouth Ave. Bridge, a variety of bridge parameters were studied in detail. These included deck thickness, modulus of elasticity, shear transfer between deck and girders, sidewalk model, diaphragm model, and the presence of horizontal bracing. For each, a sensitivity study was performed to investigate the importance of these parameters in accurately predicting absolute and differential deflections. Some parameters, such as deck thickness and modulus of elasticity, were chosen for study because of uncertainty in the properties of the actual bridge. Others, such as the diaphragms and horizontal braces, were studied because they had not been included in Berglund's parameter studies [2]. The results presented here give an overview of the calibration of the model.

9.4.1 Deck Thickness

The plans for the Plymouth Ave. Bridge specify a minimum total deck thickness of 22.86 cm (9 in), including a minimum of 3.81 to 5.08 cm (1.5 to 2 in) of a high-strength, low-slump wearing course over 17.78 cm (7 in) of regular strength concrete. While no additional overlays have been made during the service of the bridge, the actual deck thickness is unknown. Deck thickness is therefore a potential source of uncertainty in the finite element model of the bridge. In his model of the I94/694 Bridge, which has identical provisions for deck thickness, Berglund assumed a 22.86 cm (9 in) deck, as was assumed in the subassembly model of Plymouth Ave (Chapter 7). During the calibration of the full model of the Plymouth Ave. Bridge, deck thickness was adjusted to find the best agreement with field measurements of mid-span and diaphragm deflections. Results are shown in Figure 9.8 and Table 9.2.

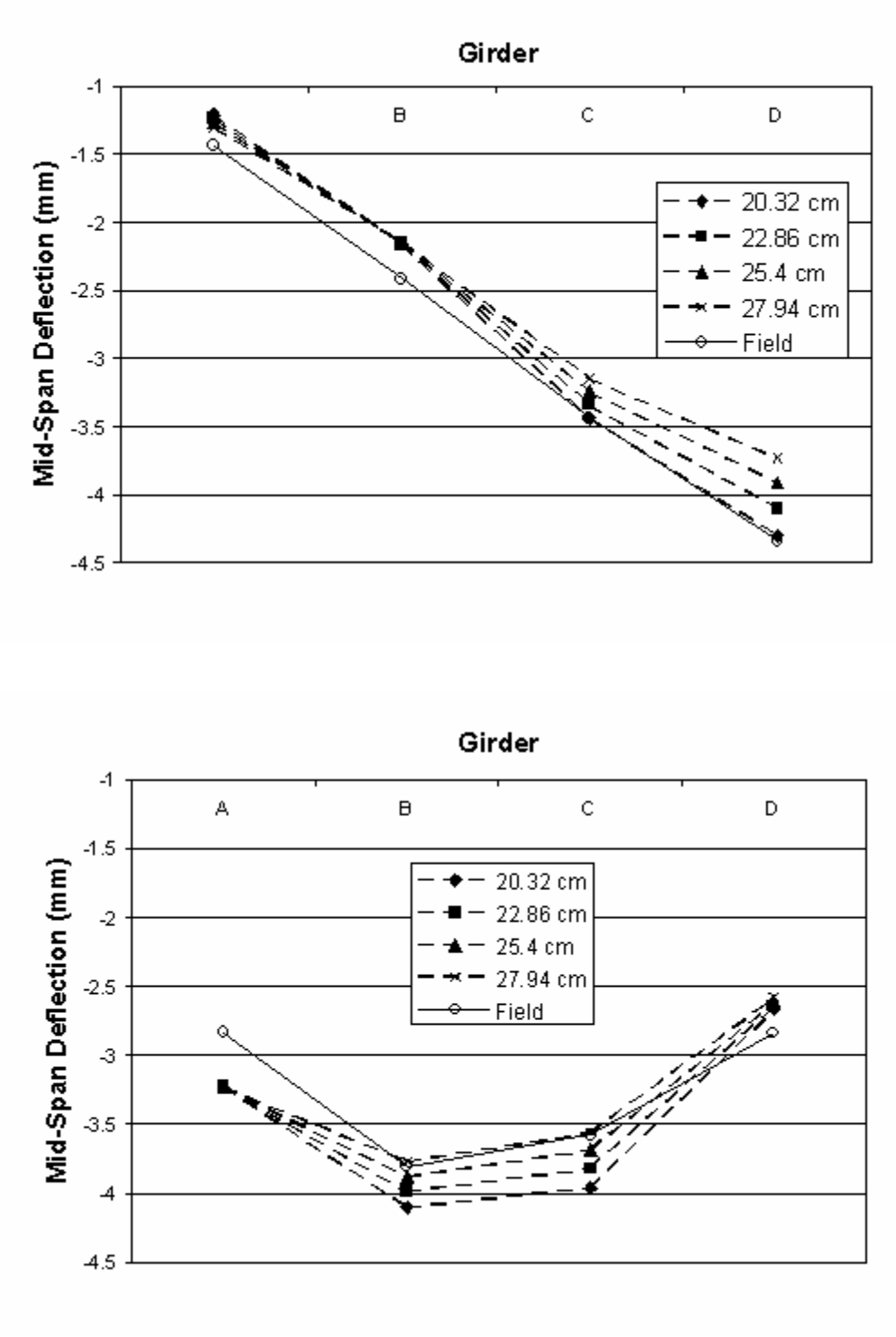

Figure 9.8 Effects of Deck Thickness on Mid-Span Deflection for (top) Left-Lane Loading, (bottom) Right-Lane Loading

Table 9.2 Effects of Deck Thickness on Differential Deflection of Instrumented Diaphragms

Deck Thickness	Left Lane Loaded		Right Lane Loaded	
	Diaphragm		Diaphragm	
	AB	CD	AB	CD
cm	mm	mm	mm	mm
20.32	0.936	1.049	1.141	0.370
22.86	0.921	0.954	1.062	0.314
25.40	0.900	0.868	0.983	0.265
27.94	0.875	0.791	0.906	0.223
Field Test	0.945	0.620	0.926	0.036

On the basis of these data, the given deck thickness of 22.86 cm (9 in) was selected for overall agreement of both absolute and differential deflections to field results. The finite element computations do not make a compelling case for a deck thickness other than the one specified in the bridge plans, namely 22.86 cm (9 in).

9.4.2 Modulus of Elasticity

The modulus of elasticity for the concrete of the Plymouth Ave. Bridge is not specified in the bridge plans. Instead, the nominal concrete compressive strength is specified to be 27.6 MPa (4000 psi). However, the strength of the wearing course is not specified, except that it is referred to as high strength. Berglund used the equation for concrete modulus of elasticity for normal weight concrete from the American Concrete Institute Building Code 318-99 (reprinted in ACI 318-02), $E_c = 57000\ (f'_c)^{0.5}$, with E_c and f'_c in units of psi. For the model of the I94/694 Bridge, Berglund selected a modulus of elasticity of 24.8 GPa (3600 ksi) for the edge rails, and 28.3 GPa (4100 ksi) for the deck, accounting for the higher strength surface. The same values were used for the sidewalks and deck in this model of the Plymouth Ave. Bridge.

Quality control standards and the strength gain of concrete over time can contribute to an underestimation of concrete strength and therefore modulus of elasticity. With this in mind, the effect of changes in modulus of elasticity on absolute and differential deflections in the model was tested. Four combinations of modulus for the sidewalk and deck were considered, shown in Table 9.3.

Table 9.3 Modulus of Elasticity for Sidewalks, Deck—Four Test Cases

	ksi		Gpa	
	Sidewalk	Deck	Sidewalk	Deck
1	3500	4000	24.1	27.6
2	3750	4250	25.9	29.3
3	4000	4500	27.6	31
4	4250	4750	29.3	32.8

The sensitivity of absolute deflections in the model to these changes in modulus are shown in Figure 9.9 and Table 9.4.

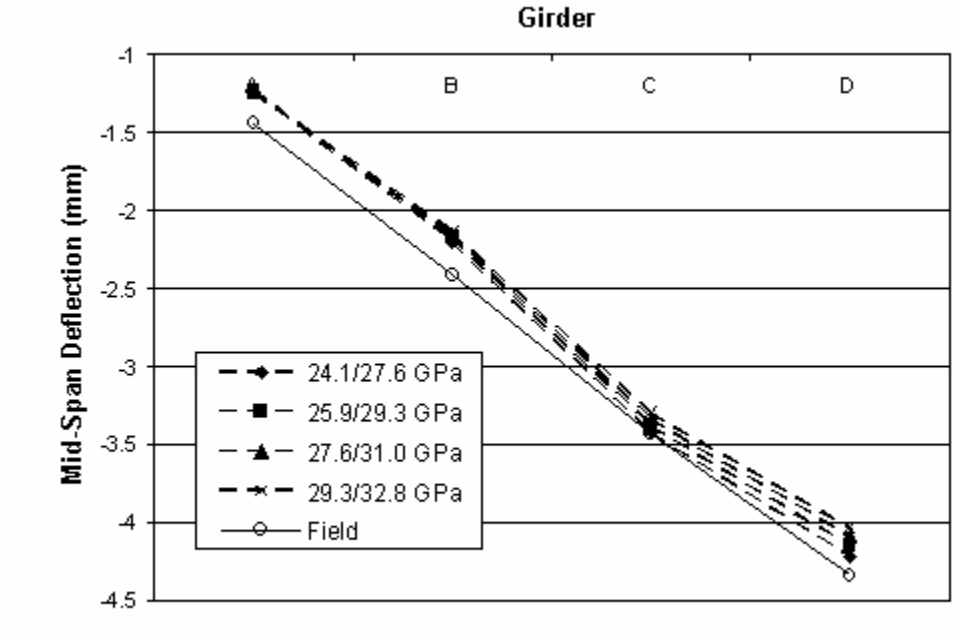

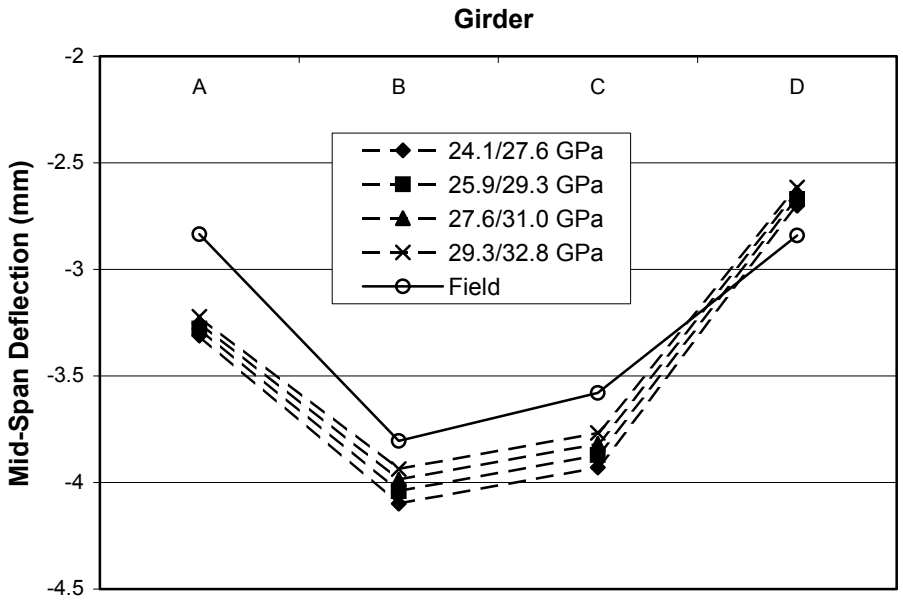

Figure 9.9 Effects of Modulus of Elasticity on Mid-Span Deflection for (top) Left-Lane Loading, (bottom) Right-Lane Loading

Table 9.4 Effects of Modulus of Elasticity on Differential Deflection of Instrumented Diaphragms

	Left Lane Loaded		Right Lane Loaded	
Modulus of Sidewalk/Deck	Diaphragm AB	CD	Diaphragm AB	CD
GPa	mm	mm	mm	mm
24.1/27.6	0.952	0.988	1.110	0.332
25.9/29.3	0.936	0.969	1.084	0.322
27.6/31.0	0.921	0.951	1.060	0.313
29.3/32.8	0.907	0.934	1.037	0.304
Field Test	0.945	0.620	0.926	0.036

Plots of differential deflection versus sidewalk and deck modulus of elasticity (Figure 9.10) show that modulus of elasticity does not have a significant effect on differential deflection in the model. Therefore the initial values of 24.8 GPa (3600 ksi) for the sidewalk and 28.3 GPa (4100 ksi) for the deck were used in the final calibration of the model.

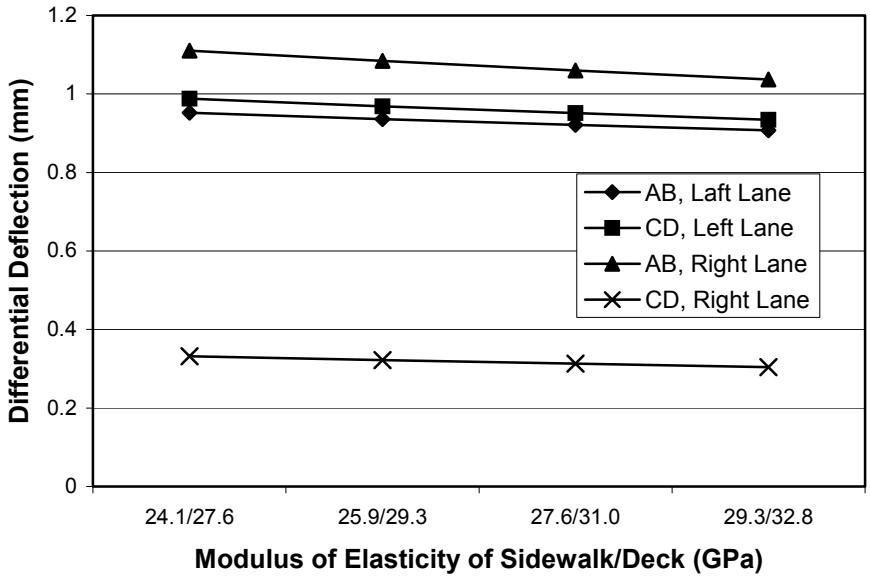

Figure 9.10 Effect of Modulus of Elasticity on Differential Deflection

9.4.3 Shear Transfer Between Girders and Deck

Current bridge design practice, as set forth in the 2001 Interim AASHTO LRFD Bridge Design Specification [18], assumes a varying degree of composite action along the length of a girder under ultimate loads, based on the amount of shear transfer provided by connections of the girder to the concrete. Under service loads, however, some composite action may be provided in the absence of shear connectors by friction between the girder and deck. Such shear transfer has been observed in field tests on decommissioned non-composite steel girder bridges. [19] But this mechanism cannot be taken into account during design, especially when using the LRFD method.

The Plymouth Ave. Bridge features shear studs, spaced at varying intervals along the lengths of the girders. In the areas of negative flexure near the piers, no shear studs are called for. The I94/694 Bridge is designed similarly, with varied shear stud spacing and no studs in negative moment regions. The Berglund model of that bridge featured rigid elements connecting the top chord of the girder to the centroid of the deck, to model the compatibility and transfer of shear provided by these connectors. The rigid connections in the Berglund model were spaced equally at intervals of 101.6 cm (40 in, equal to the depth of the girder web) all along the girder lengths. The model of the Plymouth Ave. Bridge in this study has the same configuration: rigid connections spaced equally at 182.88 cm (72 in, equal to the depth of the girder web). However, initial results from the model using mid-span deflections indicated that it was too rigid, so an attempt was made to model the reduction in shear transfer in negative flexure regions. The in-plane rotational fixity of the rigid members in these regions was released. The selective release of rotational fixity resulted in an increase in accuracy of modeled mid-span deflections in some cases, as shown in Figure 9.11, but not in all cases.

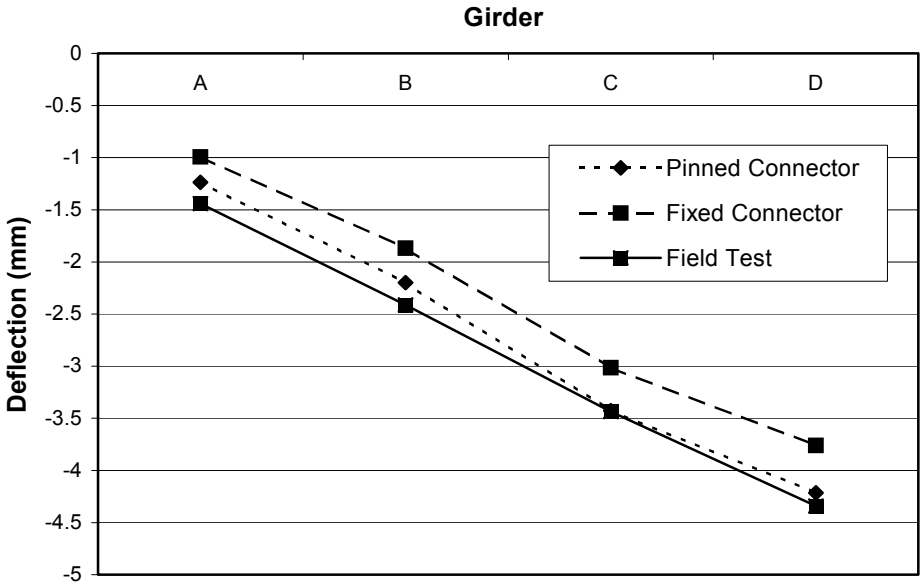

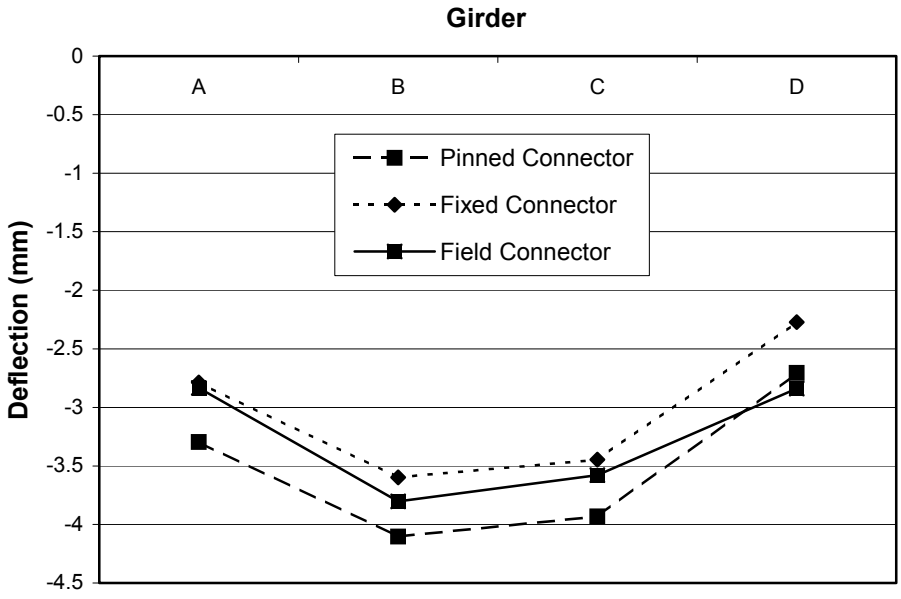

Figure 9.11 Effects of Connector Fixity on Mid-Span Deflections for (top) Left-Lane Loading, (bottom) Right Lane Loading

Some amount of shear transfer is still provided in the negative moment regions by the high axial stiffness of the rigid members. Any relative longitudinal displacement between deck and flange will engage the rigid members in tension. An examination of rigid member axial forces in a load test confirms this. This modeling of the composite action is a somewhat simple approximation that could be refined upon further study. However, within the scope and time restraints of this study, the selective release of rotational fixity of the connectors over the supports is assumed to provide an acceptable level of accuracy.

9.4.4 Sidewalk Model

The Berglund model included the integral edge rail of the I94/694 Bridge as a series of frame members connected to the deck by rigid frame members. For this study, a similar model of the sidewalk was originally considered. However, it was suggested that the single line element would not accurately represent the full width of the sidewalk's restraint on the deck. Therefore, three different configurations of the sidewalk model were considered: the single-frame-element model, shell elements connected on both sides of the sidewalk, and a model that neglected the sidewalk altogether. As shown in Figure 9.12, the shell model provided the best accuracy as compared to field measurements.

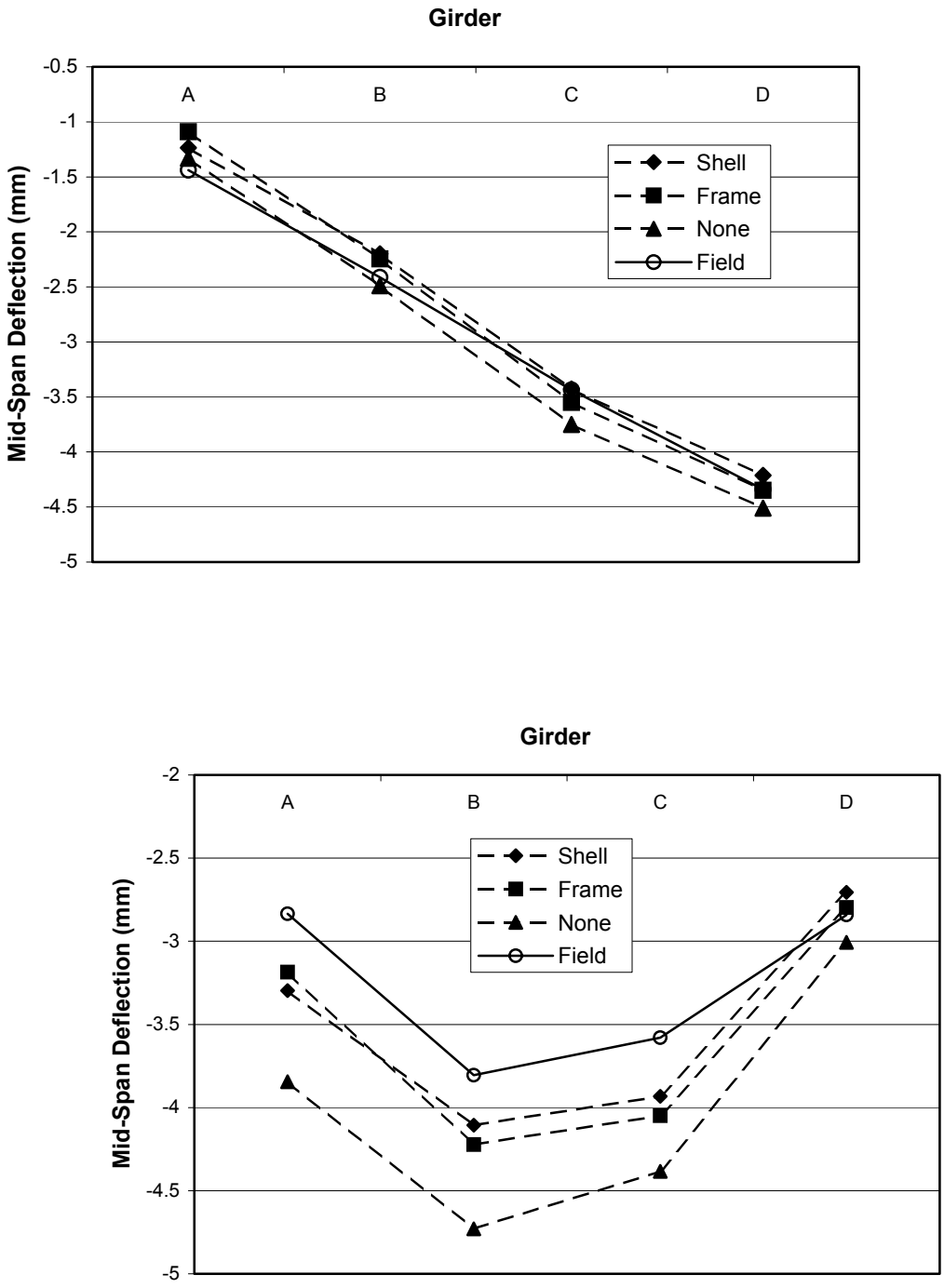

Figure 9.12 Effects of Sidewalk Model on Mid-Span Deflection for (top) Left-Lane Loading, (bottom) Right-Lane Loading

The sidewalk on the Plymouth Ave. Bridge has four expansion joints that cut through half of their depth, parallel to and aligned with the centerlines of the bridge piers. A somewhat crude model was used to estimate the effect: the sidewalk shell element directly over the pier was simply removed. Figure 9.13 shows that even this drastic measure had little effect on deflections. Therefore, in the final model, the sidewalks were modeled as being continuous across the piers.

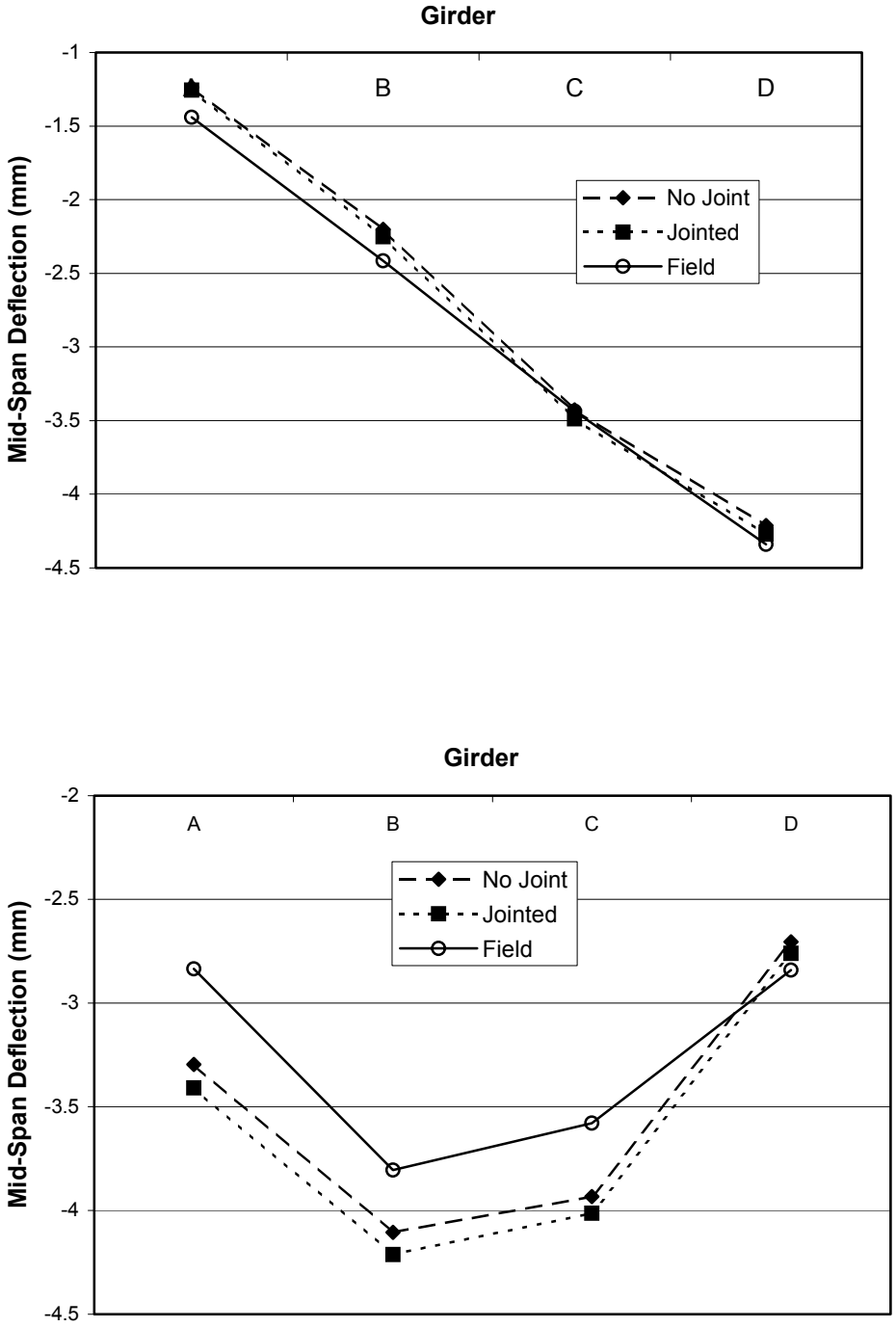

Figure 9.13 Effects of Sidewalk Expansion Joint on Mid-Span Deflection for (top) Left-Lane Loading, (bottom) Right-Lane Loading

9.4.5 Diaphragms

The straight-line, single-frame-element diaphragm configuration of the Berglund model was initially assumed to be sufficient to represent the cross braces of the Plymouth Ave. Bridge. However, it was unclear what thickness of line element should be used to model two crossing angle sections. Ultimately, the more detailed model that included all three members of the cross braces (shown in Figure 9.3b) was used. Figure 9.14 and Table 9.5 show the effect of diaphragm model choice on absolute mid-span- and differential deflections.

The single-line-element diaphragms were modeled with a depth of 162.56 cm (64 in) and thicknesses (each equally arbitrary) of 25.4 mm (1 in), 50.8 mm (2 in), and 101.6 mm (4 in). The cross-brace diaphragms are clearly the more accurate configuration for this bridge. Two variations of the cross-brace diaphragms were tested: one with the four ends fixed against in-plane rotation, and one with pinned ends (only this latter case is shown below). The difference in absolute deflections between the latter two cases was found to be negligible (i.e., on the order 0.0001 in.). Therefore it was concluded that the fixity of the brace ends has little effect on absolute or differential deflection. In the final analysis, the pinned-end model was used.

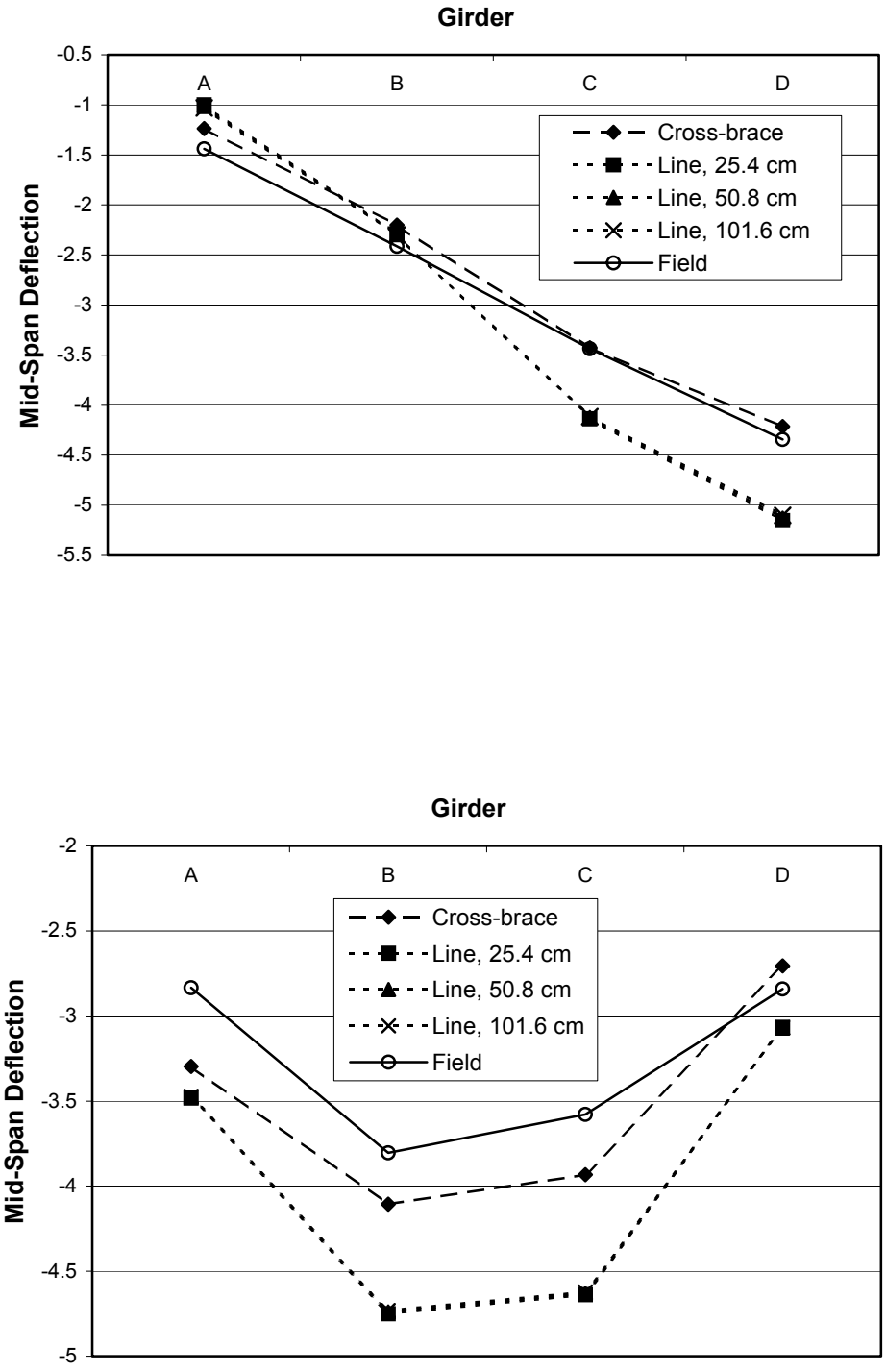

Figure 9.14 Effects of Diaphragm Model on Mid-Span Deflection for (top) Left-Lane Loading, (bottom) Right-Lane Loading

Table 9.5 Effects of Diaphragm Model on Differential Deflection of Instrumented Diaphragms

Deck Thickness	Left Lane Loaded		Right Lane Loaded	
	Diaphragm		Diaphragm	
	AB	CD	AB	CD
	mm	mm	mm	mm
Cross-brace	0.967	0.982	1.121	0.329
Line, 25.4 cm	1.237	1.268	1.331	0.458
Line, 50.8 cm	1.250	1.259	1.284	0.451
Line, 101.6 cm	1.252	1.252	1.248	0.445
Field Test	0.945	0.620	0.926	0.036

9.4.6 Horizontal Wind Bracing

The Plymouth Ave. Bridge was designed with horizontal cross braces in spans 2-4 between girders B and C, D and E, and G and H. It was not expected that neglecting these braces would have a significant effect on the model accuracy. However, at the time of replacing the single-element diaphragms with crossing multi-element braces, it was simple to also add the horizontal braces. As shown in Figure 9.15 and Table 9.6, inclusion of the bracing had a positive effect on mid-span deflection accuracy, and a very small but positive effect on differential deflection accuracy.

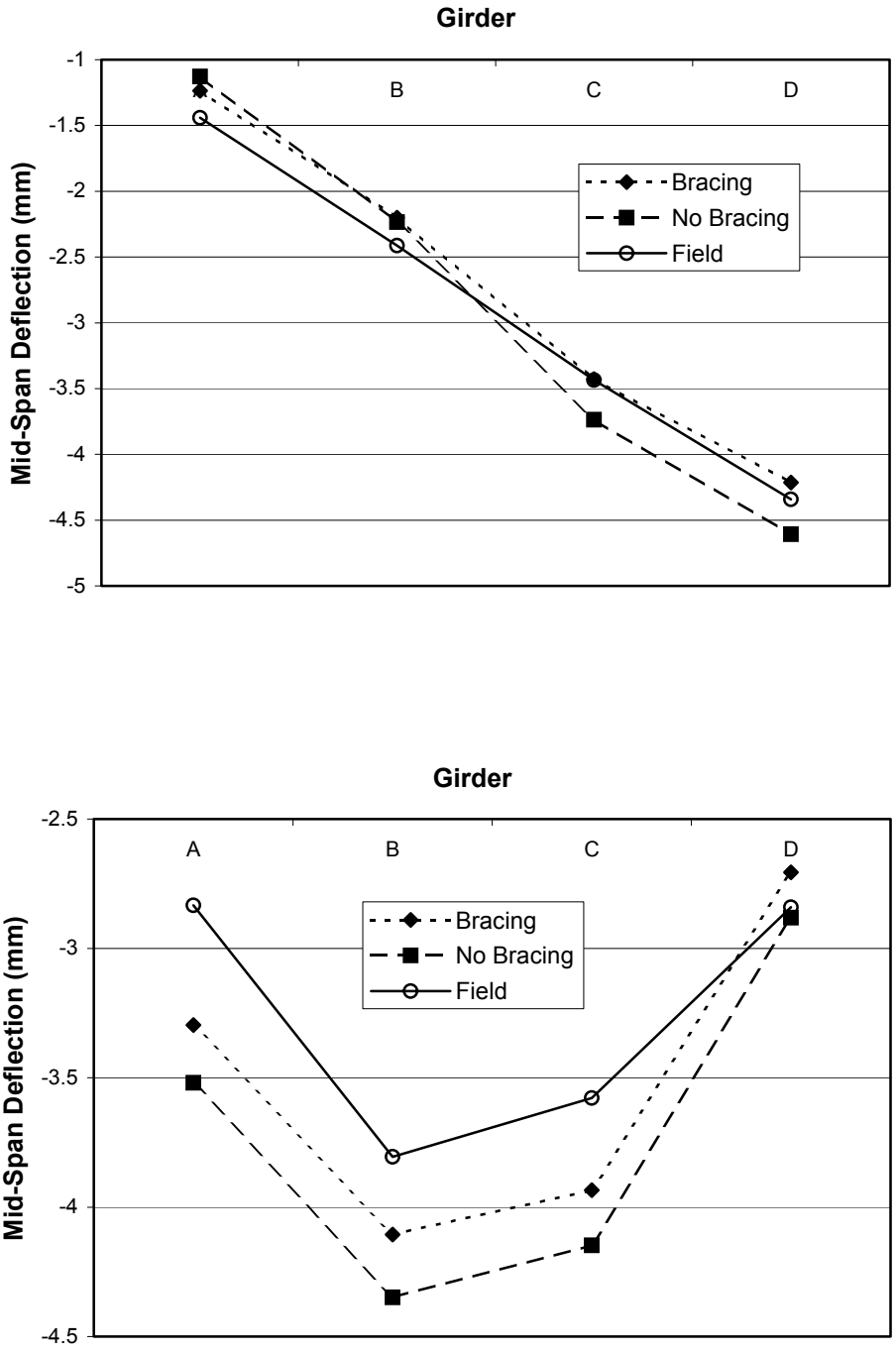

Figure 9.15 Effects of Horizontal Wind Bracing on Mid-Span Deflection for (top) Left-Lane Loading, (bottom) Right-Lane Loading

Table 9.6 Effects of Horizontal Wind Bracing on Differential Deflection of Instrumented Diaphragms

Wind Bracing?	Left Lane Loaded		Right Lane Loaded	
	Diaphragm		Diaphragm	
	AB	CD	AB	CD
	mm	mm	mm	mm
No	1.075	1.036	1.159	0.334
Yes	0.967	0.982	1.122	0.329
Field Test	0.945	0.620	0.926	0.036

Bridge design practice does not include wind bracing when evaluating strength or vertical deflection. However, when the lower chord of the girder is engaged in tension or compression during bending, the axial stiffness of the braces may participate in resisting longitudinal strains, thereby adding to the bending stiffness of the system. An analogy may be made by considering the girders and deck as a channel with its open side facing downward. The wind braces then close off this open side, forming the fourth (if less rigid) side of a tube. The effect is not large, but seems significant enough to merit inclusion when modeling the behavior of an existing bridge.

9.5 Conclusions

The calibrated values of the parameters discussed in section 9.4 are presented in Table 9.6.

Table 9.7 Calibrated Values of Finite Element Model Parameters

Deck Thickness	22.86 cm (9 in)
Deck Modulus of Elasticity	28.3 GPa (4100 ksi)
Sidewalk Modulus of Elasticity	24.8 GPa (3600 ksi)
Girder-Deck Shear Connections	selectively released
Sidewalk Model	shell element
Diaphragm Model	multiple-member cross-brace
Horizontal Bracing	present

Refinements of the finite element modeling technique used previously by Berglund resulted in an increase in accuracy for predicting mid-span and diaphragm deflections. This accuracy creates a good level of confidence in the finite element model for further

investigation of the applicability of the Berglund formula for predicting maximum differential deflection.

Chapter 10-*Truck Tests on Finite Element Model*

10.1 Overview

With the finite element model of the Plymouth Ave. Bridge satisfactorily calibrated, a series of truck tests was simulated to find the location and magnitude of the maximum diaphragm differential deflection on the bridge. Special attention was paid to the diaphragms near the obtuse corners of each span, as previous research showed this to be the typical location of maximum differential deflection [2]. The finite element model was then altered to reflect possible design differences, in order to identify factors that could result in the overestimation of differential deflection by the prediction equation.

10.2 Testing Procedure

Berglund [2] identified an "obtuse corner effect," whereby load is transferred along a line that is approximately perpendicular to the skewed supports of a bridge (Figure 10.1). The plan shown in Fig. 10.1 does not correspond to the Plymouth Ave. Bridge. Rather, it is an idealization used to explain the "obtuse corner effect", and traffic is moving in a single direction, from left to right on the bridge, with Lane 1 being the leftmost lane and Lane 4 being the rightmost one. The maximum diaphragm differential deflection was typically found at locations in the obtuse corners of a given loaded lane. Thus, truck tests were simulated using the Plymouth Ave. Bridge model, with special attention given to the differential deflections in the obtuse corners of the main spans.

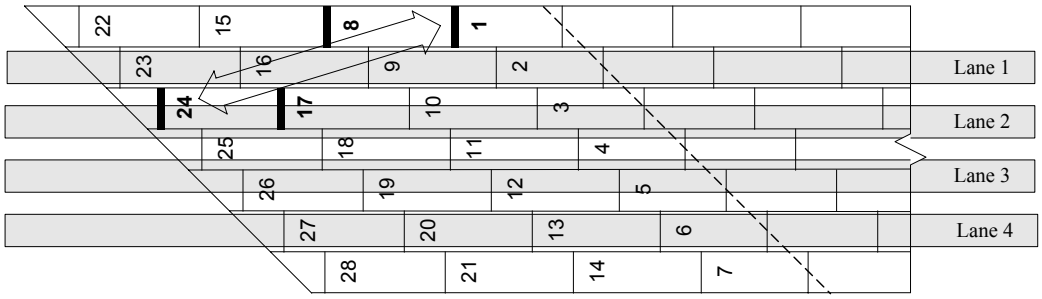

Figure 10.1 Obtuse Corner Effect for Loading of Lane 1

It was decided to perform these tests using the AASHTO HS-20 axle load configuration (Figure 10.2), so that comparisons may be made between the finite element analysis and the differential deflection prediction equation without any modification factors for axle loading. That equation was developed using HS-20 loads, so using the same loads for these tests results in the most applicable conditions for the equation.

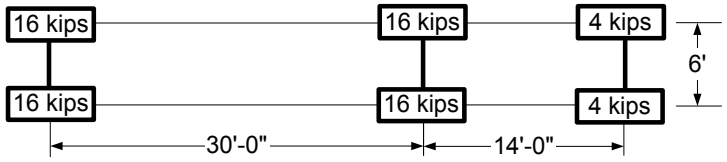

Figure 10.2 AASHTO HS-20 Axle Load Configuration

To identify the diaphragms in these tests, the nomenclature used by Berglund in the previous University of Minnesota study [2] was used. This nomenclature names the first diaphragm in the outside row of the main span, nearest the obtuse corner, A, the next as H, and the third as O (Figure 10.3).

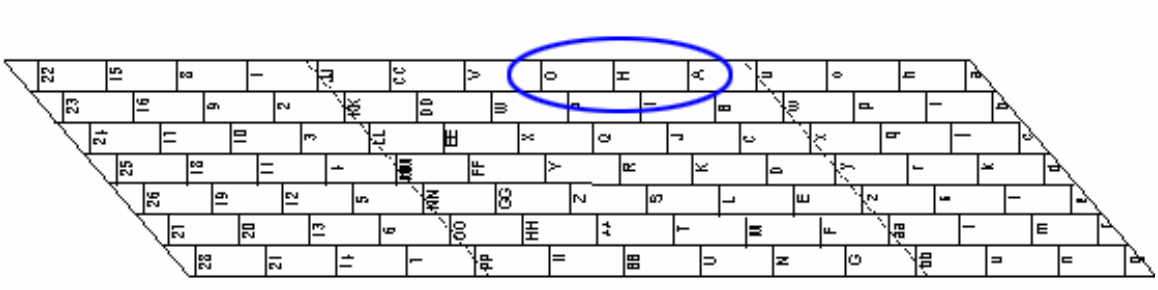

Figure 10.3 Labeling Scheme for Diaphragms

The Plymouth Ave. Bridge features a detail of diaphragm arrangement different from the bridges previously considered in the University of Minnesota research program. Some of the diaphragms near the supports in the outside rows are back-to-back with diaphragms in the adjacent rows. These "extra" diaphragms are not part of the regular, staggered pattern seen in the framing plan. Preliminary analyses showed differential deflections of these diaphragms to be generally much lower than those of nearby diaphragms in the regular pattern, possibly due to the added restraint of the adjacent diaphragm between the second and third girders. As such, these diaphragms were not labeled or considered in these truck tests.

Figure 10.4 shows the framing plan for Span 4 with Diaphragms A, H, and O indicated. This bridge carries traffic lanes in two directions, and the instrumented diaphragms are under the westbound lanes. For the westbound lanes, the right lane is closest to Girder A, and the left lane is closest to Girder D. Note that the instrumented diaphragm was identified previously as Diaphragm AB when calibrating the finite element model to the measured field data, and is labeled as Diaphragm 4H in the present analysis.

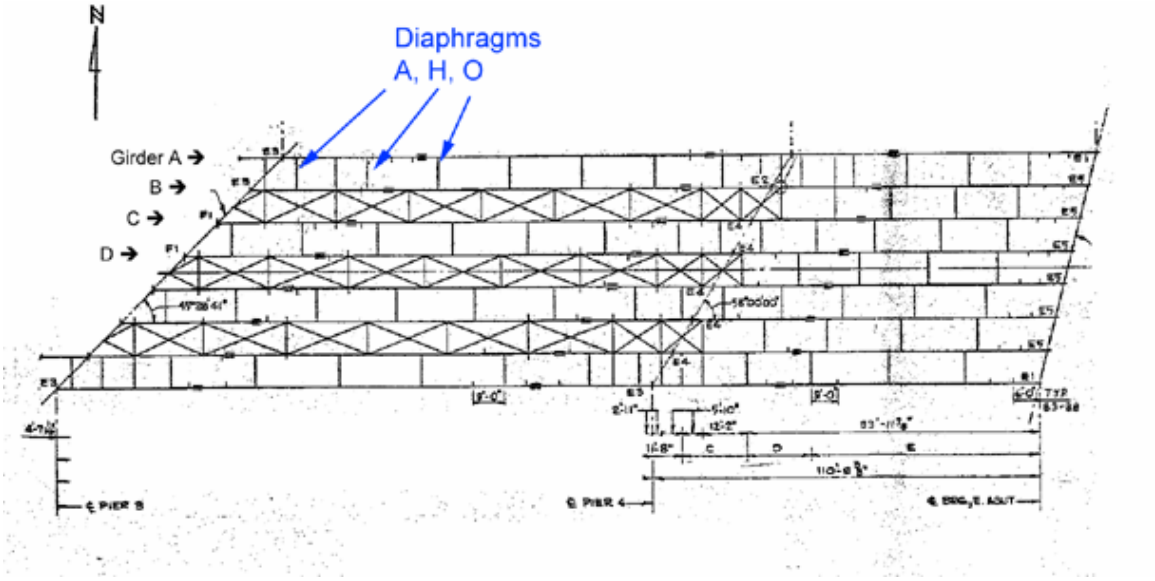

Figure 10.4 Framing Plan of Plymouth Ave. Spans 4 and 5 Highlighting Diaphragms 4A, 4H, and 4O

The deflections predicted by the Berglund formula for these tests were calculated using the length and skew angle of the central span (Span 3) of the bridge: 40-degrees and 51.21 m (168 ft). Span 3 was chosen for assessment because it is the longest in the bridge, and because it was not possible to instrument this span for field testing. Using the geometry of this span, the Berglund formula predicts a maximum differential deflection of 2.10 mm (0.0825 in). This prediction is larger than the deflections obtained from the finite element analysis of the bridge, as described in the following section.

10.3 Results and Factors Influencing Differential Deflection

Placing truck loads at various locations on the bridge, the maximum differential deflection was found to be 1.49 mm (0.0585 in) at Diaphragm 3A. This is 29.1 % less than the Berglund formula prediction of 2.10 mm (0.0825 in). The first line of Table 10.1 (i.e., finite element model as calibrated) shows results (differential deflections near the obtuse corners of the three main spans) for this test. Note that the differential deflections in the obtuse corners of all three main spans are approximately equal. This suggests that

the location instrumented was an appropriate choice, and a significantly higher value would not have been found if the obtuse corners of the other main spans (over north- and south-bound Interstate 94) had been instrumented. (Table 10.1 also shows results for the analyses to follow.)

Table 10.1 Differential Deflections of Diaphragms in Obtuse Corners of Main Spans for Various Model Configurations (Maximum Values Highlighted)

Diaphragm Location	2A		2H		3A		3H		4A		4H	
Model configuration	(mm)	(in)	(mm)	(in)	(mm)	(in)	(mm)	(in)	(mm)	(in)	(mm)	(in)
1. As Calibrated	1.359	0.054	1.227	0.048	1.486	0.059	1.213	0.048	1.024	0.04	1.376	0.054
2. Extra Diaphragms Removed	1.423	0.056	1.236	0.049	1.564	0.062	1.223	0.048	1.09	0.043	1.226	0.048
3. End Spans Removed	1.778	0.07	1.224	0.048	1.586	0.062	1.221	0.048	N/A	N/A	1.562	0.061
4. Bent Plates Replace Cross Braces	1.677	0.066	1.745	0.069	1.882	0.074	1.795	0.071	1.242	0.049	1.874	0.074
5. Bent Plates, No Extra Diaphragms	1.746	0.069	1.768	0.07	1.972	0.078	1.823	0.072	1.341	0.053	2.026	0.08

The goal of modeling the entirety of the Plymouth Ave. Bridge using finite element analysis was to resolve the differences between the field tests on that bridge and the equation prediction of maximum differential deflection. To that end, differences between the Plymouth Ave. Bridge and the assumptions of bridge design in formulation of that equation were identified and the model altered accordingly to study their effects:

- *Doubled diaphragms near supports. It was believed that these "extra" back-to-back diaphragms, described previously, could conceivably provide an alternate load path in the obtuse corner, influencing the maximum differential deflection.*
- *Extra end spans. In his primary study to formulate the equation predicting differential deflection, Berglund only considered bridges having three spans. The Plymouth Ave. Bridge has five, and the continuity provided over piers 1 and 4 by the two shorter end spans could result in different boundary conditions than the ends of the bridge would.*
- *Cross-brace diaphragms. The Plymouth Ave. Bridge was selected for study in part because it had cross-braces instead of the bent-plate diaphragms assumed in creating the prediction model. The field tests were performed to confirm or deny the applicability of the model to such a bridge.*

A set of numerical tests was performed on the finite element model with the extra diaphragms near the supports removed (Line 2, Table 10.1). The maximum differential deflection from the finite element analysis was found to be 1.56 mm (0.0615 in) at

Diaphragm 3A, 25.4 % less than predicted using the Berglund formula. While the finite element result is closer to the Berglund formula prediction without these extra diaphragms than with them, the improvement is very small and does not appear to explain the discrepancy between finite element analysis and Berglund formula prediction.

In a separate test with the extra diaphragms left in place, the first and fifth spans of the bridge were removed, with girders and deck terminated along the support lines of piers 1 and 4. The finite element result (Line 3, Table 10.1) was a maximum differential deflection of 1.78 mm (0.700 in) at Diaphragm 2A, only 15.2 % less than the Berglund formula prediction. Note that the girders at the point of termination were originally proportioned for the bridge at its full length with five spans, and were not changed for this test.

Finally, the cross-braces were replaced with single-elements representing bent plate diaphragms. These diaphragms were proportioned according to Mn/DOT rules and practice in the same method Berglund used in his primary study. Diaphragm depth was defined as ¾ of web depth, up to an allowed maximum of 1.22 m (48 in), with a depth-to-flange-width ratio of 6:1. Thus, with a 1.83 m (78 in) web depth, the diaphragms were 1.22 m (48 in) deep with 20.32 cm (8 in) flanges and 7.94 mm (0.3125 in) web and flange thickness.

The single-frame-element brace configuration resulted in a maximum differential deflection (Line 4, Table 10.1) of 1.88 mm (0.0741 in) at Diaphragm 3A, which is 10.2 % less than the predicted maximum. Therefore, it is concluded that cross-brace diaphragms seem to have a significant effect in reducing differential deflection, as compared to bent-plate diaphragms. This conclusion is intuitive, as the cross-braces rely on the axial stiffness of the diagonals, while the bent-plate diaphragms rely on the smaller flexural stiffness and shear stiffness of the bent plates. Thus, a more robust load path is offered by cross-braced bridges resulting in more effective lateral load path and smaller differential displacements between adjacent girders.

If the extra diaphragms near the supports are also removed from the cross-braced diaphragm model (Line 5, Table 10.1), the maximum differential deflection is 2.03 mm (0.0798 in) at Diaphragm 4H, which is 3.4% larger than the Berglund prediction. However, the presence or lack of these extra diaphragms would be difficult to quantify as a modification to the prediction equation, and the effect is much less than that of the cross-braces. Therefore the influence of the cross-braces is considered the main reason for the discrepancy between the Berglund prediction of differential deflection, and the calculation of this quantity using finite element analysis.

10.4 Discrepancy Between Prediction and Field Data

In Chapter 6, a maximum differential deflection for the Plymouth Ave. Bridge of 1.63 mm (0.0642 in) was predicted using the analytic Berglund Formula (see 6.2.1). This prediction was based on the 45.48-degree skew of the main spans and the average length of the fourth span, 47.76 m (156.71 ft). Also, this value was obtained using the 75% scaling factor for predicting the deflections from a 240-kN (54-kip) AASHTO HS-15 axle configuration load rather than a 311-kN (72 kip) HS-20 load. The Mn/DOT sand-filled dump trucks that were used in the field tests are 222-kN (50-kip) vehicles, and do not have the same axle configuration as an AASHTO HS truck. The Mn/DOT dump trucks feature a wheelbase of approximately 2.11 m (6.92 ft) and a spacing between the front axle and the centroid of the twin rear axles of about 5.21 m (17.1 ft, or 205 in). Throughout this and previous studies of distortional stresses for Mn/DOT, these trucks have been modeled (Figure 10.5) as a 66.7-kN (15-kip) axle and a 155.7-kN (35-kip) axle, spaced at 5.08 m (16.7 ft or 200 in).

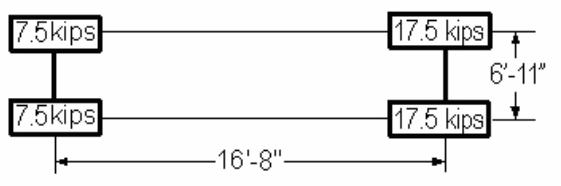

Figure 10.5 Sand Truck Axle Load Configuration in Finite Element Model

Placing such a load on the finite element model for the Plymouth Ave. Bridge, modified with bent-plate diaphragms results in a differential deflection of diaphragm 4H of 1.49 mm (0.0589 in). The deflection of that diaphragm by an HS-15 load is 1.41 mm (0.0553 in), or ¾ of the value for an HS-20 load. Thus, the use of the prediction equation with the HS-15 scaling factor is not necessarily inappropriate for estimating the response due to a 222-kn (50-kip) sand-filled dump truck in this case.

The sand-filled dump truck load configuration produces a finite element differential deflection on the bent-plate model—at the location instrumented for field tests—only 8.5 % less than the Berglund predicted value of 1.63 mm (0.0642 in). The same load on the cross-brace model produces a differential deflection at that location of 1.06 mm (0.0418 in), 34.9% less than the Berglund prediction. Therefore, it seems that the discrepancy between the field tests and the original Berglund prediction of differential deflection may be explained by the use of cross-brace diaphragms instead of bent plates.

10.5 Conclusions

The simulated truck tests that were performed on the calibrated finite element model create confidence in the results of field tests. Changes to the finite element model show that differences in design details between the Plymouth Ave. Bridge and the bridges in the study that was used to develop the Berglund prediction formula can explain the discrepancy between those predictions and field test measurements. In particular, the effect of cross-braces in reducing differential deflection is shown to be significant.

Chapter 11-*Differential Deflection Model for Cross-Brace Diaphragms*

11.1 Overview

The results of the simulated truck tests on the calibrated finite element model of the Plymouth Ave. Bridge show that cross-brace diaphragms can have a more significant effect on differential deflection than bent plate diaphragms. However, the Berglund formula for analytically predicting differential deflections was predicated on the use of bent plate diaphragms [2]. Therefore, a modification factor was developed in the present study to reduce the maximum differential deflections from the Berglund for bridges with cross-brace diaphragms.

11.2 Derivation and Justification of Modification Factor

A sample of the finite element bridge models used by Berglund in the primary parameter study was selected for modification. The single-line elements representing bent-plate diaphragms were replaced with cross-brace elements in the style of those used in the model of Plymouth Ave. The models were each tested, with both diaphragm configurations, to find the magnitude and location of the maximum diaphragm differential deflection. The results are summarized in Table 11.1.

Table 11.1 Differential Deflection Data for Parameter Study Models with Bent Plate, Cross-Brace Diaphragms

Analysis Parameters					Maximum Differential Deflection, Δ								
Girder Spacing		Span Length		Skew	Predicted		Bent Plate Diaphragms			Cross Brace Diaphragms			% Reduction of Δ
ft.	m	ft.	m	deg.	in.	mm	in	mm	Location	in	mm	Location	
10.5	3.20	60	18.3	20	0.097	2.47	0.096	2.43	A	0.094	2.38	A	2.3
10.5	3.20	60	18.3	40	0.093	2.35	0.095	2.41	A	0.094	2.39	A	0.9
10.5	3.20	60	18.3	60	0.076	1.92	0.072	1.84	A	0.067	1.71	A	7.2
10.5	3.20	100	30.5	20	0.101	2.55	0.099	2.50	H	0.075	1.90	H	24.3
10.5	3.20	100	30.5	40	0.102	2.59	0.092	2.34	A	0.089	2.25	A	3.8
10.5	3.20	100	30.5	60	0.113	2.88	0.115	2.92	A	0.085	2.17	A	25.9
10.5	3.20	140	42.7	20	0.090	2.30	0.087	2.21	H	0.059	1.51	H	31.6
10.5	3.20	140	42.7	40	0.095	2.42	0.093	2.35	H	0.073	1.84	H	21.7
10.5	3.20	140	42.7	60	0.115	2.91	0.102	2.59	A	0.081	2.05	A	20.7
10.5	3.20	180	54.9	20	0.076	1.92	0.066	1.68	O	0.021	0.52	A	68.9
10.5	3.20	180	54.9	40	0.083	2.12	0.075	1.90	O	0.040	1.01	H	47.0
10.5	3.20	180	54.9	60	0.103	2.63	0.092	2.33	H	0.047	1.19	A	48.8

The data for percent reduction, due to the cross-brace diaphragms, of maximum differential deflection from the Berglund formula (Figure 11.1) indicate an overall dependence on span length, but no strong trend with respect to skew angle. Therefore, the differential deflection reduction factor was assumed to be a function only of span length.

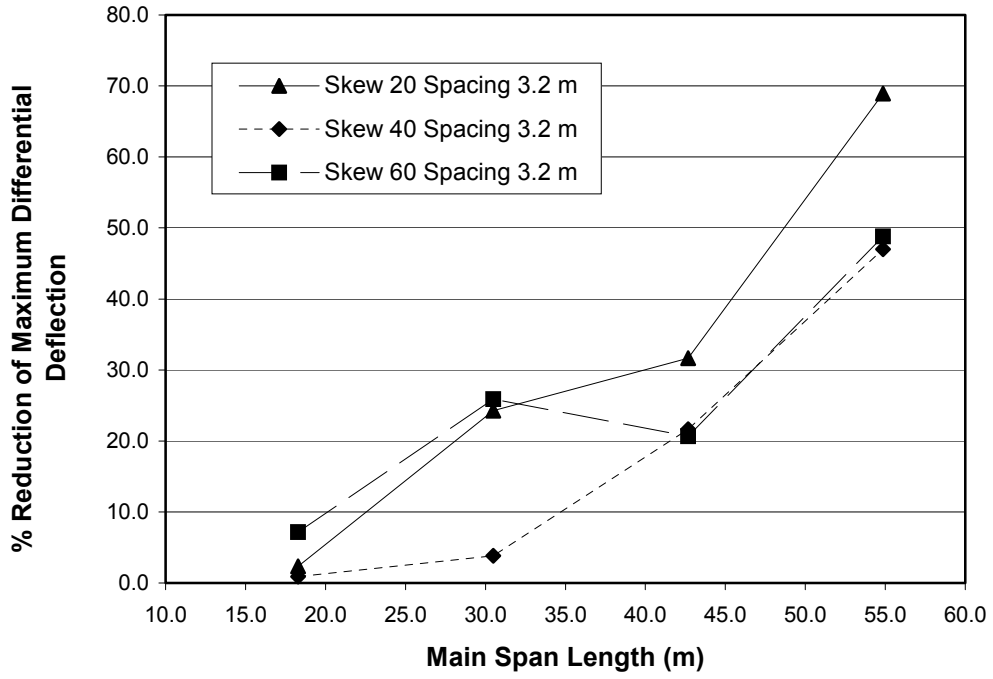

Figure 11.1 Reduction of Maximum Differential Deflection by Cross-Brace Diaphragms

The percent reduction was converted into a decimal scaling correction factor, R_x, relative to a value of 1 for zero-percent reduction, where $R_x = 1 - \%\,\text{Reduction}/100$. The percent reduction was defined as $\%\,\text{Reduction} = 100\left(\Delta_{bp} - \Delta_{cb}\right)/\Delta_{bp}$, where Δ_{bp} and Δ_{cb}, respectively, are the maximum differential deflections in bridges with bent-plate and cross-braced diaphragms. The polynomial trend line (Equation 11.1), shown in Figure 11.2, gives a reasonably accurate estimate for the scaling of differential deflections from the Berglund formula, Δ_{bp}, so that it is representative of deflections in bridges with cross-brace diaphragms, Δ_{cb}. That is, $\boldsymbol{\Delta}_{cb} = \boldsymbol{R}_x\boldsymbol{\Delta}_{bp}$ and Δ_{bp} is obtained from Equation 2-3. The

coefficients D and E are given in Table 11.2 for several units of span length. It was assumed that as the span length continued to decrease, the difference in load distribution mechanisms between cross-brace and bent-plate diaphragms would become negligible, consistent with the indication of the finite element data. As such, the trend line is assumed to intercept the y-axis at unity (Figure 11.2).

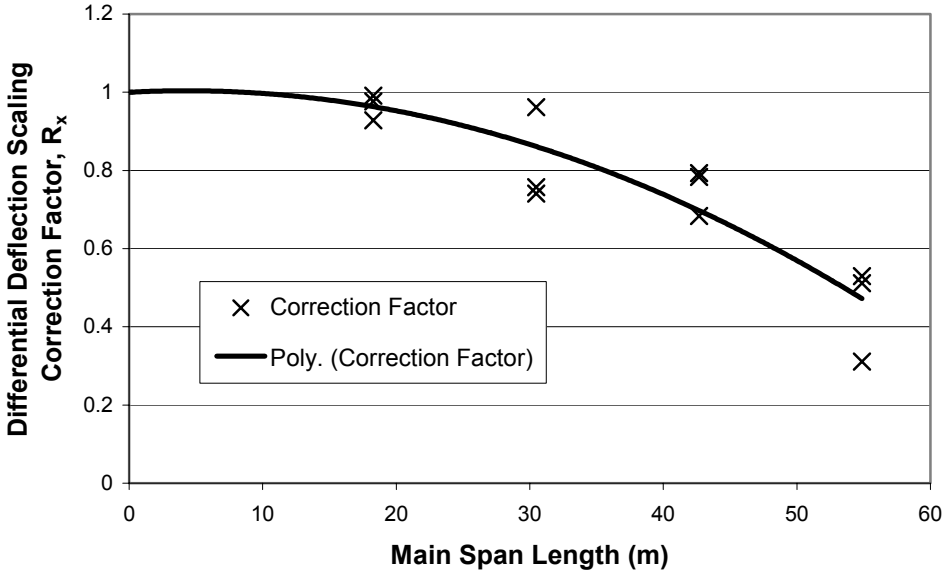

Figure 11.2 Correction Factor for Prediction of Maximum Differential Deflection in Cross-Brace Diaphragms

$$R_x = 1 + D \cdot L^2 + E \cdot L \qquad \text{Equation 11.1}$$

Table 10.2 Polynomial Equation Constants

Dimension of L	Constants	
	D	E
ft	-1.931E-05	5.432E-04
in	-1.341E-07	4.527E-05
m	-2.078E-04	1.782E-03

Thus, in practice, predictions of maximum differential deflection made by Equation 2.3 would then be scaled by the factor Rx if the bridge in consideration features cross-braces rather than bent-plate diaphragms, as noted earlier.

11.3 Application of Correction Factor to Plymouth Ave. Assessment

As discussed in section 10.4, Equation 2.3 predicted a maximum differential deflection in the Plymouth Ave. Bridge of 1.63 mm (0.0642 in), based upon a span length of 47.76 m (156.71 ft). Using that length in Equation 11.1 yields a correction factor:

$$R_x = 1 - 2.078 \cdot 10^{-4} (47.76)^2 + 1.782 \cdot 10^{-3} (47.76) = 0.6111$$

Scaling the prediction of Equation 2.3 by this factor gives a corrected prediction of 0.997 mm (0.0392 in). This value matches, to within about five percent, the maximum differential deflection of 0.945 mm (0.0372 in) measured in truck tests of the Plymouth Ave. Bridge.

11.4 Other Parameters

The correction factor R_x was developed using only those bridges in Berglund's primary parameter study having a girder spacing of 3.2 m (10.5 ft). Given time constraints, the same modification and analysis were not performed on the set of bridges with girders spaced at 2.44 m (8 ft). (Berglund's Bridge survey showed that girder spacing for steel highway bridges generally varied between 2.44 m (8 ft) and 3.2 m (10.5 ft), with no particular trend towards either extreme [2].) One such case study was performed on the bridge model calibrated with a 2.44 m girder spacing, 40-degree skew, and a span length of 42.7 m (140 ft). The reduction of maximum differential deflection for this bridge is 13.3%, less than one-half of that for the polynomial trend line, Equation 11.1, at a span length of 42.7 m (140 ft). However, this single data point is insufficient to determine the influence of girder spacing when span length is also a variable. Given the good agreement of the correction factor with field data for the Plymouth Ave. Bridge, which has a girder spacing of 2.84 m (9.33 ft), no correction for girder spacing is proposed unless further analysis shows that it is needed.

Another effect unaccounted for in the development of the correction factor, R_x, is an assumption of the finite element model. As shown in Chapter 9, the cross-brace members are modeled as extending from the top chord to the bottom chord of the girder web. This model was assumed in part due to the difficulty of adding cross-brace elements to the

SAP2000 finite element model. Mn/DOT bridge design practice is to make cross-braces as deep as possible, with 15.24 cm (6 in) of clearance to the top of the web, and a minimum of 7.62 cm (3 in) clearance to the bottom of the web for construction. Therefore the depth of the cross-brace is generally 22.86 cm (9 in) less than the depth of the web. For longer spans (with correspondingly deeper girders), the effect of this difference in depths should be minimal. But the shortest spans considered in this study have girders that are only 67.7 cm (29.67 in) deep. Thus the cross-brace clearances described above may represent a reduction of diaphragm depth equal to 33% of the web depth.

For long spans, as described above, the difference between diaphragm and web depths is less significant. Figure 11.1 seems to suggest that for shorter spans, the diaphragm plays less of a role in load distribution, because the change in diaphragm does not greatly affect the maximum differential deflection. To see whether the modeling of diaphragm depth could have a significant effect on reduction of differential deflection for intermediate spans, a conservative case was analyzed. The bridge model with a 3.2-m girder spacing, a 40-degree angle of skew, and a 42.67-m span was modified so that the cross braces only extend to 75% of the web depth. The result was a 7.8% reduction in differential deflection relative to the bent-plate case. This is only about one-fourth the value computed using the polynomial trend line, Equation 11.1, at that span length. Again, the significance of this result is uncertain, and it could not be investigated within the time frame of the current study. Clearly, this effect, and the influence of girder spacing should be studied in subsequent research on assessment of distortional fatigue.

Chapter 12-*Summary and Conclusions*

The current research increases the understanding of the distortional stress mechanism in multi-girder steel bridges. The distortional stress phenomenon is well documented by field and laboratory work performed by previous researchers, and the present study adds to that knowledge base. The literature review provides a definition of the distortional stress problem, mechanics of its behavior, and the effectiveness of various retrofit solutions.

Research previously performed by Jajich et al. for Mn/DOT as Phase I of a program to develop rapid assessment tools for distortional stresses in steel bridges led to the development of a simple equation for the prediction of web gap stresses [1]. The Jajich web gap stress formula requires knowledge of bridge geometry and the maximum amount of diaphragm differential deflection to provide an estimate of the peak web gap stress. In Phase II of the program to develop rapid assessment tools for distortional stresses in steel bridges, a method for the estimation of the maximum differential deflection at diaphragm locations was proposed by Berglund et al. for skewed steel bridges with staggered bent-plate diaphragms [2]. This method requires only knowledge of bridge geometry for its use. Both of these methods were developed using field data collected from a skewed multi-girder steel bridge with staggered bent plate diaphragms. The study documented in this report, which comprises Phase III of the program to develop rapid assessment tools for distortional stresses in steel bridges, was undertaken to determine the susceptibility of different bridge designs to distortional stresses, as well as to test the applicability of the previously developed prediction methods to these designs.

Phase III of the distortional stress rapid assessment program was conducted in two parts, with Phase IIIA focusing on the monitoring and field testing of two bridges: the Plymouth Ave. (Bridge #27796) and the 7th St. (Bridge #62028) bridges. Analysis of the data collected shows that the displacements and stresses measured for the 7th St. Bridge, which was not skewed (i.e., a square bridge), do not agree well with the predictions of the Berglund and Jajich formulas. The observed lack of agreement was not entirely

unexpected because the Berglund and Jajich formulas were developed using data collected from a skew supported bridge with staggered bent plate diaphragms, and their findings were never intended to be applied to square bridges, such as the 7th St. Bridge with its back-to-back diaphragms. Further research into the behavior the 7th St. Bridge is required if its distortional fatigue behavior is to be fully understood. However, given the low amounts of differential deflection and stress measured during truck testing, as well as knowledge of the mode of deformation that leads to higher stresses in the Plymouth Ave. Bridge, it is believed that the 7th St. Bridge, and other square bridges with back-to-back diaphragms will not suffer from distortional fatigue problems.

Web gap stresses measured on the Plymouth Ave. Bridge were also not predicted well by the equations proposed by Fisher and Jajich. Finite element modeling of a portion of the bridge revealed an out-of-plane deformation mode for this bridge that was different than that assumed by either of these prediction methods. Finite element analyses by Jajich in Phase I suggested that web gap deformation is dominated by rotation of the stiffener end. Finite element analyses in the present study reveal a web gap mechanism whereby both ends undergo deformation. In addition, the long-term monitoring studies performed on both bridges (Plymouth Ave. and 7th St.) confirmed the findings of the truck testing, even though the monitoring also showed that higher stresses than those recorded during truck testing do occur in the bridges under service conditions, but not with high frequency.

An important contribution of the first part of the present research (Phase IIIA) is Equation 8.1, which is a modification of the Jajich equation for the prediction of peak web gap stresses. This equation is based upon observations from the finite element parameter study (Chapter 7) of the diaphragm connecting girders C and D in the Plymouth Ave. Bridge. The most significant finding of this parameter study is that the web gap stress is generated by the rotations of both the top flange and the transverse stiffener, whereas Jajich assumed that web gap deformations were dominated by rotation of the transverse stiffener only.

Equation 8.1 neglects the lateral deflection of the web gap, which some researchers have accredited as the major cause of the out-of-plane distortion of the web gap. The lateral deflection is neglected for several reasons, with the first being that the accuracy of web gap stress estimates in the finite element parameter study was not significantly affected by neglecting the lateral deflection when the amount of differential vertical deflection, Δ, or the girder spacing, S, is varied. Another reason is that the finite element study performed by Jajich indicated that lateral deflection of the web gap was negligible in the diaphragm model that was refined to match the field data. It should still be cautioned that the proposed web gap stress prediction equation may have underpredicted the actual web gap stress for those bridges with values of g larger and/or values of t_w smaller than those of the Plymouth Ave. Bridge (g = 2.5 in, and t_w = 9/16 in.).

One of the significant differences between the current finite element model and that used by Jajich is the modeling of the concrete deck connecting the girders. The findings of the parameter study show that the deck plays a significant role in the distortional stress problem. Of particular interest is the manner in which the edges of the deck are restrained in the finite element diaphragm model. Jajich assumed that the edge of the deck was restrained from rotation by the headed stud connections to the girders. Rotational fixity at the edges translates to a stiffer deck that is better able to transfer live load laterally than a more flexible deck, and the supporting girders directly below the live loads are subjected to less force and, therefore, undergo less deflection. In Phase IIIA, the edges of the concrete deck in the diaphragm model were assumed to be rotationally unrestrained, and the corresponding deck flexibility led to less efficient lateral transfer of live loads, and larger differential deflections of the diaphragms. Additional research is required and it is recommended that any subsequent field monitoring projects pay particular attention to the measurement of displacements in the web gap region. Such research could also help to determine what, if any, role the lateral deflection of the web gap region plays in distortional fatigue.

The differential deflection prediction method proposed by Berglund in Phase II did not predict the differential deflection measured during field testing of the Plymouth Ave. Bridge. This lack of accuracy was addressed in the second part of this project (i.e., Phase IIIB) which contributes a heightened understanding of the role of cross-braces in differential deflection. Specifically, the use of cross-braces in place of bent-plate diaphragms is shown in Chapter 9 and 10 to significantly reduce maximum differential deflection, an effect not reflected in the development of the Berglund equation. A parametric study in Chapter 11 shows that the amount of that reduction is dependent on span length, and was used to develop a simple factor, dependent only on that length, for reducing the prediction of the Berglund equation for bridges with cross-brace diaphragms.

The reduction factor for use with the Berglund formula when considering cross-brace diaphragms, R_x, and its use are described in Chapter 11, and Equation 11.1 and Table 11.2 fully define this parameter. It is suggested that there may be some correlation between girder spacing and the extent of the reduction of differential deflections by cross-braces, which may be confirmed by additional study. However, the research in Phase IIIB has already improved the ability to successfully assess the risk of distortional fatigue in bridges with cross-brace diaphragms.

As a closing note, a recommendation is made regarding future research on distortional stresses in steel bridges. A class of bridge that may be vulnerable to this problem and which should be considered in future research is the curved girder bridge. These bridges often feature staggered diaphragms, and their geometry is likely to generate measurable differential deflections between adjacent girders that straddle a diaphragm. A field testing program and finite element study of such a curved girder bridge with staggered diaphragms is highly desirable to ascertain if the current assessment procedure for distortional stresses in steel bridges needs to further modification.

References

1. Jajich, D., Schultz, A.E., Bergson, P.M., and Galambos, T.V. "Distortion-Induced Fatigue in Multi-Girder Steel Bridges." Minnesota Department of Transportation, Final Report, May 2000.

2. Berglund, E., Schultz, A.E. "Girder Differential Deflection and Assessing Distortional Fatigue in Skewed Steel Bridges." Minnesota Department of Transportation, Final Report, Dec. 2002.

3. Keating, Peter. "Focusing on Fatigue." Civil Engineering, Nov. 1994, 54—57.

4. Fisher, J.W. *Fatigue and Fracture in Steel Bridges.* John Wiley and Sons, New York, 1984.

5. Fisher, John W., Yen, Ben, and Wagner, David. "Review of Field Measurements for Distortion Induced Fatigue Cracking in Steel Bridges." Transportation Research Record, n1118, 1987, 49—55.

6. Cousins, T. E., et al. "Field Evaluation of Fatigue Cracking in Diaphragm-Girder Connections." Journal of Performance of Constructed Facilities, 12(1), 1998, 25—32.

7. Fisher, John W., Jin, Jian, Wagner, David, and Yen, Ben. "Distortion Induced Fatigue Cracking in Steel Bridges." NCHRP Report 336, Transportation Research Board, National Research Council, Washington D.C., Dec. 1990.

8. Fisher, John W. "Fatigue Cracking in Bridges from Out-of-Plane Distortion." Canadian Journal of Civil Engineering, 5(4), 1978, 542—556.

9. Fisher, John W., Hausammann, Hans, Sullivan, Michael D., and Pense, Allan W. "Detection and Repair of Fatigue Damage in Welded Highway Bridges." NCHRP

Report 206, Transportation Research Board, National Research Council, Washington D.C., June 1979.

10. Keating, Peter and Fisher, John W. "Fatigue Behavior of Variable Loaded Bridge Details Near the Fatigue Limit." Transportation Research Record n1118, 1987, 56—64.

11. Stallings, J.M. and Cousins, T.E. "Laboratory Tests of Bolted Diaphragm-Girder Connections." Journal of Bridge Engineering, May 1998.

12. *Standard Specifications for Highway Bridges*, AASHTO, 16th Edition, Washington, D.C., 1996.

13. Moses, F., Schilling, C.G., and Raju, K.S. "Fatigue Evaluation Procedures for Steel Bridges." NCHRP Report 299, Transportation Research Board, National Research Council, Washington D.C., Nov. 1987.

14. Wipf, T.J., et. al. "Retrofit Methods for Distortion Cracking Problems in Plate Girder Bridges." Iowa Department of Transportation, Final Report, Jan. 2003.

15. Stallings, J.M., Cousins, T.E., and Stafford, T.E. "Effects of Removing Diaphragms from a Steel Girder Bridge." Transportation Research Record, n1541, Nov 1996, 183—188.

16. Computers and Structures, Inc. *SAP2000 NonLinear Version 7.44 Structural Analysis Program*. Berkeley, CA, 2001.

17. Ollgaard, Slutter and Fisher. "Shear Strength of Stud Connectors in Lightweight and Normal-Weight Concrete." *Engineering Journal,* AISC, Q2, 1971, 55-64.

18. *Interim LRFD Bridge Design Specification*, AASHTO, Washington, D.C., 2001.

Jáuregui, Yura, Frank, and Wood. "Field Evaluation of Decommissioned Noncomposite Steel Girder Bridge." Journal of Bridge Engineeringg, Jan. 2002.

Appendix A – Truck Testing Summary Data

This appendix contains summaries of the data taken during truck testing of the Plymouth Ave. and 7th St. Bridges. The procedures used to obtain these data sets are described in Section 6.2. A description of the geometry of the instrumented portions of the bridges is given in Section 3.4, with instrumentation plans shown in Figures 3.8 and 3.9, respectively, for the Plymouth Ave. and 7th St. Bridges. Truck configurations used during the truck tests is given in Figure 4.1.

The summaries presented in the Appendix are differentiated on the basis of bridge monitored, lane loading, and location of position transducers along the bridge, either diaphragm or mid-span locations. The minimum and maximum values recorded, as well as the number of truck passes used to determine these values for each instrument are reported. The greatest absolute value of either the maximum or minimum measurement represents the behavior of the instrument when the truck passed over the instrumented span, with the other value likely occurring when the truck was on an adjacent span.

The designations "Stiffener" and "Non-Stiffener " refer to the instrumented side of the girder, where the former includes attachment to the diaphragm, while the latter is the opposing side (i.e., without an attachment to a stiffener). The designations "Near", "Middle", "Far" and "Flange" refer to the position of the strain gages, with the first three being on the girder web, and the latter on the bottom flange. The "Near" gages are those closest to, but offset from, the stiffener, while the "Far" gages were adjacent to the "Near" gages but furthest from the stiffener. The "Middle" gages are those on the "Stiffener" side of the web which are directly opposite to the stiffener (i.e., on the "Non-Stiffener" side). All of there designations are summarized in Figure 3.10.

Table A.1 Plymouth Ave. - Left Lane - Diaphragm Deflection

LVDT Data

Girder Web-Gap Location	A		B	
Instrument Location	Vertical	Horizontal	Vertical	Horizontal
Min Displacement (in)	-0.00015	-0.0002	-0.00052	-0.00068
Max Displacement (in)	0.000157	0.000296	0.000611	0.000646
Number of Runs Used	11	11	11	11

Girder Web-Gap Location	C		D	
Instrument Location	Vertical	Horizontal	Vertical	Horizontal
Min Displacement (in)	-0.00251	-0.00037	-0.00344	-0.00071
Max Displacement (in)	0.000299	0.001467	0.000522	0.000171
Number of Runs Used	11	11	11	11

Position Transducers Measuring: **Diaphragm Deflection**

Girder Location	A	B	C	D
Min Displacement (in)	-0.02742	-0.06463	-0.05366	-0.07808
Max Displacement (in)	0.017314	0.0291	0.022875	0.031718
Number of Runs Used	11	11	11	11

Strain Gage Data

Girder A	Stiffener		Non-Stiffener			
Instrument Location	Near	Far	Middle	Near	Far	Flange
Min Stress (ksi)	-0.21143	-0.16859	-0.15782	-0.08063	-0.07134	-0.29561
Max Stress (ksi)	0.211587	0.158599	0.193401	0.086183	0.110797	0.260055
Number of Runs Used	11	11	11	10	11	11

Girder B	Stiffener		Non-Stiffener			
Instrument Location	Near	Far	Middle	Near	Far	Flange
Min Stress (ksi)	-0.17764	-0.17762	-0.15556	-0.14811	-0.15227	-0.34161
Max Stress (ksi)	0.176956	0.180476	0.170805	0.170621	0.151405	0.428332
Number of Runs Used	11	11	11	11	11	11

Girder C	Stiffener		Non-Stiffener			
Instrument Location	Near	Far	Middle	Near	Far	Flange
Min Stress (ksi)	-0.26003	-0.26292	-2.07687	-2.08351	0	-0.40861
Max Stress (ksi)	1.468123	1.363006	0.330987	0.358319	0	0.398969
Number of Runs Used	11	11	11	11	0	11

Girder D	Stiffener		Non-Stiffener			
Instrument Location	Near	Far	Middle	Near	Far	Flange
Min Stress (ksi)	-0.87898	-0.87407	-0.2776	-0.43138	-0.33755	-0.56545
Max Stress (ksi)	0.241776	0.172391	0.900045	1.272596	1.105813	1.926552
Number of Runs Used	11	11	11	11	11	11

Table A.2 Plymouth Ave. - Left Lane – Mid-span Deflection

LVDT Data

Girder Web Gap Location	**A**		**B**	
Instrument Location	Vertical	Horizontal	Vertical	Horizontal
Min Displacement (in)	-9.3E-05	-0.00018	-0.00056	-0.00074
Max Displacement (in)	0.000107	0.000263	0.000639	0.000735
Number of Runs Used	11	11	11	11

Girder Web Gap Location	**C**		**D**	
Instrument Location	Vertical	Horizontal	Vertical	Horizontal
Min Displacement (in)	-0.00248	-0.00043	-0.0034	-0.00084
Max Displacement (in)	0.000303	0.001433	0.000596	0.000247
Number of Runs Used	11	11	11	11

Position Transducers Measuring: **Mid-span Deflection**

Girder Location	**A**	**B**	**C**	**D**
Min Displacement (in)	-0.0567	-0.09503	-0.13528	-0.1709
Max Displacement (in)	0.036283	0.040909	0.04063	0.043257
Number of Runs Used	11	11	11	11

Strain Gage Data

Girder A	**Stiffener**		**Non-Stiffener**			
Instrument Location	Near	Far	Middle	Near	Far	Flange
Min Stress (ksi)	-0.209	-0.16283	-0.16464	-0.07096	-0.06085	-0.29663
Max Stress (ksi)	0.215983	0.162499	0.197545	0.077657	0.108091	0.274862
Number of Runs Used	11	11	11	11	11	11

Girder B	**Stiffener**		**Non-Stiffener**			
Instrument Location	Near	Far	Middle	Near	Far	Flange
Min Stress (ksi)	-0.18456	-0.18886	-0.15797	-0.18012	-0.16467	-0.38529
Max Stress (ksi)	0.2069	0.203905	0.188394	0.19952	0.18512	0.449378
Number of Runs Used	11	11	11	11	11	11

Girder C	**Stiffener**		**Non-Stiffener**			
Instrument Location	Near	Far	Middle	Near	Far	Flange
Min Stress (ksi)	-0.28104	-0.28706	-2.07733	-2.09772	0	-0.39354
Max Stress (ksi)	1.447886	1.356138	0.338637	0.365176	0	0.39721
Number of Runs Used	11	11	11	11	0	11

Girder D	**Stiffener**		**Non-Stiffener**			
Instrument Location	Near	Far	Middle	Near	Far	Flange
Min Stress (ksi)	-0.92165	-0.91898	-0.25463	-0.38494	-0.31892	-0.55396
Max Stress (ksi)	0.249056	0.172103	0.935634	1.235313	1.155493	1.945995
Number of Runs Used	11	11	11	11	11	11

Table A.3 Plymouth Ave. - Right Lane - Diaphragm Deflection

LVDT Data

Girder Web-Gap Location	A		B	
Instrument Location	Vertical	Horizontal	Vertical	Horizontal
Min Displacement (in)	-0.00014	-0.0002	-0.00051	-0.00067
Max Displacement (in)	0.000159	0.000249	0.000596	0.000687
Number of Runs Used	11	11	11	11

Girder Web-Gap Location	C		D	
Instrument Location	Vertical	Horizontal	Vertical	Horizontal
Min Displacement (in)	-0.00111	-0.00048	-0.00146	-0.00035
Max Displacement (in)	0.00057	0.000521	0.000805	0.000829
Number of Runs Used	11	11	11	11

Position Transducers Measuring: **Diaphragm Deflection**

Girder Location	A	B	C	D
Min Displacement (in)	-0.05151	-0.08797	-0.05146	-0.05004
Max Displacement (in)	0.024932	0.036952	0.0263	0.029746
Number of Runs Used	11	11	11	11

Strain Gage Data

Girder A	Stiffener		Non-Stiffener			
Instrument Location	Near	Far	Middle	Near	Far	Flange
Min Stress (ksi)	-0.32826	-0.15131	-0.17389	-0.11337	-0.1063	-0.47799
Max Stress (ksi)	0.301901	0.21214	0.171436	0.077033	0.097317	0.333421
Number of Runs Used	11	11	11	11	11	11

Girder B	Stiffener		Non-Stiffener			
Instrument Location	Near	Far	Middle	Near	Far	Flange
Min Stress (ksi)	-0.21247	-0.1934	-0.14323	-0.17546	-0.15097	-0.56326
Max Stress (ksi)	0.190498	0.178581	0.211504	0.204928	0.205187	1.09995
Number of Runs Used	11	11	11	11	11	11

Girder C	Stiffener		Non-Stiffener			
Instrument Location	Near	Far	Middle	Near	Far	Flange
Min Stress (ksi)	-0.70087	-0.71257	-0.49283	-0.50721	0	-0.63648
Max Stress (ksi)	0.46898	0.416017	0.511466	0.513058	0	1.04419
Number of Runs Used	11	11	11	11	0	10

Girder D	Stiffener		Non-Stiffener			
Instrument Location	Near	Far	Middle	Near	Far	Flange
Min Stress (ksi)	-0.44834	-0.40471	-1.67055	-2.58873	-2.30684	-0.46652
Max Stress (ksi)	1.173752	1.156101	0.554193	0.70116	0.759398	3.229655
Number of Runs Used	11	11	11	11	11	11

Table A.4 Plymouth Ave. - Right Lane - Mid-span Deflection

LVDT Data

Girder Web-Gap Location	A		B	
Instrument Location	Vertical	Horizontal	Vertical	Horizontal
Min Displacement (in)	-9.3E-05	-0.0002	-0.00058	-0.00074
Max Displacement (in)	0.000102	0.000237	0.000642	0.000766
Number of Runs Used	12	12	12	12

Girder Web-Gap Location	C		D	
Instrument Location	Vertical	Horizontal	Vertical	Horizontal
Min Displacement (in)	-0.00106	-0.00052	-0.00138	-0.00046
Max Displacement (in)	0.000594	0.000557	0.000906	0.00088
Number of Runs Used	12	12	12	12

Position Transducers Measuring: **Mid-span Deflection**

Girder Location	A	B	C	D
Min Displacement (in)	-0.11158	-0.1498	-0.1409	-0.11185
Max Displacement (in)	0.044863	0.04719	0.040744	0.039354
Number of Runs Used	12	12	12	12

Strain Gage Data

Girder A	Stiffener		Non-Stiffener			
Instrument Location	Near	Far	Middle	Near	Far	Flange
Min Stress (ksi)	-0.19613	-0.15869	-0.17574	-0.09125	-0.08987	-0.48916
Max Stress (ksi)	0.3017	0.21058	0.188933	0.072715	0.105057	0.339316
Number of Runs Used	12	12	12	12	12	12

Girder B	Stiffener		Non-Stiffener			
Instrument Location	Near	Far	Middle	Near	Far	Flange
Min Stress (ksi)	-0.18585	-0.19793	-0.17167	-0.1664	-0.16493	-0.51305
Max Stress (ksi)	0.195534	0.201739	0.236091	0.237766	0.222796	1.083155
Number of Runs Used	12	12	12	12	12	12

Girder C	Stiffener		Non-Stiffener			
Instrument Location	Near	Far	Middle	Near	Far	Flange
Min Stress (ksi)	-0.65181	-0.64718	-0.5593	-0.59361	0	-0.6114
Max Stress (ksi)	0.489344	0.460424	0.458264	0.478419	0	0.945422
Number of Runs Used	12	12	12	12	0	12

Girder D	Stiffener		Non-Stiffener			
Instrument Location	Near	Far	Middle	Near	Far	Flange
Min Stress (ksi)	-0.49101	-0.41913	-1.54622	-2.18459	-2.13766	-0.47936
Max Stress (ksi)	1.10723	1.062672	0.560725	0.861978	0.79111	0.541251
Number of Runs Used	12	12	12	12	12	12

Table A.5 Plymouth Ave. - Side-by-Side - Diaphragm Deflection

LVDT Data

Girder Web-Gap Location	A		B	
Instrument Location	Vertical	Horizontal	Vertical	Horizontal
Min Displacement (in)	-0.00014	-0.00017	-0.00053	-0.00069
Max Displacement (in)	0.000159	0.000274	0.000634	0.000707
Number of Runs Used	3	3	3	3

Girder Web-Gap Location	C		D	
Instrument Location	Vertical	Horizontal	Vertical	Horizontal
Min Displacement (in)	-0.00286	-0.00054	-0.00359	-0.00045
Max Displacement (in)	0.00081	0.001309	0.001189	0.0004
Number of Runs Used	3	3	3	3

Position Transducers Measuring: **Diaphragm Deflection**

Girder Location	A	B	C	D
Min Displacement (in)	-0.0737	-0.1431	-0.1019	-0.12033
Max Displacement (in)	0.041817	0.065508	0.048802	0.057449
Number of Runs Used	3	3	3	3

Strain Gage Data

Girder A	Stiffener		Non-Stiffener			
Instrument Location	Near	Far	Middle	Near	Far	Flange
Min Stress (ksi)	-0.26638	-0.26716	-0.13825	-0.19168	-0.1586	-0.58724
Max Stress (ksi)	0.352288	0.295436	0.164898	0.170608	0.167936	0.395855
Number of Runs Used	3	3	3	3	3	3

Girder B	Stiffener		Non-Stiffener			
Instrument Location	Near	Far	Middle	Near	Far	Flange
Min Stress (ksi)	-0.14265	-0.16411	-0.13286	-0.11486	-0.11287	-0.77941
Max Stress (ksi)	0.160976	0.153344	0.187527	0.243776	0.193374	1.471188
Number of Runs Used	3	3	3	3	3	3

Girder C	Stiffener		Non-Stiffener			
Instrument Location	Near	Far	Middle	Near	Far	Flange
Min Stress (ksi)	-0.32415	-0.33401	-1.81106	-1.80254	0	-1.02167
Max Stress (ksi)	1.417784	1.258087	0.45423	0.41693	0	1.368699
Number of Runs Used	3	3	3	3	0	3

Girder D	Stiffener		Non-Stiffener			
Instrument Location	Near	Far	Middle	Near	Far	Flange
Min Stress (ksi)	-0.47157	-0.43481	-0.94109	-1.82417	-1.40231	-0.97573
Max Stress (ksi)	0.985196	0.928578	0.555307	1.232604	0.798248	2.117993
Number of Runs Used	3	3	3	3	3	3

Table A.6 Plymouth Ave. - Side-by-Side - Mid-span Deflection

LVDT Data

Girder Web-Gap Location	A		B	
Instrument Location	Vertical	Horizontal	Vertical	Horizontal
Min Displacement (in)	-0.00012	-0.00017	-0.00054	-0.00071
Max Displacement (in)	0.000134	0.00025	0.000623	0.000696
Number of Runs Used	3	3	3	3

Girder Web-Gap Location	C		D	
Instrument Location	Vertical	Horizontal	Vertical	Horizontal
Min Displacement (in)	-0.00259	-0.00055	-0.00343	-0.00045
Max Displacement (in)	0.000773	0.001256	0.001234	0.000371
Number of Runs Used	3	3	3	3

Position Transducers Measuring**: Mid-span Deflection**

Girder Location	A	B	C	D
Min Displacement (in)	-0.15907	-0.23776	-0.27365	-0.27305
Max Displacement (in)	0.068828	0.079158	0.077984	0.079327
Number of Runs Used	3	3	3	3

Strain Gage Data

Girder A	Stiffener		Non-Stiffener			
Instrument Location	Near	Far	Middle	Near	Far	Flange
Min Stress (ksi)	-0.19998	-0.1799	-0.19981	-0.09909	-0.09008	-0.62087
Max Stress (ksi)	0.302691	0.185504	0.212567	0.077365	0.101127	0.490357
Number of Runs Used	3	3	3	3	3	3

Girder B	Stiffener		Non-Stiffener			
Instrument Location	Near	Far	Middle	Near	Far	Flange
Min Stress (ksi)	-0.19787	-0.18849	-0.16129	-0.20678	-0.164	-0.77329
Max Stress (ksi)	0.212965	0.205331	0.27634	0.253544	0.241223	1.474016
Number of Runs Used	3	3	3	3	3	3

Girder C	Stiffener		Non-Stiffener			
Instrument Location	Near	Far	Middle	Near	Far	Flange
Min Stress (ksi)	-0.42246	-0.41718	-1.83763	-1.885	0	-0.94881
Max Stress (ksi)	1.431605	1.27623	0.518138	0.535534	0	1.285736
Number of Runs Used	3	3	3	3	0	3

Girder D	Stiffener		Non-Stiffener			
Instrument Location	Near	Far	Middle	Near	Far	Flange
Min Stress (ksi)	-0.39957	-0.37002	-0.854	-1.27745	-1.27188	-1.03773
Max Stress (ksi)	0.892092	0.801776	0.481936	0.73637	0.658731	2.135453
Number of Runs Used	3	3	3	3	3	3

Table A.7 7th St. - Left Lane - Diaphragm Deflection

LVDT Data

Girder Web-Gap Location	A		B	
Instrument Location	Vertical	Horizontal	Vertical	Horizontal
Min Displacement (in)	-0.00095	-0.00044	-0.00054	0
Max Displacement (in)	0.000237	0.003024	0.000391	0
Number of Runs Used	9	9	9	0

Girder Web-Gap Location	C		D	
Instrument Location	Vertical	Horizontal	Vertical	Horizontal
Min Displacement (in)	-0.00036	-0.00101	-0.00089	-0.00173
Max Displacement (in)	0.000752	0.000517	0.000929	0.00084
Number of Runs Used	9	9	9	9

Position Transducers Measuring: **Diaphragm Deflection**

Girder Location	A	B	C	D
Min Displacement (in)	-0.02279	-0.04917	-0.0638	-0.06775
Max Displacement (in)	0.0119	0.024652	0.025392	0.028379
Number of Runs Used	9	9	9	9

Strain Gage Data

Girder A	Stiffener		Non-Stiffener			
Instrument Location	Near	Far	Middle	Near	Far	Flange
Min Stress (ksi)	-0.11476	-0.09766	-0.53997	-0.54593	-0.46078	-0.36576
Max Stress (ksi)	0.400187	0.296065	0.093065	0.084826	0.077918	0.221547
Number of Runs Used	9	9	9	9	9	8

Girder B	Stiffener		Non-Stiffener			
Instrument Location	Near	Far	Middle	Near	Far	Flange
Min Stress (ksi)	-0.47264	-0.37025	0	-0.19018	-0.15587	-0.4562
Max Stress (ksi)	0.195774	0.176467	0	0.537822	0.456359	0.490845
Number of Runs Used	9	9	0	9	9	9

Girder C	Stiffener		Non-Stiffener			
Instrument Location	Near	Far	Middle	Near	Far	Flange
Min Stress (ksi)	-0.47876	-0.61116	0	-0.35842	-0.26806	-0.8113
Max Stress (ksi)	0.362577	0.417928	0	0.943974	0.856533	0.80062
Number of Runs Used	9	9	0	9	9	9

Girder D	Stiffener		Non-Stiffener			
Instrument Location	Near	Far	Middle	Near	Far	Flange
Min Stress (ksi)	-0.12757	-0.08839	0	-0.40178	-0.34206	-1.01183
Max Stress (ksi)	0.39403	0.300498	0	0.157629	0.154531	1.260093
Number of Runs Used	9	9	0	9	9	9

Table A.8 7th St. - Left Lane - Mid-span Deflection

LVDT Data

Girder Web-Gap Location	**A**		**B**	
Instrument Location	Vertical	Horizontal	Vertical	Horizontal
Min Displacement (in)	-0.00066	-0.00036	-0.00055	0
Max Displacement (in)	0.000261	0.001951	0.00026	0
Number of Runs Used	9	9	9	0

Girder Web-Gap Location	**C**		**D**	
Instrument Location	Vertical	Horizontal	Vertical	Horizontal
Min Displacement (in)	-0.00029	-0.0007	-0.00084	-0.00162
Max Displacement (in)	0.000699	0.000438	0.000885	0.000703
Number of Runs Used	9	9	9	9

Position Transducers Measuring**: Mid-span Deflection**

Girder Location	**A**	**B**	**C**	**D**
Min Displacement (in)	-0.03035	-0.07453	-0.12681	-0.16504
Max Displacement (in)	0.019375	0.03794	0.035727	0.037162
Number of Runs Used	9	9	9	9

Strain Gage Data

Girder A	**Stiffener**		**Non-Stiffener**			
Instrument Location	Near	Far	Middle	Near	Far	Flange
Min Stress (ksi)	-0.12204	-0.1182	-0.33775	-0.32651	-0.28888	-0.21499
Max Stress (ksi)	0.270879	0.210144	0.096932	0.091602	0.084256	0.157178
Number of Runs Used	9	9	9	9	9	9

Girder B	**Stiffener**		**Non-Stiffener**			
Instrument Location	Near	Far	Middle	Near	Far	Flange
Min Stress (ksi)	-0.485	-0.37963	0	-0.18783	-0.15073	-0.34827
Max Stress (ksi)	0.198757	0.178459	0	0.480326	0.395563	0.347598
Number of Runs Used	9	9	0	9	9	9

Girder C	**Stiffener**		**Non-Stiffener**			
Instrument Location	Near	Far	Middle	Near	Far	Flange
Min Stress (ksi)	-0.56346	-0.71603	0	-0.27396	-0.23881	-0.70082
Max Stress (ksi)	0.231347	0.253989	0	1.103989	0.972553	0.828863
Number of Runs Used	9	9	0	9	9	9

Girder D	**Stiffener**		**Non-Stiffener**			
Instrument Location	Near	Far	Middle	Near	Far	Flange
Min Stress (ksi)	-0.13465	-0.07266	0	-0.26173	-0.24547	-0.98335
Max Stress (ksi)	0.264101	0.213205	0	0.177471	0.191709	1.454327
Number of Runs Used	8	8	0	8	8	9

Table A.9 7th St. - Right Lane - Diaphragm Deflection

LVDT Data

Girder Web-Gap Location	A		B	
Instrument Location	Vertical	Horizontal	Vertical	Horizontal
Min Displacement (in)	-0.00161	-0.00069	-0.00029	0
Max Displacement (in)	0.000276	0.005126	0.000764	0
Number of Runs Used	9	9	9	0

Girder Web-Gap Location	C		D	
Instrument Location	Vertical	Horizontal	Vertical	Horizontal
Min Displacement (in)	-0.00062	-0.0011	-0.00094	-0.00167
Max Displacement (in)	0.000681	0.000457	0.000865	0.001445
Number of Runs Used	9	9	9	9

Position Transducers Measuring: **Diaphragm Deflection**

Girder Location	A	B	C	D
Min Displacement (in)	-0.0405	-0.06891	-0.06726	-0.04529
Max Displacement (in)	0.016967	0.026548	0.021308	0.017207
Number of Runs Used	9	9	9	9

Strain Gage Data

Girder A	Stiffener		Non-Stiffener			
Instrument Location	Near	Far	Middle	Near	Far	Flange
Min Stress (ksi)	-0.09782	-0.09369	-1.00512	-1.01521	-0.87718	-0.55003
Max Stress (ksi)	0.734341	0.526914	0.114343	0.107453	0.102573	0.414018
Number of Runs Used	9	9	9	9	9	9

Girder B	Stiffener		Non-Stiffener			
Instrument Location	Near	Far	Middle	Near	Far	Flange
Min Stress (ksi)	-0.46792	-0.30431	0	-0.15555	-0.12854	-0.59336
Max Stress (ksi)	0.21293	0.187857	0	0.725423	0.643465	1.184971
Number of Runs Used	9	9	0	9	9	9

Girder C	Stiffener		Non-Stiffener			
Instrument Location	Near	Far	Middle	Near	Far	Flange
Min Stress (ksi)	-0.17135	-0.21514	0	-0.71537	-0.49372	-0.78832
Max Stress (ksi)	0.867989	0.990683	0	0.317954	0.281131	1.127365
Number of Runs Used	9	9	0	9	9	9

Girder D	Stiffener		Non-Stiffener			
Instrument Location	Near	Far	Middle	Near	Far	Flange
Min Stress (ksi)	-0.19577	-0.14712	0	-1.21226	-1.0017	-0.67923
Max Stress (ksi)	1.127702	0.811404	0	0.203193	0.192596	0.623025
Number of Runs Used	9	9	0	9	9	9

Table A.10 7th St. Bridge - Right Lane - Mid-span Deflection

LVDT Data

Girder Web-Gap Location	**A**		**B**	
Instrument Location	Vertical	Horizontal	Vertical	Horizontal
Min Displacement (in)	-0.00162	-0.00062	-0.00015	0
Max Displacement (in)	0.000302	0.005093	0.000759	0
Number of Runs Used	9	9	9	0

Girder Web-Gap Location	**C**		**D**	
Instrument Location	Vertical	Horizontal	Vertical	Horizontal
Min Displacement (in)	-0.00067	-0.00094	-0.0011	-0.00158
Max Displacement (in)	0.000432	0.000403	0.001102	0.001447
Number of Runs Used	9	9	9	9

Position Transducers Measuring**: Mid-span Deflection**

Girder Location	**A**	**B**	**C**	**D**
Min Displacement (in)	-0.09255	-0.13986	-0.13462	-0.09529
Max Displacement (in)	0.036954	0.042098	0.037208	0.031327
Number of Runs Used	9	9	9	9

Strain Gage Data

Girder A	**Stiffener**		**Non-Stiffener**			
Instrument Location	Near	Far	Middle	Near	Far	Flange
Min Stress (ksi)	-0.12953	-0.11398	-1.02487	-1.03161	-0.8915	-0.55886
Max Stress (ksi)	0.745436	0.529304	0.125982	0.106287	0.100941	0.417542
Number of Runs Used	9	9	9	9	9	9

Girder B	**Stiffener**		**Non-Stiffener**			
Instrument Location	Near	Far	Middle	Near	Far	Flange
Min Stress (ksi)	-0.45603	-0.28281	0	-0.16266	-0.12723	-0.61979
Max Stress (ksi)	0.220318	0.197626	0	0.716747	0.639082	1.163449
Number of Runs Used	9	9	0	9	9	9

Girder C	**Stiffener**		**Non-Stiffener**			
Instrument Location	Near	Far	Middle	Near	Far	Flange
Min Stress (ksi)	-0.12178	-0.14057	0	-0.70218	-0.50899	-0.74184
Max Stress (ksi)	0.860853	0.990429	0	0.177297	0.185273	1.082884
Number of Runs Used	9	9	0	9	9	9

Girder D	**Stiffener**		**Non-Stiffener**			
Instrument Location	Near	Far	Middle	Near	Far	Flange
Min Stress (ksi)	-0.17263	-0.12499	0	-1.23945	-1.02342	-0.61444
Max Stress (ksi)	1.152988	0.819248	0	0.183359	0.1978	0.513205
Number of Runs Used	9	9	0	9	9	9

Table A.11 7th St. - Side-by-Side - Diaphragm Deflection

LVDT Data

Girder Web-Gap Location	A		B	
Instrument Location	Vertical	Horizontal	Vertical	Horizontal
Min Displacement (in)	-0.00205	-0.00106	-0.00014	-0.01211
Max Displacement (in)	0.000253	0.007045	0.00027	0.011439
Number of Runs Used	3	3	3	3

Girder Web-Gap Location	C		D	
Instrument Location	Vertical	Horizontal	Vertical	Horizontal
Min Displacement (in)	-0.00037	-0.00059	-0.00096	-0.00057
Max Displacement (in)	0.000415	0.000365	0.000811	0.000965
Number of Runs Used	3	3	3	3

Position Transducers Measuring: **Diaphragm Deflection**

Girder Location	A	B	C	D
Min Displacement (in)	-0.06019	-0.10629	-0.12485	-0.10612
Max Displacement (in)	0.026291	0.038732	0.045607	0.045241
Number of Runs Used	3	3	3	3

Strain Gage Data

Girder A	Stiffener		Non-Stiffener			
Instrument Location	Near	Far	Middle	Near	Far	Flange
Min Stress (ksi)	-0.10231	-0.11373	-1.31679	-1.30081	-1.13436	-0.77125
Max Stress (ksi)	0.919555	0.701585	0.150763	0.112013	0.127295	0.59467
Number of Runs Used	3	3	3	3	3	3

Girder B	Stiffener		Non-Stiffener			
Instrument Location	Near	Far	Middle	Near	Far	Flange
Min Stress (ksi)	-0.81217	-0.54407	0	-0.31075	-0.22565	-0.9518
Max Stress (ksi)	0.356399	0.31655	0	1.110162	0.941296	1.506702
Number of Runs Used	3	3	0	3	3	3

Girder C	Stiffener		Non-Stiffener			
Instrument Location	Near	Far	Middle	Near	Far	Flange
Min Stress (ksi)	-0.17563	-0.20195	0	-0.27216	-0.22264	-1.4709
Max Stress (ksi)	0.548301	0.582212	0	0.473478	0.496955	1.766678
Number of Runs Used	3	3	0	3	3	3

Girder D	Stiffener		Non-Stiffener			
Instrument Location	Near	Far	Middle	Near	Far	Flange
Min Stress (ksi)	-0.22769	-0.17169	0	-1.07158	-0.84561	-1.51386
Max Stress (ksi)	1.085943	0.81753	0	0.167361	0.166497	1.729477
Number of Runs Used	3	3	0	3	3	3

Table A.12 7th St. - Side-by-Side - Mid-span Deflection

LVDT Data

Girder Web-Gap Location	A		B	
Instrument Location	Vertical	Horizontal	Vertical	Horizontal
Min Displacement (in)	-0.00196	-0.00094	-0.00022	0
Max Displacement (in)	0.000282	0.006618	0.000416	0
Number of Runs Used	3	3	3	0

Girder Web-Gap Location	C		D	
Instrument Location	Vertical	Horizontal	Vertical	Horizontal
Min Displacement (in)	-0.00041	-0.00095	-0.00087	-0.00162
Max Displacement (in)	0.00041	0.000363	0.00087	0.00109
Number of Runs Used	3	3	3	3

Position Transducers Measuring**: Mid-span Deflection**

Girder Location	A	B	C	D
Min Displacement (in)	-0.1271	-0.20807	-0.25089	-0.24481
Max Displacement (in)	0.046344	0.063348	0.062796	0.063217
Number of Runs Used	3	3	3	3

Strain Gage Data

Girder A	Stiffener		Non-Stiffener			
Instrument Location	Near	Far	Middle	Near	Far	Flange
Min Stress (ksi)	-0.10638	-0.09775	-1.21812	-1.22726	-1.06412	-0.77987
Max Stress (ksi)	0.869562	0.625321	0.139853	0.129164	0.119081	0.5058
Number of Runs Used	3	3	3	3	3	3

Girder B	Stiffener		Non-Stiffener			
Instrument Location	Near	Far	Middle	Near	Far	Flange
Min Stress (ksi)	-0.761	-0.50788	0	-0.29842	-0.23213	-0.94924
Max Stress (ksi)	0.36188	0.284977	0	1.092029	0.97002	1.425663
Number of Runs Used	3	3	0	3	3	3

Girder C	Stiffener		Non-Stiffener			
Instrument Location	Near	Far	Middle	Near	Far	Flange
Min Stress (ksi)	-0.11938	-0.11692	0	-0.36139	-0.2913	-1.44206
Max Stress (ksi)	0.500515	0.513537	0	0.481926	0.51819	1.848649
Number of Runs Used	3	3	0	3	3	3

Girder D	Stiffener		Non-Stiffener			
Instrument Location	Near	Far	Middle	Near	Far	Flange
Min Stress (ksi)	-0.16699	-0.12479	0	-1.35293	-1.11048	-1.47613
Max Stress (ksi)	1.368073	1.06711	0	0.152366	0.155854	1.803056
Number of Runs Used	3	3	0	3	3	3